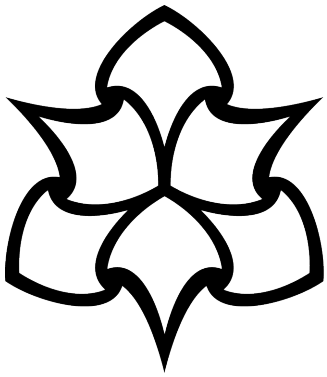

MANCHESTER METROPOLITAN
UNIVERSITY

Inductive Wireless Power Transmission for Automotive Applications

---

Author:
Matjaz ROZMAN

A thesis submitted in partial fulfilment of the requirements of Manchester Metropolitan University for the degree of Doctor of Philosophy

2019

Declaration of Authorship

I, Matjaz ROZMAN, declare that this thesis titled, "Inductive Wireless Power Transmission for Automotive Applications" and the work presented in it are my own. I confirm that:

- This work was done wholly or mainly while in candidature for a research degree at this university.
- Parts of this thesis that have been previously submitted for a degree or any other qualification at this university or any other institution, this has been clearly indicated.
- If I have consulted the published work of others, I have clearly attributed them.
- Where I have quoted from the work of others, I have provided the source. With the exception of such quotations, this thesis is entirely my own work.
- I have acknowledged all main sources of help.
- Where the thesis is based on work done by myself jointly with others, I have made clear exactly what was done by others and what I have contributed myself.

Sign:

Date:

"To my wonderful wife Upeksha, parents and parents-in-law. "

Matjaz Rozman

MANCHESTER METROPOLITAN UNIVERSITY

Abstract

Manchester Metropolitan University
School of Engineering

Doctor of Philosophy

Inductive Wireless Power Transmission for Automotive Applications

by Matjaz ROZMAN

Technology has revolutionised all aspects of human life at all consecutive intervals and Fourth Industrial Revolution is no different. Daily transport and energy industries not only shape the future of a country's economy, but also make the economy highly yielding due to recent advances. Electric vehicles (EV) have been rapidly invading the market share during recent years.The advancements in EV and enhanced market share demand EV charging, being more reliant on either conventional plug-in charging or wireless charging. Given the limitations within battery related apparatus such as escalating battery costs, higher weight and lower power density, wireless power transfer (WPT) is a novel state of the art technology in energising. WPT has remarkable characteristics such as enhanced flexibility, mobility, convenience and safety, indicating potential benefits, if it is adopted for EV with similar efficiency; for example, it can eliminate the use of charging cables.

Despite the fact that the wireless charges for EV, have undergone significant development phase during the last decade, many design limitations are yet to be addressed. Although the technology has been commercially outgrown, key limitations such as limited efficiency over distance, limited driving range, vulnerability to misalignments, or positional offsets are yet to be researched. Moreover, although high system efficiency can be attained, the distance variations between the transmitter and receiver and the misalignments will impact the system efficiency. This thesis addresses the aforementioned limitations and design challenges of the magnetic resonance WPT system, and proposes a novel transmitter and receiver circuit and coil designs, to minimise the impact of distance variations and coil misplacement, reduce the size and improve charging performance.

This thesis focusses on inductive wireless power transfer (IWPT) which is also referred to as magnetic resonance and reviews and contrasts other WPT mechanisms. Additionally, it presents a detailed mathematical analysis of inductive wireless power circuit model to obtain accurate modelling parameters. Two and four loop strongly coupled magnetic resonance (SCMR) wireless power systems have been mathematically analysed and their performance has been evaluated. A novel combined, conformal strongly coupled magnetic resonance system (CSCMR) has been combined with SCMR, in order to minimise the dimensions of the receiver and compensate the coupling factor due to distance variations between the transmitter and receiver. In the second phase, additional inductors were added to the existing loosely coupled system to obtain higher efficiencies over higher distances. The size of

the system has significantly reduced due to the additional smaller transmitter and receiver inductor which were added to the existing system to achieve better performance. The validity of each design has been discussed via a set of simulations, and their measurements have been obtained via prototypes.

Finally, a smart WPT charging system, consisting of six transmitter loops and a sensor network array, for an autonomous parking space was developed. The proposed method reduces the energy required for determining a car's location, eventually increasing the performance of the charger.

Acknowledgements

This journey would not have been as delightful without the fascinating people I met along the journey. My first and foremost, thank goes to my supervisor, Prof. Bamidele Adebisi for the opportunity, forthrightness and the continuous support during the entire research project. I am indeed privileged to have had him as my MSc lecturer, project supervisor many years ago, and then his insightful supervision during my PhD. The guidance, trust and 'the freedom to create' during the entire time, which was essential for our first paper.

I would like to convey my gratitude to Prof. Michael Fernando for the brainstorming sessions as well as the leisurely chats. I am highly grateful for the encouragement and the inspirational support I was given. I would like to thank Dr. Kheral Rupak for his supervision and experience guidance. I am also extremely appreciative to Dr. Khalid M. Rabie, Dr. Augustine Ikpehai and Dr. Kelvin Anoh for their many insightful recommendations and his continuous support throughout my research. My sincere appreciation for the tremendous support provided by University of Manchester Metropolitan's workshop staff.

I would also like to convey my profound gratitude to Dr. Ed Huang and Mr. Markus Mohsen for the support till the completion of my research. You have played a huge role in making this possible for me, which I am beyond thankful. My heartfelt appreciation goes out to my parents, parents in-law and finally, to my loving wife Upeksha, for tolerating my eccentric ways during the past three years standing by me till the end of time...

Contents

List of Figures

List of Tables

List of Abbreviations

AC	**A**lternating **C**urrent
ADS	**A**dvanced **D**esign **S**ystem
A4WP	**A**lliance for **W**ireless **P**ower
BLE	**B**luetooth **L**ow **E**nergy
CSCMR	**C**onformal **S**trongly **C**oupled **M**agnetic **R**esonance
CWPT	**C**apacitive **W**ireless **P**ower
DC	**D**irect **C**urrent
EMI	**E**lectromagnetic **I**nterference
EV	**E**lectrical **V**ehicles
GaN	**G**allium **N**itride
GWP	**G**lobal **W**arming **P**otential
IC	**I**ntegrated **C**ircuit
ICE	**I**nternal **C**ombustion **E**ngine
ICEV	**I**nternal **C**ombustion **E**ngine **V**ehicle
IGBT	**I**nsulated **G**ate **B**ipolar **T**ransistor
ISM	**I**ndustrial **S**cientific **M**edical
IWPT	**I**nductive **W**ireless **P**ower **T**ransmission
k	**C**oupling **F**actor
LED	**L**ight **E**mitting **D**iode
Li-ion	**L**ithium-ion
LoS	**L**ine of **S**ight
LPF	**L**ow **P**ass **F**ilter
MEMS	**M**icro-electromechanical **S**ystem
MC	**M**icro **C**ap
MOSFET	**M**etal **O**xide **F**ield **E**ffect **T**ransistor
MPE	**M**aximum **P**ermitted **E**mission
MRCWPT	**M**agnetic **R**esonance **C**apacitive **W**ireless **P**ower **T**ransfer
MWPT	**M**icrowave **W**ireless **P**ower **T**ransfer
NASA	**N**ational **A**eronautic **S**pace **A**dministration
Ni-Cd	**N**ickel **C**admium
NiMh	**N**ickel **M**etal **H**ydride
NMC	**L**ithium **N**ickel **C**obalt **M**anganese **O**xide

Pb-Acid	**L**ead **A**cid
PMA	**P**ower **M**atters **A**lliance
PRU	**P**ower **R**eceiving **U**nit
PTU	**P**ower **T**ransmitting **U**nit
R_X	**R**eceiver **C**oil
RF	**R**adio **F**requency
S	**S**ource **L**oop
SA	**S**pecific **A**bsorption
SC	**S**uper **C**apacitor
SCR	**S**ilicon **C**ontrolled **R**ectifier **D**iode
SCMR	**S**trongly **C**oupled **M**agnetic **R**esonance
SERT	**S**olar power **E**xploratory **R**esearch and **T**echnology
SPS	**S**olar **P**ower **S**atellite
T_X	**T**ransmitter **C**oil
TWT	**T**ravelling **W**ave **T**ube
UGV	**U**nmanned **G**round **V**ehicle
UK	**U**nited **K**ingdom
WP	**W**ireless **P**ower
WPC	**W**ireless **P**ower **C**onsortium
WPT	**W**ireless **P**ower **T**ransmission
WSN	**W**ireless **S**ensor **N**etwork
ZVS	**Z**ero **V**oltage **S**witching

Physical Constants

Speed of Light	$c_0 = 2.99792458e8\ m/s$
Relative Permeability	$\mu = 4\pi 10^{-}7\ H/m$
Wave Impedance	$\eta = 377$

List of Symbols

d	distance	m
R	power	Ω
P	power	W
U	voltage	V
I	current	A
f	frequency	Hz
t	time	s
Q	quality factor	
k	coupling factor	
B	flux density	Wb/m^2
H	electromagnetic field	T
L	inductance	L
C	capacitance	F
r	radius	m
S	scattering parameter	
Z	impedance	Ω
G	gain	
M	mutual inductance	
ω	angular frequency	rad
δ	angle	^{o}
η	efficiency	%

Chapter 1

Introduction

TRANSPORTATION plays a major role in day to day life where commuters spend the majority of their day stuck in traffic jams while travelling to their jobs in the cities. These traffic jams are caused due to yearly increase in the number of automobiles. According to a study in [1], approximately 70% of UK households owns at least one vehicle. In 2016, UK alone had more than 30 million registered cars that were driven on the roads. Vehicle licensing statistics indicate that, in 2016, around 3.3 million cars were registered for the first time and 42,000 vehicles were ultra-low emission vehicles (ULEVs) [2]. ULEVs can be defined as the vehicles that have less than $75g$ of carbon dioxide (CO_2) emission per kilometre and purchasing ULEV are further encouraged by eliminating the vehicle exercise duty (VED). As the emission standards surge, both new and conventional auto-makers anticipate in Electrical vehicle (EV) manufacturing, and thus investing in significant research efforts. Irrespective of the smaller percentage of EV on the road, considering the environmental aspect, Electrical vehicles (EV) are not just a greener, it is also an investment for the future being an eco-friendly material.

Over the conventional petrol cars, an EV offers health, ubiquity and a safety benefit. Charging cables are still used to connect the vehicles to the charging stations, which are not sustainable [3] in the long-term. One of the obvious advantages of Wireless power transmission (WPT) over wired transmission system is, its significantly lower cost of infrastructure maintenance. Thus, WPT is also the only feasible alternative to the bulky cables that are currently being used. WPT gained utmost popularity over the last two decades, due to its simplicity and functionality [4].

If we look back at history, we find that prior to Marconi's successful radio-wave transmission in 1902, only a handful of alternative solutions has been tested to fulfil the means of both energy and information transfer over long distances in attempt to eliminate the use of wires. During the late 19th century, both Nikola Tesla and Heinrich Hertz, had theorised the achievability of

wireless power transmission and Tesla's Wardenclyffe Tower experiment is among the list of widely spoken practical experiments by the scientific community. In contrast to Marconi, Tesla's method focusses on non-radiative technology which was adopted by Poynting and Lamor [5]. The main feature of Tesla's concept was based on Maxwell's proposition of non-radiative magnetic frenzies.

Near field transfer can be obtained via capacitive effect and mutually inductive coils. This transmission is then exhibited in a conventional transformer. Both mid and near field wireless systems have a distinct influence over far field technologies in a wide range of environments, including underground, underwater and in-body tissues. This thesis will investigate the efficiency of near field power delivery to charge electrical vehicles irrespective of the orientation and position of the transmitter and the receiver. In a nutshell, Tesla, Poynting and Larmor agreed on two fundamental facts, which have been listed as follows:

1. The earth acts as an acceptable conductor corridor, a charged shell which is a sustainable transmission medium [5].

2. A pathway to transfer electrical current between two distinct locations can be achieved via a suitable circuit to fulfil the requirements.

A breakthrough was made in 2007 by a group of scientists led by Professor Marin Soljacic of Massachusetts Institute of Technology (MIT), making Tesla's dormant vision, a reality. A 60 Watt bulb was light wirelessly at 8 feet distance via two larger copper coils which were tuned to resonate at the same frequency. Magnetic resonance phenomena, was initially proposed by Soljacic et. al [6], WPT has been implemented in a wide range of applications, ranging from household applications [7] to medical implants [8]. In the past few years, researchers have been working towards the implementation of WPT technology in the EVs [9, 10]. They have been able to develop a methodology to transmit power to the EV via inductive wireless power transmission (IWPT) [11] as well as capacitive wireless power transmission (CWPT) techniques [12]. Transmission efficiency has also been significantly improved over the passing years. Currently, the efficiency of the WPT system can reach up to 96%, however, it strongly depends on the transmitter and the receiver loop alignments [13].

It is also crucial to note the disadvantages of wireless charging while listing down the advantages. Upon the accuracy of the setting between the

charger and the receiver which is the vehicle, efficiency runs between 30%-80%. However, even with the most ideal setting power could be wasted. Wireless charging has come a long way that it has given endless possibilities to improve the entire EV industry.

1.1 Motivation

Since mid-2000s, when Marin Soljacic founded WiTricity after ultimately receiving the patent, company's business interest shifted from consumer electronics, mobile phone industry to exclusively on car chargers. The BMW-WiTricity partnership was able to release the first magnetic resonance based remote electric car charging system on the market, leading WiTricity to work together with the globes leading auto-manufactures to standardize the wireless car charging. Toyota adopted the wireless charging for Prius hybrid, eventually investing in the research while the rest of the Japanese auto manufacturers were working on prototypes. BMW 2018 530e iPerformance has gained potential market attention being able to charge a 9.2kWh battery in a couple of hours and under way to be released in Asia, Europe and US markets. However, the range is yet limited to 16miles at 90% efficiency, which is the highest level of efficiency so far been achieved via a WiTricity technology. Despite luxury, 530e iPerformance charging pad requires following the directions as given on infotainment manual limiting the receiver's degree of freedom. In contrast, Tesla model S comprises a battery which is approximately 100-75kWh and requires of being charged for 24 hours. Extraordinary competition among the auto makers has relentlessly accelerated, leaving the battery manufacturers enhance the battery sizes and techniques that are currently being used with rapid charging capabilities. Despite the fact that Resonance phenomena is not exclusively unique to electrical charging, energy transfer to take place, given the coinciding coil orientation which resonate at the same frequency. WiTricity system designs are based on conventional circular coils with a charging rate of 3.6-11kW [14] which is a potential charging mechanism for low capacity batteries. Given that a single charging pad being able to charge a wide range of vehicles between sports cars to SUV, charging facility can be integrated with a broad range of locations, making the technology prevalent in the years to come. WiTricity is not the standalone technology provider in the market as it appears, number of smaller manufactures such as Plugless Power and Qualcomm's Halo has emerged, adopting akin design with similar functionality to WiTricity with a different charging

infrastructure, known as dynamic charging. In contrast, dynamic charging offers a further level of freedom by allowing the EV to be charged while they are in motion. Particularly, given the number of the technology providers, products and brands, it is crucial to commercially establish the interoperability, which is a crucial stepping stone to the accelerated adoption. As a result, a draft of wireless charging standard (J2954) has been released, but yet to be closely developed over by standards organization SAE. While J2954 is being developed, a second-generation standard is already being worked on by Plugless which is already existing on the Tesla Model S in North America.

1.2 Research Aims and Objectives

The main aim of the research is to improve the performance of the WPT system by Increasing the distance between the resonators, decreasing the system dimensions, improving the spatial freedom and efficiencies. This research also aims to investigate the magnetic resonance base four-loop wireless power transmission system to facilitate a highly efficient and stable power transmission between the car and the charging panel.

- Literature review has been conducted by a tandem mathematical review, to get a thorough understanding of the short and mid-range wireless power phenomena, historical discoveries and current system limitations. Multiple system limitations will be addressed opposed to the system efficiency and the applicability within the applications which are yet to be advanced.

- Designing the system components may require a coalition of mathematical analysis, modelling, followed by the measurements. An investigation has been conducted using the free space as the transmission medium, given the conditions may vary upon the parameter which is to be enhanced. The goal is to yield a prototype model of the magnetic resonance wireless power system, which could transfer energy over the free space by magnetic resonance. Signal dynamics opposed to the system efficiency has been of greater interest.

- A prototype was built in response to the MATLAB based mathematical simulation and the mathematical behaviour, rendering in terms of Maxwell, Ohm and Faraday concepts. Theory of Maxwell and Faraday will be applied during the design of the physical model and initially

it will consist of two major segments: Receiver and the Transmitter. Experiments initially will begin placing the transmitter away from the receiver and crucial parameters such as the distance and receiver orientation will be varied to observe the efficiency variations.

- Later chapters of the thesis will emphasise how the overall system efficiency can be enhanced and discussed opposed to the experimental results obtained by the prototype built to converge the approach. Conclusions were driven based upon the results obtained by both the simulation and the built prototype.

1.3 Key Contribution

This research focusses on development of high performance models of a strongly coupled magnetic resonance (SCMR) system. Therefore, the main contributions of of this thesis are:

- Develop an optimal and cost effective SCMR for WPT charging of electric vehicle (EV), which satisfies the size and spatial freedom requirements.
- Develop various SCMR designs and examine their performance varying crucial parameters such as distance, coil dimensions and the geometry. The system was developed for wireless charging of hand-held electronic devices and EV charging as potential applications.
- Miniaturise the SCMR-WPT system for EV charging. Analysis SCMR geometrics to reduce the size and weight of the WPT system. The miniaturization will enhance the users comfort and enhance the travelling distance.
- Derive an analytical model of SCMR system. The effect of size, the distance and the frequency was formulated. The efficiency of the system is calculated using proposed analytical model as a function of geometrical and material parameters.
- Propose a novel method of WPT system design, using multiple inductors to improve the coupling between the coils.

It is believed that within the next few years there will be many thriving ubiquitous wireless power applications for hand-held and EV charging, with enhanced charging efficiency at minimum cost.

1.4 Thesis Organisation

The remaining part of this thesis is organised as follows. Chapter 2 provides a general background theory on the WPT and car charging. It covers a literature review of WPT, from long range to short range and its applications. This chapter also describes the basic mathematics of IWPT and offers an insight on the EV components. In Chapter 3, a four loop SCMR-WPT system is described and combined with conformal SCMR (CSCMR) system to offer more spatial freedom to the application. In this chapter rather than SCMR or CSCMR a combined system which consist of SCMR on the transmitter and CSCMR on the receiver side is used. The system is analysed with a mathematical model and the results are compared with the measured results. With this approach the power transmission can be achieved from a very short distances to a maximum distance, without adjusting the frequency. Chapter 4 demonstrates a inductor-capacitor-inductor (LCL) design of transmitter and receiver loop oscillation circuit. The design is mathematically described and simulated, the results are compared. The main advantage of this method is to reduce the size of the transmitter and receiver resonator, which reduce the weight of the vehicle. In Chapter 5, a novel approach of wireless car charging is proposed. The new method include sensors embedded in the parking place, which sense the car position. The method is described and simulated with the test circuit. With this new charging method, the maximum efficiency of a transmitter coil in a multicoil charger is determined mathematically based on the sensors feedback. This method increase the charging time and reduces losses. It can also sense any change in a car's position, which can increase losses.

1.5 List of Publications

1.5.1 Journal papers

1. Rozman, Matjaz, Michael Fernando, Bamidele Adebisi, Khaled M. Rabie, Tim Collins, Rupak Kharel, and Augustine Ikpehai. "A New Technique for Reducing Size of a WPT System Using Two-Loop Strongly-Resonant Inductors." *Energies* 10, no. 10 (2017): 1614.

2. Rozman Matjaz, Michael Fernando, Bamidele Adebisi, Khaled M. Rabie, Rupak Kharel, Augustine Ikpehai, and Haris Gacanin. "Combined

conformal strongly-coupled magnetic resonance for efficient wireless power transfer." *Energies* 10, no. 4 (2017): 498.

3. Matjaz Rozman, Augustine Ikpehai, Bamidele Adebisi, Khaled M. Rabie, Haris Gacanin and Helen Ji. "Smart Wireless Power Transmission System For Autonomous EV Charging." Access-2019-10457- IEEE access, DOI (identifier) 10.1109/ACCESS.2019.2912931.

1.5.2 Conference Papers

1. Rozman Matjaz, Khaled M. Rabie, and Bamidele Adebisi. "Wireless Power and Communication Transmission for Industrial Robots." In 2018 11th International Symposium on Communication Systems, Networks and Digital Signal Processing (CSNDSP), pp. 1-5., 2018.

2. Gheth Waled, Matjaz Rozman, Khaled M. Rabie, and Bamidele Adebisi. "Emc measurements in indoor power line communication environments." In International Telecommunications Conference, pp. 189-200. Springer, Singapore, 2019.

3. Rabie Khaled M., Bamidele Adebisi, and Matjaz Rozman. "Outage probability analysis of WPT systems with multiple-antenna access point" In 2016 10th International Symposium on Communication Systems, Networks and Digital Signal Processing (CSNDSP), pp. 1-5., 2016.

4. Rozman Matjaz, Augustine Ikpehai, Bamidele Adebisi, and Khaled M. Rabie. "Channel characterisation of cooperative relaying power line communication systems." In 2016 10th International Symposium on Communication Systems, Networks and Digital Signal Processing (CSNDSP), pp. 1-5., 2016.

Chapter 2

Background Theory

THIS chapter provides a review of EVs, inductive charging and current WPT technologies. The history of wireless power, the elementary phase of research that began during the early 18^{th} century and the most recent development in the field are presented in Section 2.1. This discussion is further backed up with various existing WPT techniques that are prominently in use, including the far and near-field techniques and, most certainly, a careful comparison between their advantages and the limitations. This chapter also outlines, a considerable amount of theoretical background which are based on areas where WPT applications are already in use. WPT has entered the mainstream with few impressive demonstrations despite the gaps between exhibiting the technology viability and commercialisation, this will shape the future of consumer electronics. Although that it is exciting to know what the future holds for the widespread adoption of wireless charging, yet the health and safety aspects of the applications cannot be neglected. Health and safety standards are presented followed by more detailed presentation of IWPT in Section 2.2, where the basic descriptions are presented. The EV, its basic design and charging are presented in Section 2.3. This section covers EV design, battery and the charging system. The main challenges and limitations are discussed in Section 2.4 followed by Section 2.5, which explains the methodology of the thesis. The conclusion of Chapter 2 is drown in Section 2.6.

2.1 Wireless Power Transmission

2.1.1 The History of Wireless Power Transmission

In this section an overview of the history of WPT is presented. The first reported experiment on WPT dates back to 1819. It was Danish physicist and chemist H.C. Oersted [15]. He discovered that the electric current, which

flows through the electric wire, generates a magnetic field around the conductor. Ampere's Force Law, Biot-Savart's Law following Faraday's Law of electromagnetic induction were later established, based on Oersted's fundamental discovery, underlining the connection between magnetism and electric current.

In 1864, J.C. Maxwell detailed how magnetic and electric field are generated and affected by each other and mathematically defined them via Maxwell's equations forming the foundation of classical electromagnetism. Later in 1873 his electricity and magnetism theory along with his other research efforts during his time in Cambridge, was unified into a publication "A Treatise on Electricity and Magnetism" [16]. His study concluded that electricity and magnetism are regulated by the same force.

In 1888, a German scientist H.R. Hertz, successfully used a pair of oscillators to transfer electrical power through a small gap between the coils, during his landmark research analysing Maxwell's equations [17]. This experiment was a breakthrough being the first ever practical observation of the existence of the electromagnetic radiation confirming Maxwell's predictions. A series of experiments based on electromagnetic radiation, were further conducted by his rival, Croatian-born American researcher Nikola Tesla spending great deal of time and capital. The primary focus of Tesla's study was to develop a technique that transfers electrical energy over a large distance, eliminating electrical wires. In 1893, he was able to successfully transmit high frequency current over a short distance using a single wire as a conductor [18]. This was followed by another breakthrough in 1899, when he transmitted 108V of high-frequency electric power to turn on Geissler tubes across the stage [19].

During Tesla's wireless transmission of electricity based research, he developed a "Tesla Coil" with an air gap between the coils, which was a great contribution towards the promotion of electromagnetic field. In 1901, Tesla's completed his famous Wardenclyffe Tower, which was designed with the intention to transmit electricity through the ionosphere over a large distance. However, the project was later shut down due to low efficiency, hazardous concerns and a lack of funding caused by a breakthrough made by an Italian researcher, Marconi, who was able to successfully transmit a radio signal across the Atlantic Ocean [20].

The early invention of magnetron was designed by H. Gerdien in 1910, whilst many reassembling devices were designed from the 1920s to 1930s. However, even though the design converts electricity into microwave which allows the energy to be transmitted over a long distance, the conversion of

the microwave back to electricity was considered a major design limitation. In 1964, W.C. Brown, who specialised in the magnetron principle, proposed WPT via microwave during a demonstration during which he also discovered a methodology that converts the incident microwaves back into DC power via a rectenna [21].

Since the development of rectenna, a numerous attempts have been made to achieve high power transmission over a long distance. The experiments were carried out mostly performed by Canadian and Japanese research institutes [22]. As the research on WPT evolved, Brown, in 1975, successfully transmitted a $30kW$ of power over a 1 mile distance with an efficiency of 84% using microwaves [23]. However, the research was discontinued due to the emergence of solar power satellites (SPS), which were firstly described in 1968 [24]. The main concept of SPS is to place a large geostationary satellites in Earth's orbit to collect energy from the sunlight and transmit it to the Earth using microwaves. At the same time, a coupling based electromagnetic transmission was introduced for a low power appliances. The technique was implemented in an implantable medical device [25].

A larger number of trendy portable electronics emerged during the late 1990 at an affordable price, due to the development of semiconductors led to far better and cheaper consumer electronics, after having competed primarily through performance which was measured by the energy consumption at the time. All approaches were pretty fruitless where the devices actually did not have a permanent power source and therefore a power source such as a battery was required. The battery offers a limited power source with shorter life time, hence the necessity for a low power inductive based wireless power transfer was raised [26]. However, during 2007, a new phenomenon of non-radiative mid-range WPT, was experimentally demonstrated by Kurs et al [6] using self resonant strongly coupled coils. The rapid proliferation of WPT techniques provides an ample growth opportunity to the consumer electronics market offering the consumer convenience, enhanced user experience due to the reduced size with higher efficiency.

Short-range wireless power technology is considerably established with the upsurge on demand for domestic and industrial applications, mid- range wireless power research has been gathering momentum in the last decade. With the surged interest of short to mid range WPT, the necessity of an implementation of an international standard has emerged. Today they are three different standards which have been implemented in the market. Most widely used is Qi standard introduced by Wireless Power Consortium (WPC) [27].

The standard is used for up to 10W (5V, 2A) of power WPT charging using 115 to 300kHz frequency band. However Qi standard is not the only one on the market. Power Matters Alliance (PMA) and Alliance for Wireless Power (A4WP) also have their own standard and uses 87 to 357kHz and 6.78MHz frequency band for power transmission respectively [28].

2.1.2 Wireless Power Transmission Techniques

WPT techniques can be classified into two main categories: radiative (far field) and non-radiative (near field) techniques. The main difference between the two is that the non-radiative techniques are coupling-based while the radiative are radio frequency (RF)-based, as shown in Fig. 2.1 .

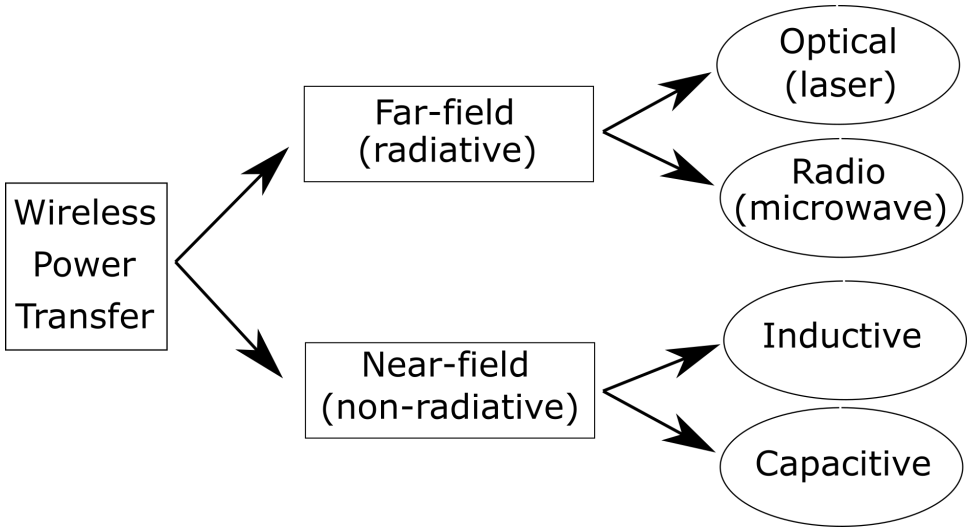

FIGURE 2.1: WPT techniques.

Fig. 2.1 also shows that both far- and near-field wireless power techniques can be further divided into two independent sub-techniques. While using far-field techniques, power can be transferred as an optical beam or as a radio frequency wave. In a near-field range, power can be transmitted via electromagnetic induction or via a capacitive charge.

2.1.3 Non-radiative WPT

2.1.3.1 Inductive Coupling

Inductive wireless power transfer (IWPT) is a near-field technique, which is based on electromagnetic field induction, as shown in Fig. 2.2. The electromagnetic field of the primary coil induces the electrical energy to the secondary coil. The received energy is then used to charge the device directly

or to store the energy in the battery. The operating frequency of the inductive WPT is typically measured in the 80-300kHz range. The secondary coil is usually tuned at the transmitting frequency to enhance the transmission distance, which is usually within 20cm. The quality factor of the coils is usually small because the transferred power attenuates quickly if the coils have a high-quality factor [29, 30, 31]. High efficiency can be achieved at a short distance, usually less than the coil's diameter.

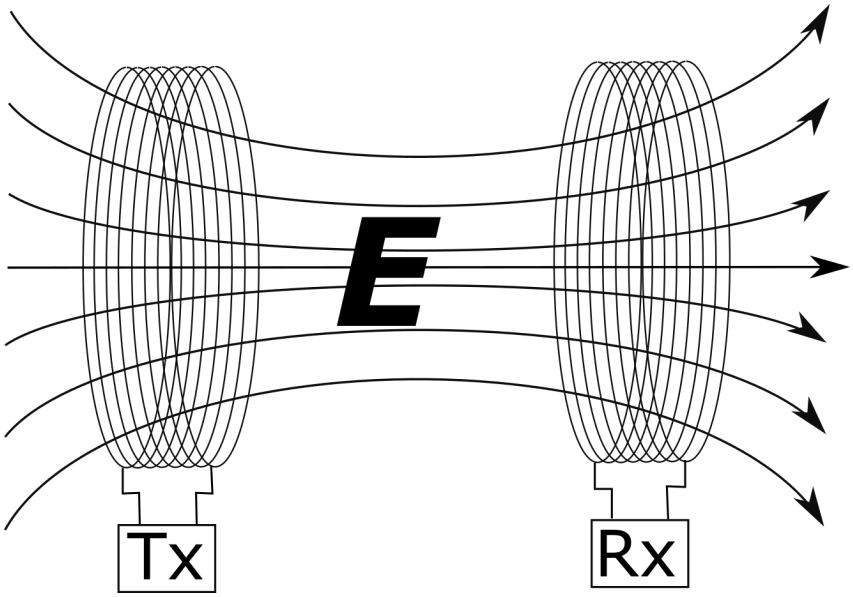

FIGURE 2.2: High-level diagram of inductive wireless power transfer system.

Advantages and disadvantages

The main advantage of using IWPT for charging is that it eliminates the use of bulky wires. Moreover, the IWPT offers a more convenient method of charging without using wires [32]. IWPT is also easy to use one can simply plug the charging pad into the power supply and attach the transmitter to the device [33, 34]. However, nowadays, many of the new devices already have an inbuilt wireless power (WP) receiver. In many cases, IWPT is considered a safer alternative to conventional charging [33], as it allows the device to be fully isolated from the outside environment [35]. With its increasing efficiency, IWPT charging has gained popularity among costumers; however, its overall efficiency is highly influenced by the misalignment between the two coils and the distance between the two. Applications using IWPT include mobile devices, cordless toothbrushes, medical implants, fitness bonds and EV chargers.

2.1.3.2 Capacitive Coupling

Capacitive wireless power transfer (CWPT) is an alternative technology that has been highly researched in recent years due to its low-cost capacitive interfaces and simplicity [36]. Both IWPT and CWPT are prevalent methods that function over a short range. However, IWPT has been most frequently used to function at various power loads and several meter ranges while CWPT uses electric field coupling, which is sustainable in kW level applications and lower electromagnetic interference with its reduced size, making it a highly feasible charging solution for battery-powered devices [37]. Based on CWPT's principle, both the transmitter and receiver are formed with a pair of parallel conductive plates. A supply current charges the plates at the transmitter's end while the plates on the receiving end are charged with the opposite polarity of the transmitter's end. Thus, the voltage on the secondary side is generated between the plates. However, existing CWPT applications have the same limitations as regular capacitors where the coupling capacitance is restricted by the available area, as is the air gap between the conductors [36]. Additionally, the medium between the plates also has a considerable effect on the capacitance. The principle circuit is presented in Fig. 2.3.

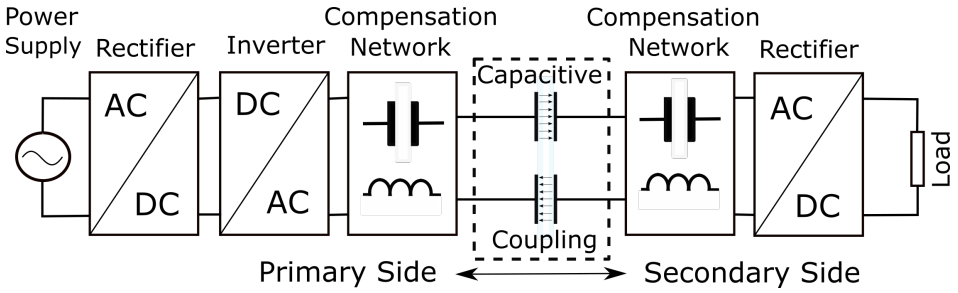

FIGURE 2.3: Principal circuit diagram of capacitive wireless power transfer system.

Advantages and Disadvantages

One of the main advantages of using CWPT over IWPT is that the losses caused by eddy current are negligible [38]. In CWPT, an inductive coil is not required to transmit power; therefore, the losses caused by eddy current only appears on the wires connecting the inverter and charging plates. The

operating frequency at which the power is transmitted between the transmitter and receiver plates is considerably lower than the operating frequency of an IWPT system [39]. Higher charging efficiencies can be achieved by adding inductors that alter the operating frequency and duty cycle to accommodate higher capacitance. Like every other commercial application, CWPT-based applications are expected to facilitate higher power. Given the fact that CWPT systems are made of metal and requires a larger coupling area to facilitate high power, the system design of the cost of applications is no exception. In a nutshell, unlike designing and assembling coils into a product, manufacturing plates of any shape, which are made of a conductive material, is cost efficient. CWPT systems are highly influenced by misalignment [39] where the alignment variations may result in capacitance variants. As the capacitor plates are also used to determine the oscillating frequency, a compensation network with a feedback loop may be required to compensate for the variation in capacitance caused by misalignment [38]. Applications of CWPT include EV charging, low-power integrated circuits (IC), biomedical devices, light emitting diode (LED) lights and mobile device chargers.

2.1.3.3 Magnetic Resonance Coupling

Magnetic resonance coupling transfers the electrical energy via electromagnetic induction between the two resonant coils through an oscillating magnetic field. In contrast, two coils which resonate at the same frequency, are strongly coupled and therefore a high efficiency of power transfer can be achieved, unlike the IWPT system efficiency which is highly dependent on the distance. Resonance phenomena only occur if the excitation frequency and the natural frequency of the receiver frequency harmonise together, thus the frequencies are usually in the range of megahertz [39, 40]. In fact, it is crucial to choose the appropriate resonant frequency to match the size of the coil. Furthermore, both coils oscillate at their maximum amplitude tunnelling the maximum power at maximum efficiency. The quality factor (Q) of the primary and secondary coil, is habitually high enabling efficient energy transfer at lower system's coupling coefficient [41]. A magnetic resonance coupled WPT (MRCWPT) can reach the distance of a few centimetres to 1 meter [41], and could simply be up to ten times the diameter of the transmitter. MRCWPT also forms a user-friendly charging platform where multiple devices could be charged simultaneously being in the vicinity by tuning multiple coupled resonators of receiving coils [42]. Additionally, this also includes

devices of variable sizes and power levels in parallel. AirFuel offers commercial applications that operate at $6.78MHz$. As shown in Fig. 2.4, the main element of the MRCWPT system are coupling capacitors. The coupling capacitors tune the transmitters and the receivers LC circuit, to achieve maximum efficiency of the transmission. Precise tuning of the resonators is vital to maintain constant high efficiency of the system upon air gap variations and to mitigate the influence of frequency splitting [42]. This technique is addressed as frequency tuning in literature and one of the techniques commonly employed in magnetic resonance based systems. Moreover, frequency tuning is not necessarily limited to the frequency range within ISM band.

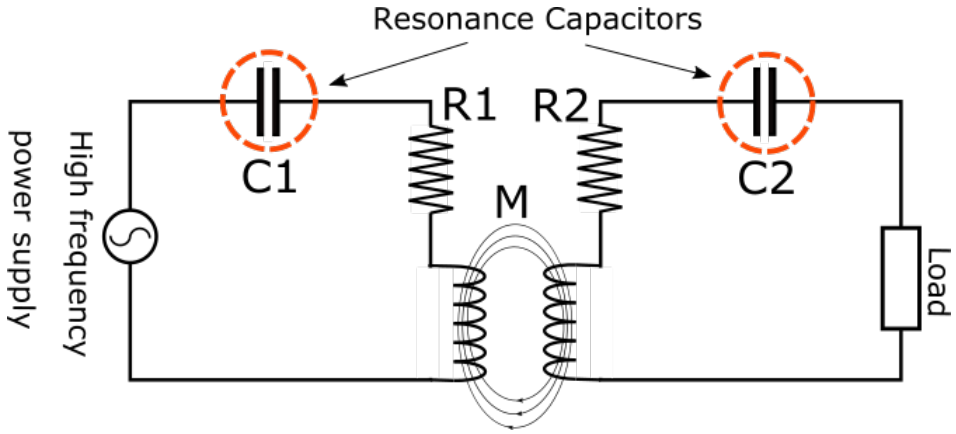

FIGURE 2.4: Circuit diagram of strongly coupled magnetic resonant WPT design with two resonant capacitors.

Advantages and Disadvantages:

Resonance approach is often contrasted with the induction phenomena for range of features. Both the IWPT and MRCWPT systems are pretty straightforward to implement [43]. However, in contrast MRCWPT operates at the high frequency end of the spectrum with enhanced efficiency [43] compared to IWPT. Safety is a common concern of any newly emerged technology. Resonance approach offers safety feature than the conventional cable connection, especially in industrial applications where the cables are exposed to various risks [44]. Despite the convenience of using MRCWPT, the size of the system is another important factor. High inductance of the coils, is required to achieve high efficiency, and may increase the weight of the system as a whole [45]. In order to achieve resonance between the transmitter and receiver, the capacitors included in the circuitry are simultaneously required to be of low tolerance being able to compensate the variable mutual inductance between the coils, the compensation circuit is required, to maintain optimum efficiency during the transmission [46]. The main applications of MRIWPT

includes household applications, medical implants and EV charging.

2.1.4 Radiative WPT

Radiative WPT is a far field wireless transmission technique which is used for power transmission over larger distances such as dozens of kilometres. Radiative approach uses electromagnetic (EM) waves which are at the high frequency end of the spectrum, such as microwave, infra-red or X-ray. A typical frequency band of radiative WPT is between 300MHz and 1000GHz. The energy is radiated anisotropically, which simply defines that the energy being transmitted towards one direction which is highly preferable for both broadcasting purposes and also for the applications which require line of sight (LoS), mitigating the power losses due to diffraction and atmospheric absorption. Directive beam forming technique is used for power transmission purposes where the directional signal transmission or reception which can be used in in both T_X and R_X, since it considerably helps to improve the efficiency [47].

2.1.4.1 Microwaves

Microwave wireless power transfer (MWPT) is considered as the most efficient far field technique which is capable of transmitting power over multiple *km* range, via microwave radiation. Initial microwave WPT was deployed in 1858 at Raytheon. With considerably smaller wavelength, circuits associated with the wave propagation such as microstrip lines, hollow waveguides coaxial lines, etc. could be scattered, therefore, the transmission distances can be larger [48]. MWPT system converts direct current (DC) in to microwaves using a microwave generator, which are then passed through a coax to the wave-guide adapter in order to isolate the wave generator to avoid detuning the selected frequency [49]. Tuner and the directional coupler are used to distinguish the waves as per the propagation directions which are then transmitted directly from the transmitting antenna which are targeted towards the receiver antenna. Upon the receipt of the signal it is then passed through low pass filter (LPF) and received microwave power is converted back into electrical energy. Monitoring is most commonly used to produce microwaves due to the lesser costs and efficiently regardless of the two types of microwave generators are available in the market, Klystron and Travelling Wave Tube (TWT). Both Klystron and TWT are extremely costly, yet TWT with limited power, making it not widely adopted for wireless power

generation purposes. Even though 2.45GHz is practically proven to be the highest efficient frequency with efficiency over 95% to be used in MWPT [50] 5.8GHz, 8.5GHz, 10GHz and 35GHz are also used with reasonable efficiencies for MWPT. Moreover, MWPT efficiency strongly depends on the microwave generator and the rectenna that is used to transmit the power from the source to target.

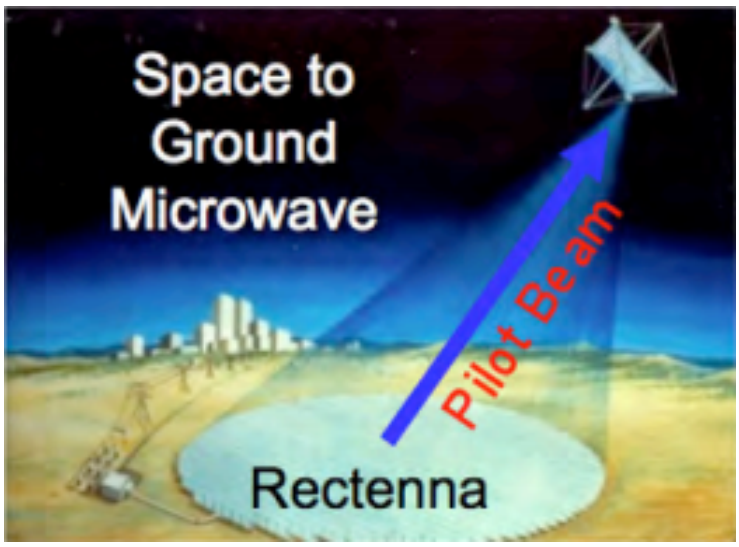

FIGURE 2.5: Satellite placed in the Earth orbit collects the solar power and transmitts it on the earth using microwaves [51].

Advantages and Disadvantages

The MWPT is used to transmit the energy on large distances. However, to enable the transmission the transmitter must be in a clear line of sight with the receiver [52]. The direction of the transmitter focus must be on the receiver at any time of the transmission [52]. The main concern of using microwaves is safety, since the microwaves represents a serious treat to the human body [53]. The main applications of microwave WPT are the unmanned ground vehicle (UGV), used for space missions, and solar power satellites (SPS).

2.1.4.2 Laser

WPT using a laser beam (laser power beaming) is a technique, which is highly researched due to the nature of the intended military applications and space application which could be highly beneficial. Prior to the transmission, electrical current is converted into high density light and transferred by pointing a light beam to a high efficiency photovoltaic cell, which act as

a receiver. Upon the reception of the light, energy is converted back into electricity. Laser energy transmission takes advantage of the atmospheric transparency window in the visible or near infra-red frequency spectrum [54]. Moreover, Laser WPT systems demonstrate 50% system efficiency.

Until recently, few actual experiments have been carried out using laser beams for power transmission. Researchers in [55] demonstrated a laser based ground to ground WPT. The ground-based laser transmits the power to a ground-based vehicle. However, the future goal is to transmit the power collected by satellites via laser beam to the UGV, as seen in Fig. 2.6.

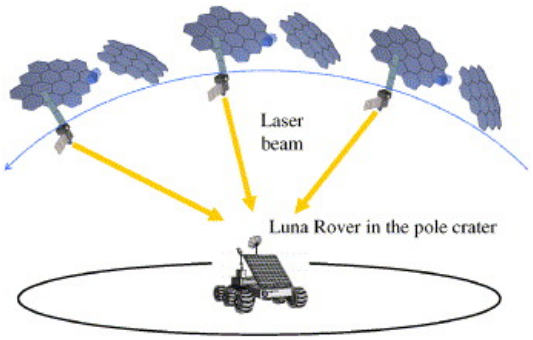

FIGURE 2.6: Lunar rover powered by laser beam from satellite [56].

Advantages and Limitations:

Similar to the microwaves, laser based WPT requires a LoS between the transmitter and the receiver [55, 57]. The efficiency of the power transmission is also typically low, which is between 40-50%. Light beams are highly influenced by atmospheric absorption [57] and therefore, in some cases whole transmitted power can be absorbed by the atmosphere before it reaches the receiver [57]. The above phenomenon is also known as transmission attenuation where the power decreases, depending on the transmission distance and air quality. The use of laser beam for power transmission can also cause a serious damage to the humans. The laser can cause blindness, burns or even kills. The main applications which uses laser WPT for its operations are Satellites, UGVs and direct energy weapon (DEW).

2.1.5 Applications of WPT applications

WPT based applications are widely used in numerous industries.

2.1.5.1 Industrial

Industrial application designers have just begun to see through the virtue of using wireless power. Portable hand-held equipment and static industrial applications in use, often operate in harsh environment. For instance, exposure to stress, dirt, oil, acid and even the slight moisture may cause damage to the conventional wires or power leads used to provide power and may also reduce the number of the potential risks to the human factor [33]. Simultaneously having no additional maintenance costs with no tethered machinery or corrosive plugs, customer service, speed and accuracy may get significantly improved. Applications such as industrial robots with higher special freedom often replace the human workforce in a hazardous environment [58]. For the robots to operate, at intended maximum speed for a maximum amount of time, charging pads have to be installed. The robot will have to return to a nearest charging pad every time the low battery power is detected in order to get recharged [58]. WPT charging pads simultaneously minimise the human intervention with the robots and therefore it also reduces risk of injury at work place. Factory environment is also a big market place for sensors manufacturers, where every manufacturing site tends to monitor their workplace environment and multiple different aspects. The sensors are usually placed in the hardly accessible areas such as rooftops, high temperature ovens or the wall embedded fire monitoring sensors [59]. The WPT charging is the most convenient solution to be implemented.

2.1.5.2 Automotive

With a maturing technology which has already widespread among multiple industries starting with consumer electronics to EV, there are certain advancements in automotive market. For instance, apart from advance features such as driver-less operation, the automotive industry is also shifting from using fossil-fuel [60]. Number of hybrid and EV in use have been increased and developed to minimise the carbon emission caused by the transportation [61]. However, EVs require additional battery as a power source [60]. As a solution, battery manufacturers are investing their time in improving the chemistry of the Lithium batteries, eliminating toxic metal having a lighter structure. Hence the 74% of the EV battery prices drifted, which was considered as a costly option by the manufacturers. However, lighter battery will also improve the overall system efficiency of the EV which will be lighter. Portability and functionality of EVs has been improved by introduction of

WPT charging into the automotive market [62]. A battery of an average EV, may take between 4 to 8 hours, depending on its capacity and the speed of the charging pad. The researchers in [63] have proposed an electric powered highway system, where vehicles receive electrical energy while being driven. This will significantly increase the range of the vehicle without interruptions, saving both time and cost. Extensively discussed electric cars are not the sole beneficiaries of WPT technology, smaller transportation vehicles such as electric bikes, electric four wheelers, heavy vehicles and also electric levitation trains are good examples of the WPT technology based applications used today.

2.1.5.3 Aerospace

The concept of placing SPS system in space was proposed in late 1970s [24]. More recently a new system was proposed by National Aeronautic and Space Administration (NASA) proving that WPT functions flawlessly $1km$ above the ground. NASA launched space solar power exploratory research and technology (SERT) program to be combined with WPT for commercial markets. A solar satellite will be used to collect the energy from the Sun and distribute the collected energy to the other receiving satellites which are stationed miles away or to the Earth via microwaves or laser beam [64]. Satellites are not the only one which WPT was proposed as a possible charging solution. Wireless sensor networks (WSN) are mainly powered by batteries [65], which significantly limit the time that the network is awake. The limitation with stored energy can be partially solved by harvesting energy [66], which increases the working time. However, in order to maximize the time that the WSN is awake, a WPT charging was proposed in [65, 67].

2.1.5.4 Consumer Electronics

Present day consumer electronics have a massive impact on both day to day professional and personal lives. Especially portable electronic devices such as mobile phones, laptops, smart watches, etc. have revolutionized the human life. However, it is also important to note that each portable device requires a battery for its functionality. The use of a battery, has a significant negative impact on the environment [68]. The implementation of WPT charging may not only reduce the size of the required battery but in some cases may also eliminate the batteries completely. Although both the capacitive and

inductive techniques can be used to charge the devices, the capacitive charging require relatively large charging area [69], or an extremely high charging frequency [69, 70]. Alternatively IWPT technique is extensively used for charging electric toothbrushes [71], charging pads for mobile phones [72] and sensors [73]. IWPT can also be implemented to charge even higher power electronics, such as TV [74], projectors [75] and heaters [76].

2.1.5.5 Medicine

Implementation of WPT into medical devices have grown rapidly over the last decade. The applications, such as battery-less wireless gastric implants [77], medical endoscopes [78] and gastrointestinal robots [79], can benefit from the advantages of implementing the WPT technology instead of conventional wires. Applications using WPT offers safer and cost effective alternative solutions while increasing mobility and utmost customer satisfaction [80]. Micro-electromechanical system (MEMS) plays an important role in medicine industry where MEMS are used for measuring pressure gradient across the heart valves in order to prevent heart diseases [80]. However, there are key challenges such as wireless signal attenuation and negative impact on surrounding tissue, which have significantly hindered the research. It is highlighted that wirelessly powered medical applications would also communicate data to the monitoring system for diagnosis, facilitating accessibility and personalised treatments [81].

2.1.5.6 Naval

Underwater vehicles and robots are often used in a various applications, varying from monitoring to mine detection [82, 83]. The vast majority of those applications are battery powered hence regular recharging or charging facility in the vicinity would be highly beneficial due to numerous facts. With the conventional approach, charging via a plug in cable, vehicle or robot have to be evacuated from the water during the recharging period, which might also interrupt the research work or data which is to be gathered. The robot is prevented from working and is out of order for a whole charging process. In order to reduce standby time due recharging period, the researcher in [84] and [85], proposed underwater WPT charging method as it would allow the robot to be used while being charged. However, as researchers in [86] pointed out, that the efficiency of underwater charging such as seawater, drops significantly if the WPT operates on a frequency above $20kHz$.

2.1.6 WPT Standards and Regulations

2.1.6.1 Qi Charging Standards

Qi is an open wireless charging standard founded by Wireless Power Consortium (WPC), built cooperatively by a collaboration of the world's largest manufacturers from a wide range of industries [26]. 8 leading companies attended the WPC inaugural meeting in December 2008 and the current member pool is 634 companies with 2565 electronic products. The initial Qi specification was published in mid-2010. Company mission, Qi being the most widely adopted global standard to build a future with no cables, WPC is constantly liaising with standard bodies and government agencies, helping to understand the potential of the wireless power phenomenon.

Its aim is to specify simple, efficient and safer WPT and data communication between a Qi charger and an array of charging device. It also offers the compatibility and flexibility between products manufactured by multiple manufacturers by entirely not having the customised wireless charging pads to be designed. Qi is a blend of both induction and resonance technologies, hence chargers' compliance with Qi standard is able to regulate transmitted power accordingly to the demands of the charging device. Based on power requirement, Qi standard can be divided into two sections, low power and medium power. Furthermore, Qi for low power supports up to 5W of power to be transmitted on a frequency, ranging from 110 to 205kHz, while Qi for medium power supporting fast charging with 120W on a frequency that ranges from 80- 300kHz [87]. The frequency band is mutually used for both power transfer and data communication between the charger and charged device. The communication protocol is the key to interoperability, which defines the functions that enhances the efficiency of the system. For instance, the standard defines the functions that detects the presence of an object placed on the charging pad and if it is a Qi compliant object, control of the power output when its idle and finish charging when the device is fully charged. Qi standard also provides guidelines for three potential approaches to achieve alignment, the guided positioning is to be achieved via magnetic attraction, free positioning by moving coil and free positioning by coil arrow.

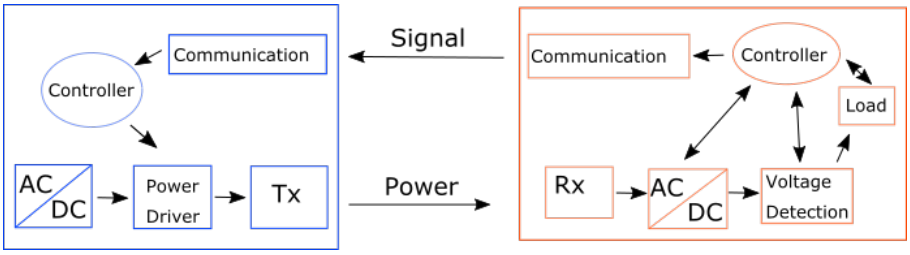

FIGURE 2.7: The diagram of Qi WPT charging system.

Guided Positioning by Magnetic Attraction

The charging pad consists of a single transmitting coil which is in a fixed position inside the charger. Furthermore, the charger and the devices consist of magnetic core with opposite poles. Once a device is placed on the charging pad, the magnetic core placed inside the transmitter and receiver forms a magnetic force. The formed magnetic force attracts the charged device on the fixed position right above the transmitting coil, where the flux density is maximum, and the charging is maximised.

Free Positioning by Moving Coil

The charging pad consists of a mechanically movable charging coil which is simple yet cost effective. The coil can determine the object's position, moving on X and Y axis. Chargers with above dynamics, has been implemented by using a motor mechanism, which moves the coil and monitor the feedback from the receiver. In a nutshell primary coil is able to tune the position to either via inductive or capacitive coupling. However, a system with mechanical components is less reliable and durable and prone to malfunction.

Free Positioning by Coil Arrow

The charging pad is capable of charging multiple devices simultaneously regardless of their position. In this scenario charger pad consists of multiple charging coils and the WPT will be taken place regardless of the orientation of the secondary coil. When the device is placed on the charging pad, the charger begins to send a power to the receiver coil while monitoring the feedback from the receiver. After the power transmitted by each coil is measured, the coil with the maximum efficiency will begin to charge the device. In contrast Free positioning is more user friendly, but costly due to the complex winding structure with advance control elements [88].

2.1.6.2 Rezence Charging Standards

Rezence WPT standard was introduced in 2012 by Alliance for Wireless Power (A4WP), which was later renamed to Air-Fuel Alliance due to merge with Power Matters Alliance. The standard proposes magnetic resonance coupling via large electromagnetic field. The devices can be placed up to several meters away from a charger without alignment restrictions. The system consists power transmitting unit (PTU) and power receiving unit (PRU) as shown in Fig. 2.8, where the power transmission is controlled by charging management protocol. Rezance standard transmits the power on $6.78MHz$ band also called Industrial Scientific Medical (ISM), while the communication signal is transmitted on the $2.4GHz$ frequency band. The protocol for communication between transmitter and receiver is also specified by the standard, which is realised by Bluetooth Low Energy (BLE) link.

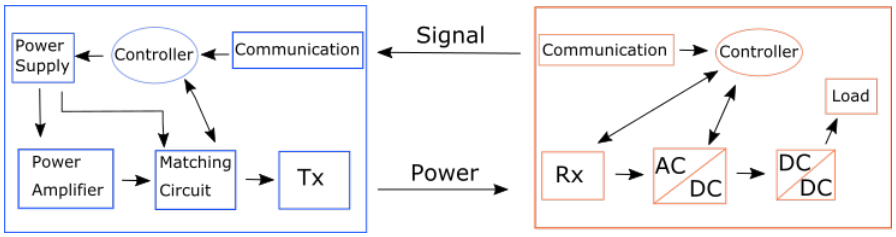

FIGURE 2.8: The diagram of Rezance WPT charging system.

The PTU unit consist of three units, LC resonator with matching circuit, inverter and control circuit. PRU unit consists of a control circuit and a power conversion circuit. The transmitter unit, initially detects the device by constantly sending advertisement and wait on respond. The receiver responds by sending connection request to the transmitter. After the connection request is received the PTU unit stops sending advertisements signal and the two units exchange their static and dynamic parameters. After the information exchange the PTU unit starts to transmit the power to the receiver. The receiver constantly update the PTU with its dynamic parameters in order to enable PTU unit to adjust power transfer based on demands.

2.1.7 Health and Safety Regulations

In order to protect humans against harmful effect of electromagnetic radiation the maximum allowed values of exposure are described in IEEE Standard for safety levels with respect to human exposure to radio frequency electromagnetic field, $3kHz$ to $300GHz$ [89]. The standard was introduced by IEEE International Committee on Electromagnetic Safety, and approved by

IEEE-SA Standards board in 2005. Its purpose is to protect and prevent the permanent damage caused by exposure to the RF electric, magnetic and electromagnetic fields over the frequency range of $3kHz$ to $300GHz$. An average exposure power (AEP) can be calculated as:

$$\overline{AEP} = \frac{1}{t_2 - t_1} \int_{t_1}^{t_2} P(t)dt \tag{2.1}$$

where $P(t)$ is instantaneous power, t_1 and t_2 represents the starting and ending time of exposure respectively. The AEP is calculated in watt (W).

Plane wave power density (S) is a commonly used term in electromagnetic wave radiation. Power density of the electromagnetic field can be calculated as:

$$S = \frac{|E|^2}{\eta} = \eta |H|^2 \tag{2.2}$$

where E and H are the root means square (rms) of the electric and electromagnetic field respectively, η represents the wave impedance ($\eta = 377$ in free space).

Specific absorption (SA) represents the quotient of the increment energy ($\triangle W$) absorbed by and incremental mass ($\triangle m$) contained in a volume ($\triangle V$) of a given density (ρ).

$$SA = \frac{\triangle W}{\triangle m} = \frac{\triangle W}{\triangle \rho \triangle V} \tag{2.3}$$

SA is calculated in watt per kilogram (W/kg).

The MPE exposure level can be divided into two sections. To the MPE level in the controlled environment, such as industrial and hospitals where emergency services and monitoring is well established and the time of the exposure is limited. The limits for this environment are higher, and can be seen in Fig. 2.9. MPE limits for living environment, where the humans are daily exposed are presented in Fig. 2.10. These limits represents a maximum allowed limits to which humans can be exposed in in-home or nature environment. All consumer electronics and kitchen appliances must be compliant with the limits, and tested before sold in the market.

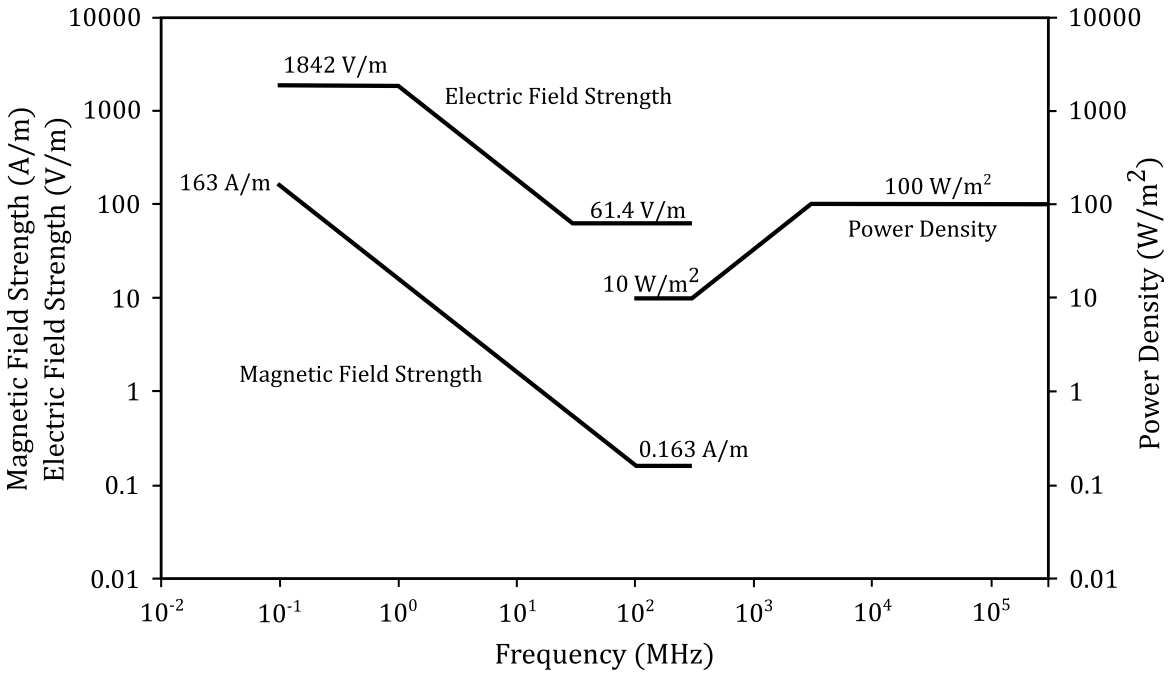

FIGURE 2.9: MPE limits in controlled environment where usual exposure time is relatively short [89].

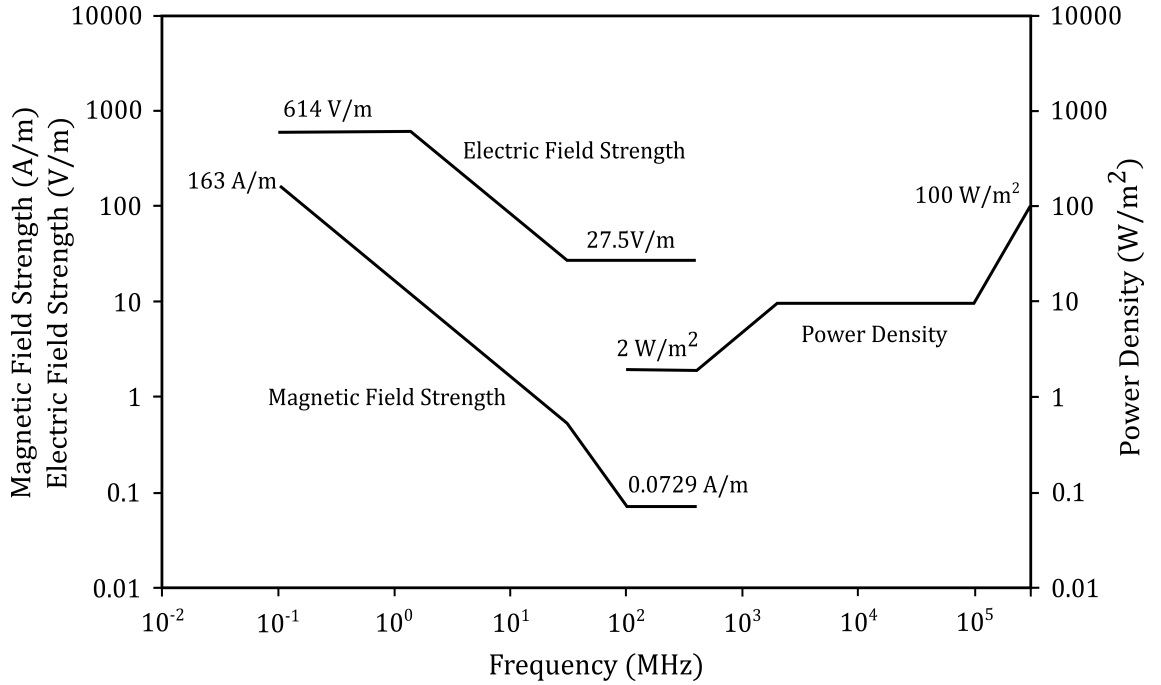

FIGURE 2.10: Daily MPE exposure limits, for the living environment [89].

2.2 Inductive Wireless Power Transmission

Energy transfer through electromagnetic induction is simply known as inductive wireless power transfer.

2.2.1 Principle of IWPT

Fundamental speculations of WPT are disciplined by Faraday Law and Ampere's Law. Fig. 2.11 exhibits the basic overview of the WPT phenomenon where the current (I) which flows through the conductor, generates a magnetic field (H) surrounding the conductor as per Ampere's Law. The secondary conductor and the primary conductor are linked by the magnetic field that is created, inducing a voltage (V), as briefed by Faraday's Law. In a nutshell, Ampere's Law defines the current which flows through the coil, is equivalent to the line integral of the magnetic field intensity around the closed loop:

$$\oint \vec{H}.\vec{dl} = I \tag{2.4}$$

The voltage induced in the secondary coil can be explained by the Faraday Law as:

$$V = -N_2 \frac{d\Phi}{dt} \tag{2.5}$$

N_2 and Φ indicate the number of turns of the secondary coil and the electric flux, respectively. The negative voltage induced in the secondary coil can be expressed by Lenz Law, which states that the induced electromagnetic force in the primary coil opposes the direction that the resulted current in secondary coil flows. An induced electromagnetic force (EMF) always gives rise to a current whose H opposes the change in original magnetic flux.

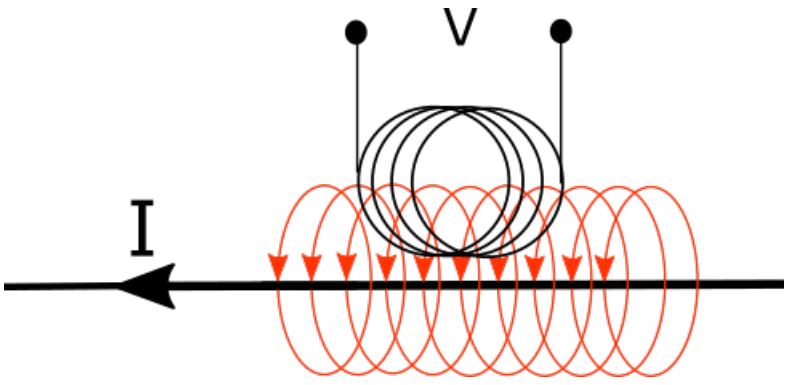

FIGURE 2.11: WPT fundamentals.

2.2.2 Magnetic Resonance and Quality Factor

Resonance is a major role in a strongly coupled WPT. To enable a good link between the transmitter and receiver, the frequency of the two have to be close match. The more precise the tuning, the lower is the coupling factor at which the system reaches it maximum efficiency. In Fig. 2.12 the series connected LC circuits is presented with parasitic resistance R. The resonance of the circuit occurs when the energy stored in the capacitor is transferred to the inductor and vice versa. The frequency of the oscillation can be calculated as

$$f_0 = \frac{\omega_0}{2\pi} \tag{2.6}$$

where ω_0 is the angular frequency and can be expressed as

$$\omega_0 = \frac{1}{\sqrt{LC}} \tag{2.7}$$

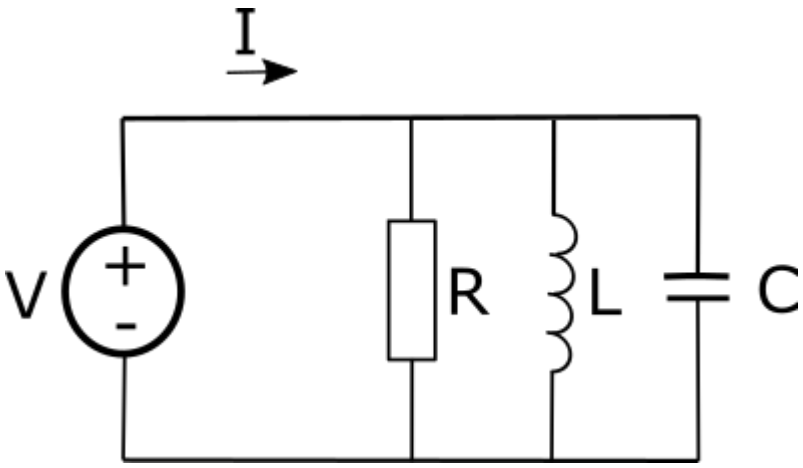

FIGURE 2.12: Series connected LC circuit with parasitic resistance R.

The quality factor (Q) is determined by a quality of the components used in the circuit. When the current oscillates between the capacitor and inductor the Q determines how much energy dissipates during the oscillation. The Q can be mathematically expressed as

$$Q = \frac{2\pi(\text{maximum energy stored during single cycle})}{\text{Energy dissipated during single cycle}} \tag{2.8}$$

Therefore, for the *RLC* circuit the *Q* can be written as

$$Q = \sqrt{\frac{L}{C}}\frac{1}{R} = \frac{\omega_0 L}{R} \tag{2.9}$$

which indicates that the Q increases with the decrease of resistance R and vice versa.

2.2.3 Coupling Factor and Mutual Inductance

The coupling factor (k) determines the amount of flux, generated by the transmitter, reaching the receiver coil, as shown in Fig. 2.13. The greater the amount of flux reaching the receiver, the greater the k is, which is in range between 0 and 1. It is important to note that the k is strongly determined by the distance between the loops and the inductance of the inductors. Therefore the k can be calculated as

$$k = \frac{M_{12}}{\sqrt{L_1 L_2}} \tag{2.10}$$

where M_{12} is the mutual inductance between the two coils and L_1 and L_2 are the inductances of the transmitter and the receiver coils. The mutual inductance between the two coils can be expressed as

$$M_{12} = \frac{N_2 \phi_{12}}{I_1} \tag{2.11}$$

where N_2 is the amount of windings of the secondary loop, ϕ_{12} is the electrical flux passing from primary coil to secondary coil and the I_1 is the current of primary coil. Self inductances of the coil L_1 and L_2 can be calculated as

$$L_x = \mu_0 \mu_r N_x^2 \frac{A}{l} \tag{2.12}$$

where A is a cross section area enclosed by the inductor in square meters (m^2) and l represents the length of the coil in metres.

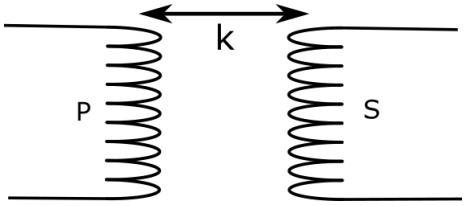

FIGURE 2.13: Coupling factor between the two coils.

2.2.4 Wireless Power Transfer Efficiency Calculation based on Two-Port Network

The WPT circuit can be analysed based on two-port network theory as shown in Fig. 2.14. The network can be characterized by a various circuit parameters, such as transfer matrix, impedance matrix or scattering matrix [90].

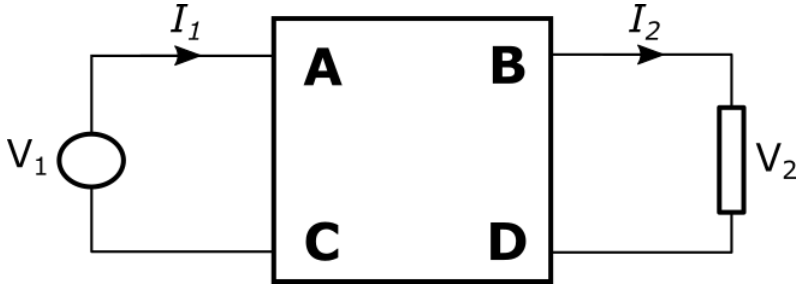

FIGURE 2.14: Two port network with power supply and load connected.

Therefore, the two-port network in Fig. 2.14 can be written as a transfer matrix as

$$\begin{bmatrix} V_1 \\ I_1 \end{bmatrix} = \begin{bmatrix} A & B \\ C & D \end{bmatrix} \begin{bmatrix} V_2 \\ I_2 \end{bmatrix} \tag{2.13}$$

where I_1 and I_2 are the input and the output currents and the V_1 and V_2 are the input and output voltages. The same circuit can be written as the impedance matrix as

$$\begin{bmatrix} V_1 \\ V_2 \end{bmatrix} = \begin{bmatrix} Z_{11} & Z_{12} \\ Z_{21} & Z_{22} \end{bmatrix} \begin{bmatrix} I_1 \\ -I_2 \end{bmatrix} \tag{2.14}$$

The transfer and impedance matrices are widely used for the electronic circuit analysis however, at the higher frequencies the measurements of the coefficients become difficult. In order to overcome the issue the scattering matrix is preferred. The scattering matrix of the system presented in Fig. 2.14 can be written as

$$\begin{bmatrix} s_{-1} \\ s_{-2} \end{bmatrix} = \begin{bmatrix} S_{11} & S_{12} \\ S_{21} & S_{22} \end{bmatrix} \begin{bmatrix} s_{+1} \\ s_{+2} \end{bmatrix} \tag{2.15}$$

where ingoing waves are presented by s_{+1} and s_{+2} and the outgoing waves of the network are represented as s_{-1} and s_{-2}.

Based on the scattering matrix the expressions for the currents and the voltages in terms of wave variables can be represented as

$$\begin{array}{ll} V_1 = \sqrt{Z_0}(s_{+1} + s_{-1}) & V_2 = \sqrt{Z_0}(s_{+2} + s_{-2}) \\ I_1 = \frac{1}{\sqrt{Z_0}}(s_{+1} + s_{-1}) & I_2 = \frac{1}{\sqrt{Z_0}}(s_{+2} + s_{-2}) \end{array} \tag{2.16}$$

where Z_0 is the reference impedance value (usually 50Ω). The voltages V_1 and V_2 can also be expressed based on impedances and current as

$$\begin{aligned} V_1 &= Z_{IN} I_1 \\ V_2 &= Z_L I_2 \end{aligned} \tag{2.17}$$

where Z_{IN} and Z_L are the input and load impedances. By combining (2.16) and (2.17) the scattering matrix equations are given

$$\begin{aligned} s_{-1} &= \Gamma_{IN} I_{+1} \\ s_{-2} &= \Gamma_L I_{+2} \end{aligned} \tag{2.18}$$

Γ_{IN} and Γ_L are the reflection coefficients given by

$$\begin{aligned} \Gamma_{IN} &= \frac{Z_{IN} - Z_0}{Z_{IN} + Z_0} \\ \Gamma_L &= \frac{Z_L - Z_0}{Z_L + Z_0} \end{aligned} \tag{2.19}$$

A load (Γ_{OUT}), generator (Γ_G) and the deflection coefficient in terms of scattering matrix parameters can be written as

$$\begin{aligned} \Gamma_{IN} &= \frac{Z_{OUT} - Z_0}{Z_{OUT} + Z_0} \\ \Gamma_L &= \frac{Z_G - Z_0}{Z_G + Z_0} \\ \Gamma_{IN} &= S_{11} + \frac{S_{12} S_{21} \Gamma_L}{1 - S_{22} \Gamma_L} \end{aligned} \tag{2.20}$$

where the Z_{OUT} is the output impedance. The reflection coefficient also depends on scattering parameters as

$$\Gamma_{OUT} = s_{22} + \frac{s_{12} s_{21} \Gamma_G}{1 - s_{11} \Gamma_G} \tag{2.21}$$

The efficiency of the system can be calculated based on the input and output power. Based on Fig. 2.14 and [91], the input power of the system can be expressed as

$$P_{IN} = \frac{1}{2}\frac{|V_G|^2 R_{IN}}{|Z_{IN} + Z_G|^2} \tag{2.22}$$

where the R_{IN} is a real part of input impedance (Z_{IN}). The output power on the load can be calculated as

$$P_L = \frac{1}{2}\frac{|V_G|^2 R_L |Z_{21}|^2}{|(Z_{11} + Z_G)Z_{OUT} + Z_L|^2} \tag{2.23}$$

where R_L is a real part of Z_L component.

Based on [91], the maximum output power will appear on the load when the input impedance is equal to the impedance of the power generator ($Z_{IN} = Z_G$), and the load impedance is the same value as output impedance ($Z_L = Z_{OUT}$). The efficiency of the circuit in terms of S-parameters can be expressed based on [91] as

$$\eta_1 = \frac{(1 - |\Gamma_G|^2)|s_{21}|^2(1 - |\Gamma_L|^2)}{|(1 - s_{11}\Gamma_G)(1 - s_{22}\Gamma_L) - s_{12}s_{21}\Gamma_G\Gamma L|^2} \tag{2.24}$$

In case when the generator and the load impedance are matched with the reference impedance (2.20) can be simplified as $\Gamma_L = \Gamma_G = 0$, $\Gamma_{IN} = s_{11}$ and $\Gamma_{OUT} = s_{22}$. Therefore (2.24) can be simplified as

$$\eta_1 = |s_{21}|^2 \tag{2.25}$$

2.2.5 Matching Circuits

The transfer efficiency of the WPT circuit is highly affected by the coupling coefficient, quality factor, frequency and load parameters. In order to overcome the efficiency drop and keep the efficiency on the maximum level, the matching circuits are used [92, 93].

To achieve maximum transfer efficiency, the optimum load value have to be used [94, 95]. However, in a real world application the load value does not always match the optimum value as design. In order to overcome the mismatch between the optimal load and real load, the impedance matching circuits are used [94]. There are many topologies used for impedance matching network which can achieve constant voltage output [95] and a numerous approach, such as LCL-T circuit proposed in [96], or LLC approach used by authors in [92].

2.2.6 Coil Losses

The winding resistance in the inductive coil plays an important factor when determining the efficiency of the transmission. The resistance of the coil is calculated based on the conductor material resistivity ρ, length (l) and cross section area (A) of the conductor as:

$$R_{DC} = \frac{\rho l}{A} \tag{2.26}$$

.

The resistance is based on the constant DC current through the conductor therefore, the magnetic field inside the conductor is constant and static. Most widely used material for the electric conductors is copper, which has $\phi = 1.68 * 10^{-8} \Omega m$. However, for the WPT applications the operational frequencies are usually high therefore, conductors carry a time varying current. Alternating current cause a change in the intensity of the current in the inductor. This cause a alternating magnetic field to be established around the conductor. The same alternating magnetic field create an electric field which oppose the change of current intensity, called counter-electromotive force. The current experiences own magnetic field and the field induced by other conductors, which cause Eddy current to be induced in to the windings. The current oppose the penetration of the conductors by producing own magnetic field and this cause an ohmic losses, due to conversion of electromagnetic energy in heat. Eddy current cause two kind of effects, skin effect and proximity effect.

2.2.6.1 Skin Effect

Regardless of the electromagnetic force, the greatest current density in the inductor is found on the conductor surface and it reduces deeper into the conductor. The decline in current density inside the conductor is called skin effect. In a high frequency condition, majority of the current will flow on the conductors skin therefore, the skin depth is the depth at which the current density falls to $1/e$ of the surface value. The e represents a mathematical constant based on natural logarithm, and its approximate value is equal to 2.71828. The skin depth can be calculated as

$$\delta = \sqrt{\frac{\rho}{\pi \mu_r \mu_0 f}} \tag{2.27}$$

where μ_r is relative permeability of the conductive material and μ_0 is the relative permeability of free space. Letter f represent the frequency of the current. For copper wire the μ_r value is very close to μ_0 of a free space, which is $4\pi 10^{-7} Hm^{-1}$.

The resistance of the round conductor based on the operating frequency can be calculated based on [97] as

$$R_{AC} = \frac{\rho l}{\pi\delta(\frac{1-e^r}{\delta})2r - \delta(\frac{1-e^r}{\delta})} \tag{2.28}$$

where r is the radius of the conductor.

2.2.6.2 Proximity Effect

When the current is flowing through more than one conductor in a close proximity, such as inductor or a transformer winding, the magnetic field around the wire influence the distribution of the current inside the conductor. The current will concentrate to flow through the smaller regions in the conductor and therefore increase the effective resistance of the conductor. The crowding of the current will increase with the increasing frequency of the current. The losses in the conductor due to proximity effect can be calculated based on Dowell method [98] as

$$R_{AC} = R_{DC}\Big(Re(M) + \frac{(m^2-1)Re(D)}{3}\Big) \tag{2.29}$$

where R_{DC} is the resistance of the coil in a direct current condition, m represents number of layers of the coil and M and D can be expressed as

$$M = \alpha h \coth(\alpha h) \tag{2.30}$$

$$D = 2\alpha h \tanh(\frac{\alpha h}{2}) \tag{2.31}$$

where h is a height of a square conductor

$$\alpha = \sqrt{\frac{j\omega\mu_0\eta}{\rho}} \tag{2.32}$$

ω represents an angular frequency and ρ can be mathematically expressed as

$$\rho = N_l \frac{a}{b} \tag{2.33}$$

where N_l is a number of turns, a is a width of a square conductor and b is a width of a winding area.

2.3 EV Charging

Even though it is hard to pinpoint the EV invention to one inventor, after a series of breakthroughs world's first EV was introduced in early 19^{th} century [99]. However, with relatively low oil prices EV had rather little advancement. It was until the second half of the 20^{th} century as the oil prices continue to rise, when EVs went into mass production. By the end of 2018 roughly 3.3 million EVs are on the UK roads, with a wide range choice available. Nevertheless, today EVs are already playing a crucial role in day to day transportation, decreasing the foreign oil dependence by approximately 30-60%.

The rapid popularity of EVs has been caused by a wide variety of principles, such as vehicle sizes and current battery technologies, that satisfy a distinct consumer pool. Whereas the EVs are to replace the vehicles with internal combustion engine (ICE), battery pack endurance and the costs associated governs the success of EVs. Furthermore, if the size is increased, batteries will simply get heavier, negatively affecting both the travel economics and driving range. The driving range of an EV is primarily determined by the battery power and energy capacity [100]. A standard battery pack in the EV, is able to store $35kWh$ of electrical energy. However, with a standard AC grid of 220-380V/15A, a battery pack can be fully charged within 6 to 8 hours. In a nutshell, a single car charger can fully charge up to 3 cars within a day.

Car manufacturers often measure the driving range under the best conditions. According to reports, the real world travelling distance may be lesser than 30–37% of the distance specified by manufacturers [101]. For instance, extra electrical loads such as headlights, wipers, heating, cooling, outside temperature and physical geography would reduce the driving range further [102]. Super-fast charging is one other aspect which is highly looked over by the battery users [103]. Atmospheric temperature is a crucial factor for battery charging duration. For instance, Li-Ion batteries cannot be charged at or below 0^oC where most novel EV battery packs may include a heating blanket. Nevertheless, fast charging technologies are available and only to be

used sparingly where fast charging over-stresses the battery while enhancing the level of dendrite growth which arbitrates the safety aspect. The basic schematic diagram of the EV can be seen in Fig. 2.15.

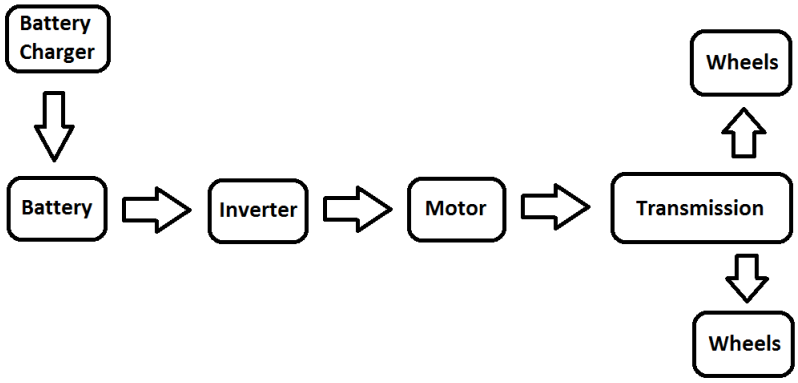

FIGURE 2.15: Schematic diagram of EV system.

There are many EV chargers already on the market, from plug-in chargers [104] to the on-board chargers [105]. The output power of chargers installed at homes, varies from 2.5kW to 7kW, while the chargers at public locations have much higher power from 25kW to 135kW [104]. It is also important that the charging standards from different bodies and charging technologies from a range of manufacturers, are being merged. Two major charging terminologies, '*level*' and '*mode*' are being widely used. While ''*level*' is mostly being used by a manufacturer in North America [106, 107], both '*level*' and '*mode*' are being used by European manufacturers. Moreover, '*mode*', consists of four different power levels of charging and the level is an aggregation of 3 charging stages. Level-1 and Level-2 chargers are deployed in residential facilities and household appliances, while Level-3 chargers are being used at commercial charging stations [108]. Additionally, wireless car chargers can be a potential alternative to plug-in car chargers where wireless based car chargers are able to operate on the 2-coil design principle [109] at different power levels, ranging from 360W [110] to hundreds of kilowatts. In contrast, plug in charging can be catered while the vehicle being parked (static charging) and WPT charging is a dynamic alternative, where the EV can get charged while moving (dynamic charging) [111]. Volume of WPT EVs charger manufacturers is rising, offering static charging solutions, nevertheless, a practical, dynamic version of charging is yet to be developed [112].

While battery manufacturers are in an arms race to develop the best battery cells, both the consumers and the car manufacturers wait for the most

sophisticated WPT car charging system. WPT phenomena have many advantages over wired charging, which offers convenience and simplicity where EVs charging will become a splash and dash event where the vehicle can be charged at the garage door with neither lifting a finger nor wires. It enhances the user experience to the next level by enabling the characteristics of the charging process to be controlled via a smart phone or computer. With the introduction of autonomous charging, human management will be further minimised improving both the safety and reliability aspects of the charger. EV WPT charging pads require minimum installation space area, hence charging facilities can be installed in the parking surface. All key benefits of the wireless charging can be seen in Fig. 2.16.

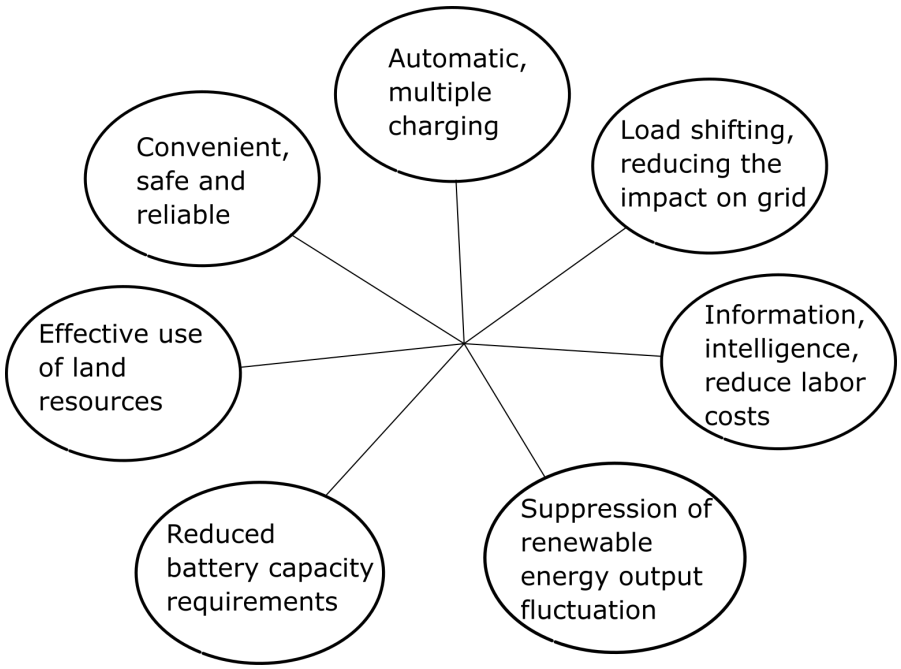

FIGURE 2.16: Benefits of wireless charging.

2.3.1 Advantages and Disadvantages of EV

Advantages:

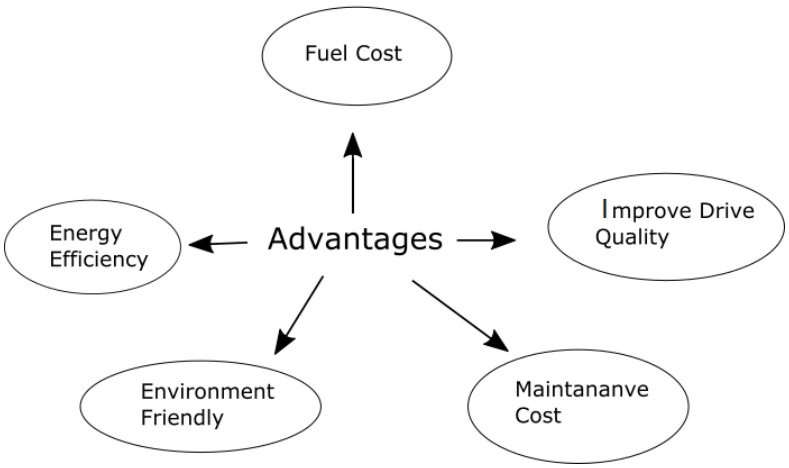

FIGURE 2.17: Advantages of EV in comparison to the other vehicles.

EVs offer many advantages over conventional ICEs, the full list of advantages can be seen in Fig. 2.17. The most notable among them are:

1. **Low energy consumption:** EVs do not require fossil fuel during the operation, but solely operate on battery power. Nevertheless, they instantly switch over to gasoline if the battery is running low. Most of the ICEVS convert only 20% of the energy provided by the fuel to the energy used for moving while the remainder dissipates mostly as heat. EV converts up to 86% of the energy stored in the battery which is used solely during the operation of the vehicle [113].

2. **Environment friendly:** Tail-pipe emissions along with the hazardous gas emission associated with ICEVs, contribute to the emission of significant percentage of greenhouse gases. EVs in 2015 have exhibited a promising future by reducing greenhouse gas emissions compared to the ICEVs during the vehicle's lifespan, which is also makes an impact on human health [114].

   Global warming potential (GWP) for a sample EV model produces approximately 105,054 pounds of green gas emissions over the full vehicle lifespan, whereas equivalent ICEV emits over 136,521 pounds. In a nutshell 23% potential advantage for the BEV. EV significantly minimises the ecological impact on the environment due to the vehicles where EVs

produce zero tail-pipe emission where the functionally entirely rely on the grids, power plants or batteries [115].

3. **Cost-Effectiveness:** In contrast electricity costs associated with the EV over the mileage is significantly lower than the fuel costs required ICEV over the same distance. EV also require limited maintenance simultaneously minimising the maintenance costs compared to the owning a ICEV. They consist of simple battery-electric motor systems compared to the costly engines of ICEVs where with the evolving EV technology current generations EV lithium-ion battery pack has decreased.

4. **Noise:** Electrical motors used for moving the vehicles are significantly quieter and require fewer maintenance than the ICEs. Frequency content of the EV noise indicates potential peaks at higher frequencies which can also be heard as a single tone.

   Many researches have been conducted to justify the noise emission between EV and ICEV. Moreover, EVs tyres are generally low rolling resistance in order to drive longer distances with the charged battery where being the most essential requirement for the noise reduction. Even though at lower speed, both the ICEV and EV exhibits considerable noise difference while higher levels indicate the contrary where tire and road noise gets dominant. In a nutshell noise caused by the traffic jams, parking zones and also streets can be decreased by introducing EV's in urban areas while at high speed EV would not a difference.

5. **Recyclable:** Almost 100% of the EV and the batteries are fully recyclable therefore, all materials used for the EVs can be reused multiple times. Moreover, battery recycling and re-fabrication has made an extensive impact on the enhance demand for both battery materials and the environment. With the expeditiously increasing volume of EV customer base, EV batteries are recycled after reaching the peak life time, by 4R Energy Co, which is a joint venture between Nissan and Sumitomo [116]. Recycled Li-Ion batteries are to be used in 1^{st} Gen - Nissan Leaf and to be sold at half of the price of a new EV battery. EV manufactures are discovering multiple roots to manufacture EV at minimum cost.

Disadvantages:

Like every other technology despite the generic advantages, variants of disadvantages in Li-Ion batteries can be listed. Currently available battery

performance of Li-Ion batteries, is not adequate to be extensively used where extensive research efforts are required in improving power density, safety, durability, and cost.

1. **Weight:** In contrast with a fossil fuel, the weight of the battery does not reduce with the depletion. Therefore, the EV have to carry same weight for a full length of the travel which leads to higher energy consumption of the EV.

2. **Longer Charging Time:** In contrast to EV charging time is significantly higher than the time required to fill up the gasoline powered vehicles which is maximum 5-6 minutes. EV car charging stations are still at their development stage and charging one vehicle requires a dedicated station for 5-6 hours hence only few EV can be charged per each day.

3. **Durability:** Researchers are making efforts to increase the battery life time with enhanced durability. For deep cycles minimum of 5 years per 100,000km. However, increased cycles swiftly decrease the battery capacity while the power is affected by the cold weather.

4. **Environmental Affect:** Even though the environmental impact of gasoline is pinpointed and weighted over Li-Ion battery, surprisingly the battery manufacturing process generates more severe set of environmental impacts offsetting overall advantages discussed. For instance, even though the greenhouse gas emission is minimised, consequences due to metal mines and battery recycling process. In particularly, underprivileged communities located near the mines are affected due to both the manufacturing waste and the recycling waste

5. **Safety:** Li-Ion batteries are highly vulnerable to short-circuiting and overcharging which are the major drawbacks. The chemical structure between the anode and the cathode of the Li-ion battery, is destroyed. Hence the short circuit is caused by the Li-metal deposits which may also potentially lead to fire. In contrast other battery types such as Pb-acid or Ni-Cd batteries, are more risk free after short-circuiting and overcharging due to their low energy capacity and inflammable electrolyte materials which are used. Potential battery short circuits may be accelerated with the increased temperature, causing damage to neighbouring devices.

2.3.2 Battery Types

Due to both the escalating environmental concerns and the limited fossil fuel resources, various renewable energy sources are being developed and researched by the automotive industry without imminent economic and social disruptions. Among all the potential alternative solutions, batteries have been the most prominent option to replace petroleum due to zero greenhouse emission. Moreover, battery is the most significant component in an EV, thus the only apparatus which is able to store energy which powers up the EV. After being charged, electrical energy is converted in to chemical energy and then back to electrical energy which powers the motors.

With the number of highly commercially successful EV models such as Tesla Model S, Nissan Leaf or affordable Renault Zoe, industry has made great investment in developing more enhanced on-board battery systems. However, there are several types of battery systems available:

1. **Lead-Acid**

   Both Pb-acid and Nickel metal hydride (NiMH) batteries are conventional battery technologies that were highly used in early EV models such as General Motor's EV1. Lead-Acid batteries, as seen in Fig. 2.18, are widely used in a motorbike applications due its proven manufacturing technique and reliability. Nevertheless, with respect to being used in EV, both techniques are obsolete even though they are rather inexpensive due to their larger weight. Pb-Acid batteries are typically seen in ICEV where they are an inexpensive source of energy with limited $34 Wh/Kg$.

FIGURE 2.18: Lead-Acid battery used in a motorbike application.

2. **Nickel Metal Hydride:**

   In contrast NiMH batteries are superior with twice the energy of a Pb-Acid battery. NiMH batteries are used in EV since they are significantly lighter, smaller with greater energy density. With regards to EV, NiMH are highly suitable with 69.4Wh/kg , which is prominently being used in many hybrid vehicles, such as Toyota Prius and Honda Civic hybrid. Moreover, they require minimum space which will allow the battery system to be contained within a smaller space. Even though, NiMH batteries may have some limitations, such as having lower charging efficiencies and being directly proportional to temperature. Thus, they self-discharge up to 12.5% per day under room temperature and the rate aggravates with the accelerated temperature which makes NiMH batteries unseemly for EV in warmer temperature. These batteries are also fully recyclable in contrast to Nickel-Cadmium batteries which are hazardous to the environment. Nickel-Cadmium battery shown in Fig. 2.19 was used in a hand tools applications.

FIGURE 2.19: Nickel-Cadmium battery used in a battery powered hand-drill.

3. **Solid State:**

   EV are widely powered by "wet" lithium-ion batteries which is essentially the larger version of the common phone batteries. However, growing research interests on solid-state batteries have significantly increased where the cells are made of solid conductive material with no liquid electrolytes for the next generation EV. Initial Solid-state research programme was begun at the University of Colorado Boulder.

   In contrast Li-Ion batteries may generate heat during liquid electrolytes motions which may lead to a quick fire under right circumstances while a solid-state cell can be both quickly charged and discharged safely

with the excluded volatile and corrosive electrolyte. In a nutshell an EV can be quickly charged with two to three times high energy over Li-Ion. It is also a highly simplified cell design which does not require much room to be stored without cooling pack, allowing more cells to be included in one car battery unit. Nevertheless, limitations such as temperature range and electrode current density are yet to be overcome. Automotive and battery manufactures are ambitious to scale up the manufacturability and full product qualification to be installed in new EV by 2019 driving the costs further down, completely displacing the Li-Ion cells.

4. **Lithium-Ion:**

   Lithium is the lightest of all metals with greatest electrochemical potential that provides the largest energy density for weight. First non-rechargeable lithium batteries were commercially available in the early 1970. Lithium-Ion battery used in a portable computer in presented in Fig. 2.20.

   Lithium-Ion batteries are preferred to be installed in EVs due to their superiority in high energy density. Compared to other types of batteries, they are also less costly, less safe and degrades over time with higher energy densities than both lead-acid and nickel-metal hydride batteries. In a nutshell they are not suitable to be used in a EV that is being used daily where the car would not be able to travel far as it was brand new.

   As a solution, latest Nissan LEAF has introduced a breakthrough battery which uses material that can store a higher density of lithium-ion, which enhances the driver range. Both higher reliability and energy density have been achieved through the novel laminated cell structure and Lithium - Nickel Cobalt Manganese Oxide (NMC) [117] electrodes. Laminated cell design offers more space that enhances both the durability and higher cooling performance over the conventional cells. Advanced NMC material enhances the capacity of high density Li-Ion storage offering an eight years warranty.

   One of the other main drawback is that they should be charged in early stages to increase their life-cycle [118]. It is also important to note that the Li-Ion batteries should never be depleted bellow their minimum voltage, in that event their lifespan is also shortened drastically [119]. However, Tesla battery packs have caught fire in accidents in few

instances escalating the safety concerns, hence even a dubious claim about solid-state cell may generate huge buzz. Despite all the disadvantages Li-Ion requires minimal maintenance which most batteries cannot claim with low self-discharge and lesser harm due to the disposal.

FIGURE 2.20: Li-Ion battery used in a laptop.

The various battery types and their energy densities have been compared in Table 2.1

Type	Lead-Acid	Nickel-metal	Lithium-Ion
Cell Voltage	2.1	1.2	3.6
Stored Energy ($\frac{Wh}{kg}$)	30-40	50-80	150-250
Efficiency (%)	70-92	66	98

TABLE 2.1: Comparison of battery types

2.3.3 Inductive EV Charging

Fig. 2.21 exhibits the fundamental concept of WPT car charger phenomena. Transmitter end consists of an AC-DC converter, which converts AC mains voltage in to DC voltage. The voltage is then passed through the DC-DC boost converter, which enhances the voltage to a higher level. High frequency (HF) inverter then inverts the DC voltage into an HF-AC voltage which is suitable for the transmission.

HF rectifier located at the Receiver end converts the received HF-AC voltage into DC voltage. DC-DC converter converts the DC voltage into the lower level DC voltage, which more closely matches charging battery.

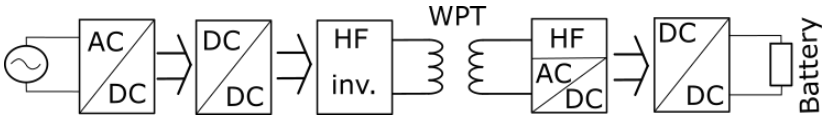

FIGURE 2.21: WPT battery charger.

2.3.3.1 AC/DC

AC-DC power converter converts the AC voltage into DC voltage. Alternatively, full wave bridge rectifier is then used as the EV charger converter. A full bridge rectifier consists of four diodes and the voltages across the resistive load can be expressed as

$$v_0(\omega t) = \begin{cases} V_m sin\omega t & for\, 0 \leq \omega t \leq \pi \\ -V_m sin\omega t & for\, \pi \leq \omega t \leq 2\pi \end{cases} \tag{2.34}$$

where V_m is a mains voltage.

The voltage across the RL load is a full wave rectified sinusoidal and the waveform is determined by the DC voltage and the harmonics which is expressed as a Fourier series.

$$v_0(t) = V_0 + \sum_{n=2,4,...}^{\infty} V_n cos(n\omega_0 t + \pi) \tag{2.35}$$

where $V_0 = \frac{2V_m}{\pi}$, and $V_n = \frac{2V_m}{\pi}(\frac{1}{n-1} - \frac{1}{n+1})$.

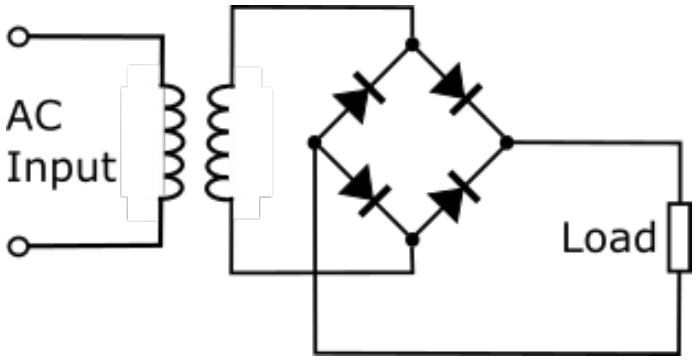

FIGURE 2.22: AC/DC power converter.

A Three phase voltage rectifier is used as a power supply which is implemented with three pairs of diodes. First three diodes are typically standard PN diodes which are connected in parallel, which conduct in series with three silicon-controlled rectifier diodes (SCR). SCR function is to act as normal diode in the blocking direction, when the potential of the cathode is higher than the potential of anode, the built-in forward bias potential is

approximately $0.7V$ difference. Forward bias SCR is to be triggered by a positive current pulse applied to the gate, which enables the SCR to accomplish the rest of half-cycle as shown in Fig. 2.23. Hence the output wave forms are phase shifted to achieve 12-step waveform.

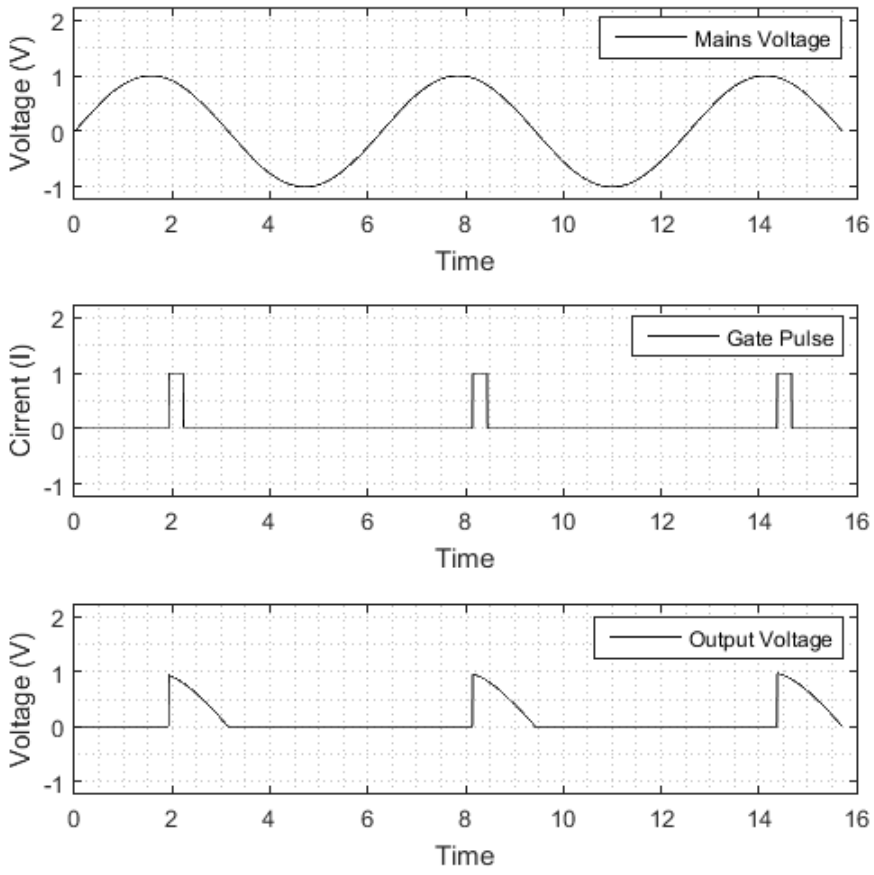

FIGURE 2.23: Operation of SCR diode, the mains voltage is applied on the device which is then triggered by gate pulse. The output voltage therefore depends on the triggering angle.

2.3.3.2 Boost converter design

A boost converter as presented in Fig. 2.24 is a circuit designed to increase the potential of the DC voltage. The voltage is increased by switching the current, which flows though the inductor L_1. When the switch is disconnected, the inductor tends to keep current flow, where the voltage potential on the inductor rises to push the current through the diode D_1 which is connected to the capacitor C_1. Depending both the switching frequency and the pulse duration, the output voltage can be determined as:

$$D = 1 - \frac{V_{in}\eta}{V_{out}} \tag{2.36}$$

where D indicates the duty cycle of the switch, while V_{in} and V_{out} input voltage and output voltage respectively. η represents the efficiency of the converter. The maximum output current is calculated by:

$$I_{maxout} = \left(I_{lim} - \frac{\triangle I_{L1}}{2}\right)(1 - D) \tag{2.37}$$

where the current limit, stated in the switch data sheet, is expressed as I_{lim} and the current ripple is expressed as $\triangle I_{L1}$ [120].

Commonly the higher the chosen inductor value is the higher the maximum output current due to the minimised ripple current. Likewise, current is inversely proportional to the inductance. From the following equations the inductance L_1 can be calculated as:

$$L_1 = \frac{V_{in}\left(V_{out} - V_{in}\right)}{\triangle I_{L1} f_s V_{out}} \tag{2.38}$$

If fs represents the minimum switching frequency of the switch and V_{out} is the desired output voltage ripple, then the output capacitance of C_1 can be calculated as:

$$C_1 = \frac{I_{out} D}{f_s \triangle V_{out}} \tag{2.39}$$

where $\triangle V_{out}$ is a desired output voltage ripple.

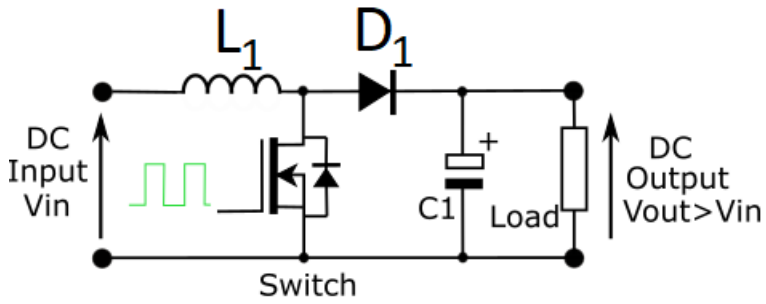

FIGURE 2.24: Circuit diagram of boost converter.

As shown in Fig. 2.25, an example of the output voltage ripples between 39 and 41VDC, has been achieved for the above circuit when the inductor value $L_1 = 500\mu H$ and the capacitor $C_1 = 5\mu F$. The diode used was type 1N4007. The switching cycle is total of a $20\mu s$ where the ON time is $13\mu s$,

which is represented by red line marked as switching time. Blue line represents the input voltage and both the input and output currents have been indicated in the graph. Generally, if the required maximum output current is slightly greater than the required L_1 higher inductance can be chosen where the higher the inductance the smaller the ripple current. Particularly, the ripple current could be further minimised with enhanced switching frequency. The graph exhibits the system's maximum output current has been determined to be $0.9A$ where the input current ripple of 3.1 to $3.5A$.

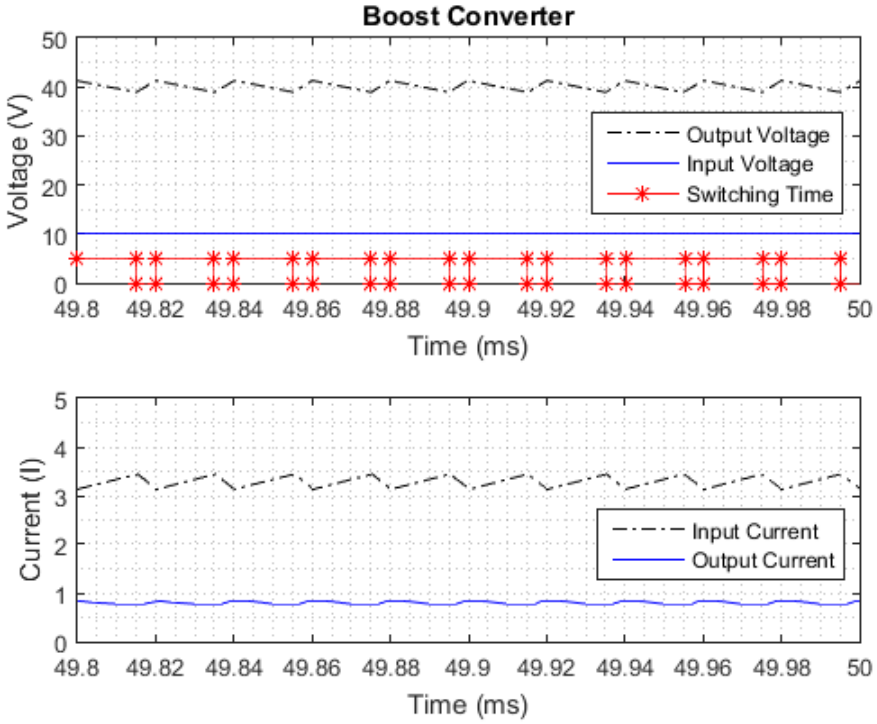

FIGURE 2.25: Simulated results of boost converter results.

2.3.3.3 Buck converter design

A buck converter as shown in Fig. 2.26 was employed to decrease the voltage, particularly in this case WPT system output voltage of $40V$ to $12V$ which is desired to charge the battery. The buck converter switches the inductor's input current at a high frequency rate. When the switch is ON, the current flows through the inductor (L_1) through the capacitor (C_1). When the switch ($SW1$) is off, the inductor is still magnetized and the voltage drop across the inductor causes output voltage to drop. However, due to the stored energy in the inductor, the current will continue to flow and the output power will remain consistent to the input power.

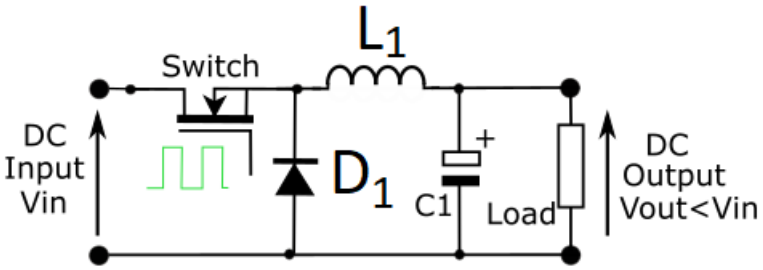

FIGURE 2.26: Circuit diagram of buck converter.

The output voltage of the buck converter can be calculated using the same (2.36) as for boost converter. The maximum input currents (I_{max}) can be calculated as follows where I_{L1min} is a minimum current of the integrator switch:

$$I_{max} = I_{L1min} - \frac{\triangle I_{L1}}{2} \tag{2.40}$$

Inductor L_1 can be calculated as

$$L_1 = \frac{V_{out}\left(V_{in} - V_{out}\right)}{\triangle I_{L1} f_s V_{in}} \tag{2.41}$$

V_{in}, V_{out}, fs and $\triangle I_l$ respectively indicate the typical input voltage, desired output voltage, minimum switching frequency and the estimated ripple current. Output capacitance is calculated as:

$$C_1 = \frac{\triangle I_{L1}}{8 f_s \triangle V_{out}} \tag{2.42}$$

note that $\triangle V_{out}$ expresses the desired output voltage ripple. Fig. 2.27 exhibits the simulated results of the example of the buck converter, when the input voltage is 40V and the output voltage is 10V. The capacitor value used in this case was $C_1 = 5\mu F$ and the inductor value of $L_1 = 80\mu H$.

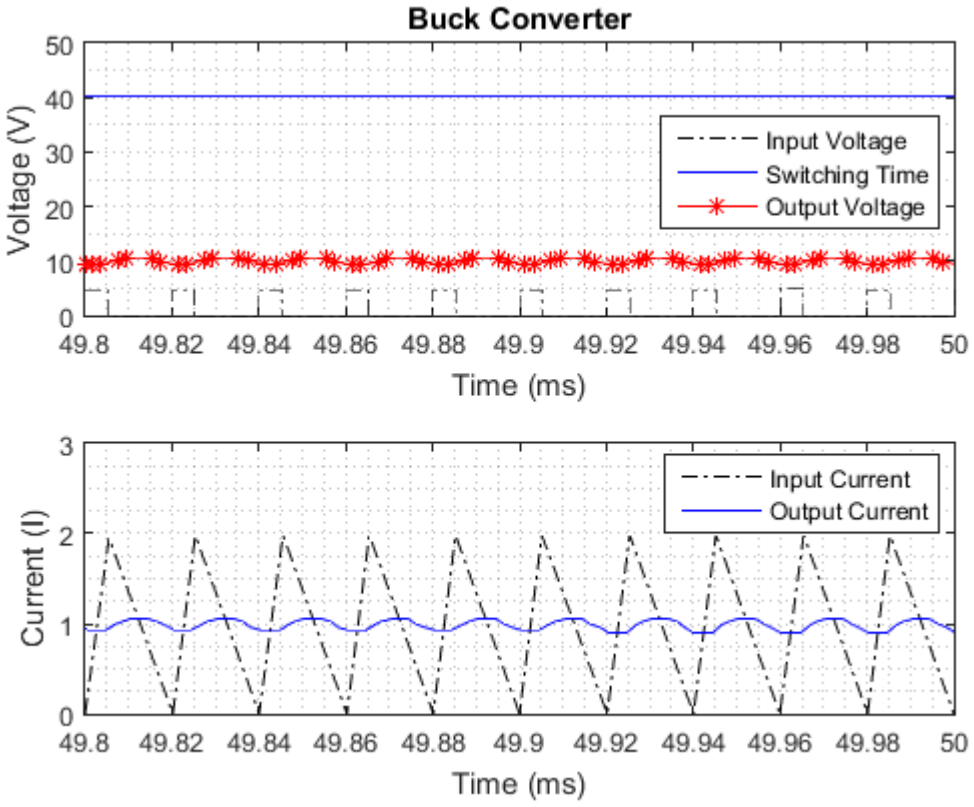

FIGURE 2.27: Buck converter results.

2.3.3.4 DC/AC inverter

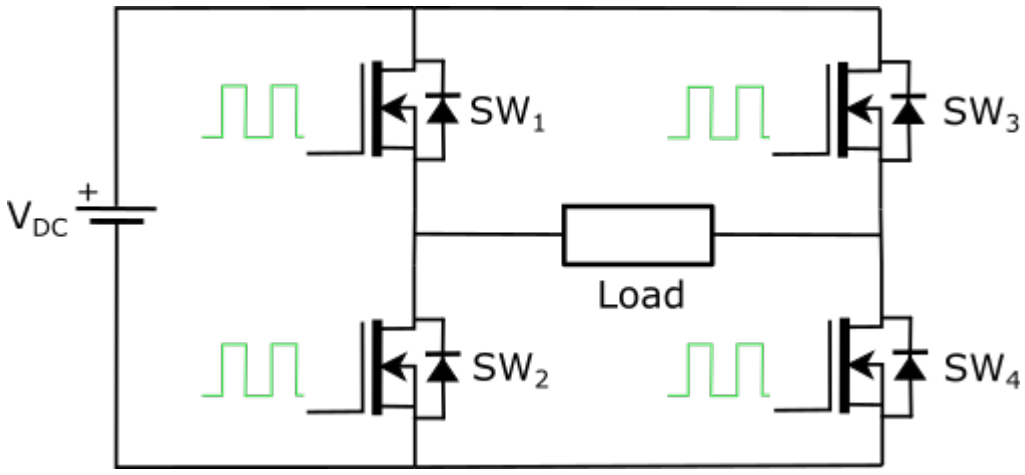

FIGURE 2.28: Circuit diagram of full bridge inverter.

DC voltage from either a battery or a DC source was converted, using a full bridge inverter. Particularly inverter transfers the power from the DC battery to the AC load, specifically in a current circuit the inverter converts DC power to $300kHz$ and $50Hz$ AC. As shown in Fig. 2.28, full bridge

inverter comprises four switches which close and open in a particular sequence. Upon switch SW_1 and SW_4 are being closed, switch SW_2 and SW_3 open, and vice versa. The output voltage across the load is reversed and the current flows through the load towards the opposite direction producing square waveform across the resistive load. By regulating the switching speed, the output frequency is controlled.

The output current strongly varies upon the load. Precisely, if the load is purely resistive, the output current will match the shape of the voltage. Particularly in a WPT system, the load is a transmitter inductive coil, current which rises exponentially will create a sinusoidal waveform. The output current can be expressed as an aggregation of currents.

$$i_0(t) = i_f(t) + i_n(t) = \frac{V_{DC}}{R} + Ae^{\frac{-t}{\tau}} \tag{2.43}$$

for $0 \leq t \leq \frac{T}{2}$, where A is a constant which is evaluated at the initial condition of $\tau = \frac{L}{R}$, thus the current across the T_X coil is calculated where $t = \frac{T}{2}$ and the voltage across T_X coil is $-V_{DC}$.

$$i_0(t) = \frac{-V_{DC}}{R} + Be^{-\frac{(t-\frac{T}{2})}{\tau}} \tag{2.44}$$

for the $\frac{T}{2} \leq t \leq T$, where the constant B is evaluated from the initial condition.

Power on the load can be determined by $I_{RMS}^2 R$, and the RMS load current can be calculated as

$$I_{RMS} = \sqrt{\frac{1}{T}\int_0^T i^2(t)d(t)} = \sqrt{\frac{2}{T}\int_o^{\frac{T}{2}} \left[\frac{V_{DC}}{R} + (I_{min} - \frac{V_{DC}}{R})e^{-\frac{t}{\tau}}\right]^2 dt} \tag{2.45}$$

In ideal case where is no loss on the switches is seen, the power of a DC source is determined from

$$P_{DC} = V_{DC} I_S \tag{2.46}$$

where V_{DC} and I_S are the voltage and the current of the DC power supply.

2.4 Challenges and Limitations

The main aim of the wireless power system is to provide the power to a movable object without being physically attached to them. The power should

be therefore transmitted through the air gap between the transmitter and the receiver [91, 121]. In order to develop such a system, a close collaboration between the design of the magnetic coils and the power electronics have to be established [122].

Improvements in the magnetic design could be based on the increasing magnetic coupling between the coils [123], improved magnetic properties of the ferromagnetic material [124, 125], or by changing the geometric design of the transmitter and receiver coil [126]. The use of Litz wire, as seen in Fig. 2.29, can in some cases significantly improve the efficiency of the WPT system [127]. However it is important to note that the Litz wire will improve the efficiency only in the system which operates bellow the frequency of $500kHz$ [127, 128]. If the operating frequency is greater than $1MHz$, the effect of Litz wire decrease gradually by increased effect of parasitic capacitance [128].

FIGURE 2.29: Litz wire.

A large gap between the transmitter and the receiver results in a large leakage inductances and a low mutual inductances between the transmitter and receivers coils [129]. High frequency, used to transmit the power increases the losses on ferromagnetic core of the inductor. Eddy current on the top of the inductors coil also increase power looses and EMI [130], and it also increases the parasitic capacitance of the coil.

The size of the system also plays a major role in a WPT system design. A v.ast majority of portable hand-held devices are small in size, while in car applications the weight of the system is a major concern [45]. Therefore, the WPT system must be as small and light as possible in order to increase functionality and decrease power consumption of a vehicle for both static [131]

or a dynamic charging [132]. When designing a system, the switching frequency of the system is an important parameter. While this parameter does not concern metal oxide field effect transistors (MOSFET) devices, which have very high switching frequency, it is very important parameter when using insulated gate bipolar transistors (IGBT). Despite higher switching frequency, MOSFET devices with similar drain to source voltage specifications (V_{DSON}) than IGBT, have significantly higher price.

With increase of power demand and in order to increase the charging speed, the WPT chargers tend to be more powerful. Simultaneously, with the increase in the transmission power, the cost of the WPT charger also increases. The relationship between the design cost and the output power is an important factor, that must be addressed prior to the system design.

2.5 Methodology

The fundamental concept of the entire thesis has been an analysis of how the IWPT phenomenon can be further simplified with no deterrents to the end user. Challenges and limitations along with variations of techniques, have been discussed to narrow down the potential challenges of upgrading the wireless charging infrastructure to simultaneously support and adapt variety of electronic devices and platforms including EVs. Particularly, the incompatibilities between the currently deployed WPT techniques and the EV charging platforms, causing commercial and technical unviability, has been further narrated. The thesis investigates multiple approaches of improving the system efficiency, spatial freedom while minimising the weight of the IWPT charging system, in order to cater the efficiency requirements that the consumer desires. The theoretical IWPT system has been simulated using both MATLAB and Wolfram Mathematica, built relying upon the mathematical equations. The analysis has been further supposed by the results, obtained via the simulation software Advance Design System (ADS) and Micro Cap (MC). Ultimately simulation results were compared with a real-life application through a laboratory built IWPT system prototype. The results generated by the prototype were measured using an oscilloscope and a spectrum analyser and compared with the calculated results. In Chapter 3, discusses an application where both the size and the spatial freedom of a four-loop WPT system, has been reduced, while in Chapter 4 the weight of the two-loop, strongly coupled loops has been reduced. Finally, in Chapter 5 proposes a rapid car detection technique for the multi-charging pad.

2.6 Chapter Summary

This chapter presented the background of the WPT technology. Its historical approaches, technological variations, operating principles, major applications, advantages, disadvantages, future advancements and system limitations have been discussed. Historical approaches with relevance to WPT, include technical breakthroughs of the electromagnetic induction to the latest laser technologies. Literature review has been provided to deliver recent industrial advancements with the real-life applications.

Basics of a WPT technology which involves two magnetically coupled coils estranged by an air gap where the receiver coil is induced by the magnetic field generated by the transmitter is connected to an AC supply. The general system overview is followed by the detailed mathematical equations, circuit model as well as the mutual inductance model. Furthermore, a comprehensive mathematical analysis of the WPT system has been conducted based on two port network theory along with the potential techniques that could be used to enhance the efficiency. A detailed analysis of the health and safety regulations were presented. Second part of this chapter provides an insight of EV charging, which includes all primary elements of a WPT charger. Challenges and the limitations associated with the WPT has been detailed.

Chapter 3

Combined Conformal and Strongly Coupled Magnetic Resonance System for Increasing Charging Capability

RESONANCE WPT is highly affected by the distance variations between the transmitter and receiver [133]. SCMR systems heavily rely upon the magnetic coupling between the resonators, which ought to be strongly coupled in order to achieve maximum transfer efficiency [3, 4]. In EV charging applications for example, the distance between the vehicle body and the charging pad strongly depend on the vehicle model and the fill. Thus, the resonant frequency of the transmitter and the receiver loop also varies accordingly to the air gap between the resonators. Therefore, in order to maintain the maximum efficiency, either the impedance matching [134, 135] or adaptive matching technique [136] must be implemented during the circuit design. Additionally, the transmission coil array technique is also being widely used [137] where the phase weights the transmission circuit according to the energy deposition profile of the receiving coil.

Both, SCMR and CSCMR four-loop techniques, are discussed in this chapter. Two independent effective systems are carefully brought together in order to address one of the common limitations where the distance varies between the car charger and receiver inbuilt in the car, counterweights the efficiency. In this section a mathematical analysis has also been conducted to support the simulated system specifications which are presented in Section 3.2. Section 3.3 elaborates the system configurations and the experimental parameters of the combined system. Moreover, it also contrasts the calculations and experimental results, which are graphically presented. The system efficiency, which is associated with the angle and misalignment is studied in

Section 3.4 while Section 3.5 presents the combined results of the combined CSCMR-SCMR system. The chapter summary is presented in Section 3.6.

3.1 Four-Loop System Model Analysis

Four-loop, strongly coupled magnetic resonance method was introduced in 2007 [6]. The primary advantage of this method is that it maximises the distance between the transmitter and receiver loop. The authors of this study pointed out that, 60W of energy can be wirelessly transmitted over 2m at 40% overall efficiency, using the above technique. In particular, the SCMR system has also demonstrated that even the higher transmission efficiencies can be achieved, simply by designing both the transmitting and receiving resonators to resonate at the same frequency. The resonant frequency of the transmitter and receiver are matched, at the maximum quality factor of the conductors [138]. However, high sensitivity to the coil misalignments [139, 29], and its bulky structure can be listed as the two fundamental drawbacks of this SCMR system. Hence the Conformal SCMR (CSCMR) concept was presented in [140], in order to prevail over these drawbacks. In accordance with this method, both the source and load loops are embedded in the same plane with transmitter and receiver resonators. Few designs of the CSCMR system were also built as printable version, see e.g. [141, 142, 143]. In practice, few printable versions of CSCMR system were built. Both, SCMR and CSCMR systems are shown in Fig. 3.1.

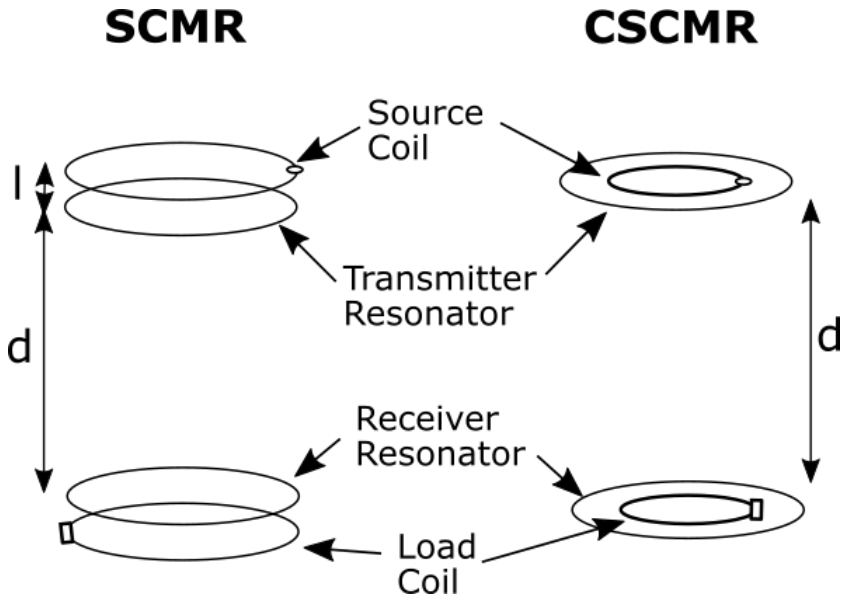

FIGURE 3.1: Comparison between SCMR and CSCMR system.

3.1.1 Combined SCMR and CSCMR Four Loop Wireless Power Transfer System

The combined SCMR and CSCMR Four-Loop Wireless Power Transfer System model is presented in Fig. 3.2. The novel concept also converts both the SCMR and CSCMR WPT system phenomenon into a single concept. The transmitting end is designed following the SCMR concept where the source loop is placed outside the transmission resonator in order to offer the flexibility of changing coupling factor between the two loops. Likewise, the load loop is placed concentrically inside the receiver resonator adhering to CSCMR technique. As a result of applying this concept, the geometrical size of the receiver end has been further minimised while the coupling factor between the two coils remains fixed.

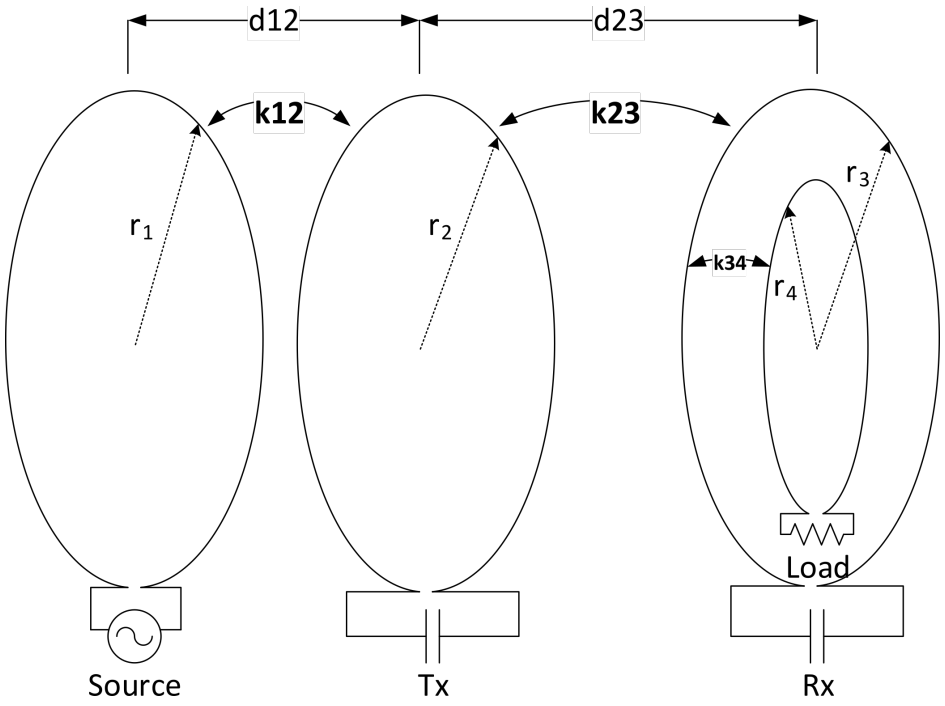

FIGURE 3.2: Combined SCMR-CSCMR system.

In Fig. 3.2, it can be shown that if the distance (d_{23}) between the transmitter (T_X) and the receiving (R_X) resonator is changed. Thus, the changed distance requires the change of the corresponding coupling factor (k_{23}) where the coupling coefficient (k) is a function of the distance between the adjacent coils. As a whole, the changes in the receiver end are required to be compensated by simultaneously altering the coupling factor (k_{12}), to maintain the system's maximum efficiency. In accordance with the CSCMR concept, the coupling factor (k_{34}) remains fixed; hence, only the coupling factor between

the source loop and the transmitter resonator (k_{12}) can be simply adjusted by altering the distance (d_{12}). Therefore, the relationship between the distances has been mathematically represented as $\left(\frac{\triangle d_{23}}{\triangle d_{12}}\right)$. Hence the system operates at its maximum efficiency under the given ratio between the distances.

3.1.2 Mathematical Analysis of Combined Conformal and Strongly Coupled Magnetic Resonance System

The combined system, which comprises both CSCMR and SCMR, include source loop, load loop, transmitter and receiver resonators. Both transmitter and receiver resonators are typically designed to oscillate at the same frequency, whereas the quality factor (Q) between the two loops are maximised. In this regard it ensures that the power transmission between these loops is maximum for electromagnetically coupled loops whose coupling factor is at a considerable level. The four-loop system can be further elaborated with an equivalent circuit diagram as shown in Fig. 3.3, which illustrates a hybrid system with two pairs of resonators.

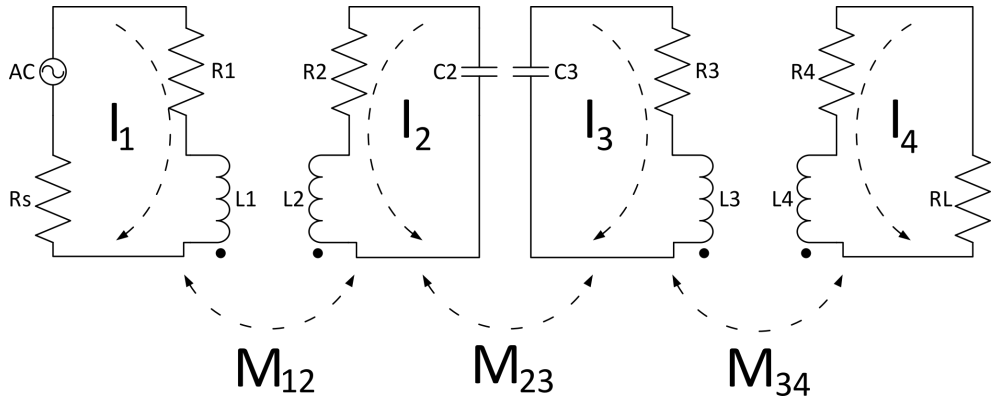

FIGURE 3.3: Equivalent hybrid SCMR and CSCMR circuit diagrams.

Based on Kirchoff's voltage law, the circuit can be derived as a four-port network model [144, 145]. The reflected voltages, can be determined as:

$$\begin{cases} V_s = (R_s + R_1 j\omega L_1) I_1 + j\omega M_{12} I_2 + j\omega M_{13} I_3 + j\omega M_{14} I_4 \\ 0 = j\omega M_{21} I_1 + (R_2 + j\omega L_2 - j\frac{1}{\omega C_2}) I_2 + j\omega M_{23} I_3 + j\omega M_{24} I_4 \\ 0 = j\omega M_{31} I_1 + j\omega M_{32} I_2 + (R_3 + j\omega L_3 - j\frac{1}{\omega C_3}) I_3 + j\omega M_{34} I_4 \\ 0 = j\omega M_{41} I_1 + j\omega M_{42} I_2 + j\omega M_{43} I_3 + (R_4 + R_L + j\omega L_4 - j\frac{1}{\omega C_4}) I_4 \end{cases} \tag{3.1}$$

which can be further simplified into a matrix form as:

$$\begin{bmatrix} V_s \\ 0 \\ 0 \\ 0 \end{bmatrix} = \begin{bmatrix} Z_1 & j\omega M_{12} & j\omega M_{13} & j\omega M_{14} \\ j\omega M_{21} & Z_2 & j\omega M_{23} & j\omega M_{24} \\ j\omega M_{31} & j\omega M_{32} & Z_3 & j\omega M_{34} \\ j\omega M_{41} & j\omega M_{42} & j\omega M_{43} & Z_4 \end{bmatrix} \begin{bmatrix} I_1 \\ I_2 \\ I_{23} \\ I_4 \end{bmatrix} \tag{3.2}$$

where the mutual inductance (M) between the two parallel loops and the magnetic flux density (B) can be expressed as:

$$B_y = \mu_0 H = \frac{\mu_0 I_y r_y^2}{2(r_y^2 + d^2)^{\frac{3}{2}}}. \tag{3.3}$$

The distance between the primary and the secondary coils is represented by d and r_y and I_y respectively indicates the loop radius and the current flow through the loop. Based on both the Ampere's law and Faraday's electromagnetic induction law, the electromagnetic induction field (H) for one of the parallel coaxial loops can be determined [26, 146], as:

$$H_y = \int \triangle H_y = \frac{I_x r_y^2}{2\left(r_y^2 + d^2\right)^{\frac{3}{2}}} \tag{3.4}$$

where I_x represents the current flow through the x^{th} loop. The mutual inductance (M) between the x^{th} and y^{th} loops including the area enclosed by the coil can be expressed as [147, 148]

$$M_{xy} = \frac{B_y A_y}{I_x} = \frac{\mu_0 H_y A_y}{I_x} = \frac{\mu_0 r_x^2 r_y^2 \pi}{2\sqrt{\left(r_y^2 + d^2\right)^3}} \tag{3.5}$$

where r_x and r_y represent the radius of the x-th and y-th loops, respectively and μ_0 denotes the permeability of free space. A_y stands in for the area of the y-th loop and can be mathematically expressed as $A_y = \pi r_y^2$.

In order to calculate M between the receiver resonator and the load loop based on the CSCMR system, which consist of two coaxial loops placed concentrically on the same plane, the magnetic field is usually attributed to the larger loop. Therefore, when the distance between the two coaxial loops is equal to 0, the mutual inductance between the two can be simplified as:

$$M_{xy} = \frac{\mu_0 r_x^2 \pi}{2 r_y}. \tag{3.6}$$

It is also important to note that $r_x \ll r_y$. A coupling coefficient between the two loops can be expressed as:

$$k_{xy} = \frac{M_{xy}}{\sqrt{L_x L_Y}}. \tag{3.7}$$

The mathematical solution of the circuit presented in Fig. 3.3 can be derived from

$$[I] = [Z]^{-1}[V] \tag{3.8}$$

Therefore, the scattering parameter S_{21}, which represents the ratio between the signal at the output port and the injected signal at the input, can be calculated as:

$$S_{21} = 2\frac{V_L}{V_S}\left(\frac{R_S}{R_L}\right)^{\frac{1}{2}} \tag{3.9}$$

where the load voltage can be written as

$$V_L = -I_4 R_L \tag{3.10}$$

By combining 3.7 and 3.9, the S_{21} parameter can be given as:

$$S_{21} = \frac{j2\omega^3 k_{12}k_{23}k_{34}L_2L_3\sqrt{L_1L_4R_sR_L}}{A+B+C+D+E} \tag{3.11}$$

where:

$$\begin{cases} A = Z_1Z_2Z_3Z_4 \\ B = k_{12}^2 L_1L_2Z_3Z_4\omega^2 \\ C = k_{23}^2 L_2L_3Z_1Z_4\omega^2 \\ D = k_{34}^2 L_3L_4Z_1Z_2\omega^2 \\ E = k_{12}^2k_{34}^2 L_1L_2L_3L_4\omega^4 \end{cases} \tag{3.12}$$

and Z_1, Z_2, Z_3 and Z_4 are the loop impedances of the four coils and can be calculated as:

$$Z_x = R_x + j\omega L_x - j\frac{1}{\omega C_x} \tag{3.13}$$

where R_x, L_x and C_x represent total resistance, the equivalent inductance and external capacitance of the x^{th} loop, respectively.

For the system to work at maximum efficiency, resonant frequency (f_0) is calculated as:

$$f_0 = \frac{1}{2\pi\sqrt{(LC)}} \tag{3.14}$$

It is also important that the Q of the transmitter and the receiver resonators are high, to reduce coil losses [144]. The Q of the y^{th} loop can be expressed as:

$$Q_y = \frac{\omega_0 L_y}{R_y} \tag{3.15}$$

where ω_0 denotes the angular frequency, which can be calculated as $\omega_0 = \omega_y = 1/\sqrt{L_y C_y}$ in terms of $[rad/s]$. Based on the above mathematical analysis the values of the loops elements for a maximum transfer efficiency are calculated and presented in Table 3.1.

TABLE 3.1: Calculated values of the loop elements.

Resistance	Capacitance	Inductance	Radius
R_1 = 0.015 Ω	C_1 = 525.97 pF	L_1 = 0.929 μH	r_1= 30 mm
R_2 = 0.03 Ω	C_2 = 203.42 pF	L_2 = 2.402 μH	r_2= 30 mm
R_3 = 0.02 Ω	C_3 = 661.2 pF	L_3 = 0.739 μH	r_2= 30 mm
R_4 = 0.012 Ω	C_4 = 2571.1 pF	L_4 = 0.19 μH	r_4= 5 mm
R_S; R_L= 50			

3.2 Numerical Analysis

SCMR based WPT has been proposed recently to overcome the limitations of IWPT such as poor efficiency, and limited range. Both IWPT and SCMR function on the same principle, despite higher operating frequencies and the high-Q allow the SCMR based systems to transfer power over larger distance compared to IWPT, at higher efficiency. Similarly, both CSCMR and SCMR share the same operating principle, yet the coil geometry slightly varies, allowing CSCMR to have a further compact system design. Particularly geometrical parameters of the loops have a strong impact on the efficiency of both the CSCMR and SCMR systems.

Based on the mathematical analysis, an experimental model has been designed with circular shaped loops. The oscillating frequency of the loop is calculated as $7.2MHz$, given the maximum operating distance to be $12mm$. The radius of the source loop is determined as $30mm$, where the transmitter and the receiver resonator loop, $(r_1 = r_2 = r_3)$, were calculated from (3.5) and (3.6) respectively.

The system will achieve the maximum distance when the k between R_X and load loops (k_{34}) is equivalent to 0.1 [149]. To ensure that the k (k_{34}) matches the above requirements, the equivalent radius of the load loop (r_4) was calculated from (3.6) as $5mm$. The inductance of the load loop was calculated as $L_4 = 0.19\mu H$. In addition, accuracy of Q requirement between the two loops is fulfilled, if the inductance of R_X is set to $L3 = 0.739\mu H$. With (3.14), the capacitance of the the R_X loop can be obtained as $C3 = 661.2pF$, so that the required loop resonating frequency is achievable. Similarly, the inductance of the T_X loop (L_2) was set at $2.402\mu H$ to ensure that the coupling factor and the Q requirements are met. The desired capacitance of the transmitter resonator loop was calculated as $C_2 = 203.42pF$, from (3.14), to ensure that the requirements for resonant frequency is met. The estimated values of the loop elements, are presented in Table 3.1.

Fig. 3.4 indicates that the system obtained maximum efficiency of 84%, when the distance between the transmitter and the receiver resonator is equivalent to $12mm$. Particularly in this scenario, the distance between the source and transmitter resonator loop is equal to $3.4mm$, and therefore, the k (k_{12}) is equal to 0.1.

Fig. 3.4 also illustrates the frequency splitting phenomenon which has a crucial impact on the system efficiency, when the load power split from a single peak to a double peak. Moreover, splitting frequencies are not equivalent to the resonant frequency and the observed splitting frequencies during the simulation is $7.15MHz$ and $7.25MHz$. The phenomenon can be further caused by the increasing coupling factor between the receiver and transmitter resonator loops when the distance between them (d_{23}), decreases to a critical point.

Hence, both higher and lower frequencies generate distinct H causing distinct k, which result in different efficiencies. For this reason, most practical yet highly controlled systems tend to employ the lower frequency as the operating frequency. Given that the relationship between transfer power and efficiency in (3.9), the notion of frequency splitting can be summarised in respect to the frequency characteristic of transfer power. Like the maximum system efficiency is attained at natural resonant frequency, while the maximum transfer power at the two splitting frequencies.

Analytical model was used to evaluate the impact on the overall system efficiency due to the alternations of the distances d_{23} and d_{12}. In addition,

it was further reviewed how the impact can be used to maintain the maximum efficiency at various distances between transmitter and receiver resonator without altering the transmitting frequency.

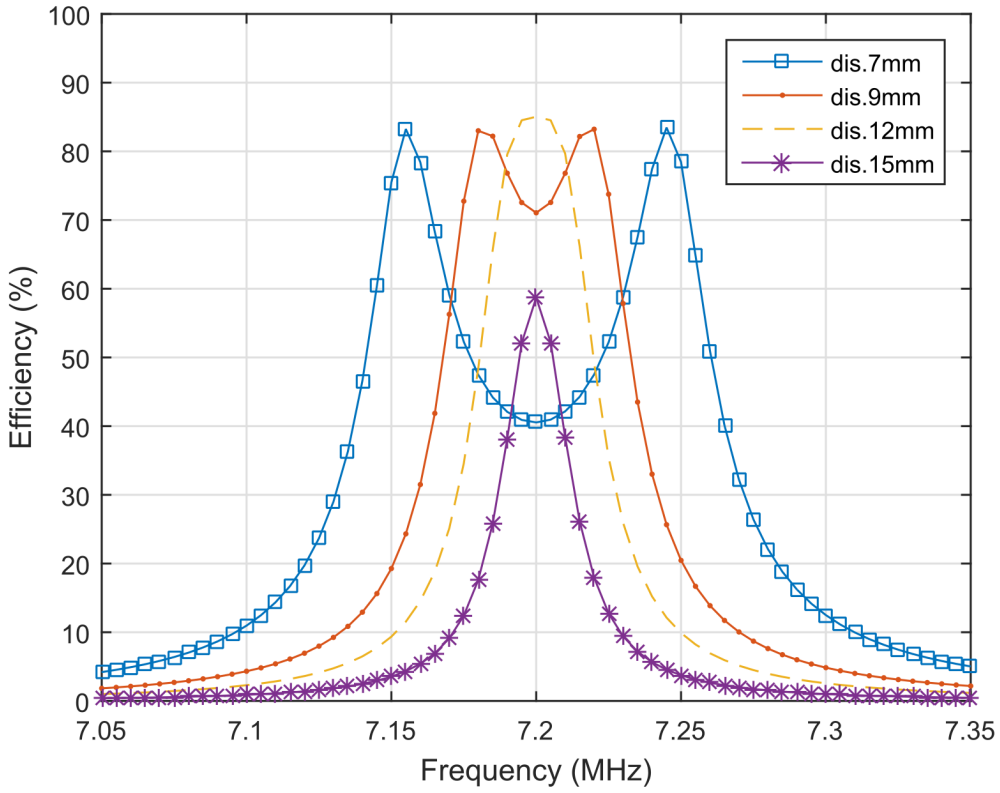

FIGURE 3.4: Maximum distance and frequency splitting phenomenon of the calculated system.

From Fig. 3.4, it is also evident that the maximum efficiency appears when the distance between transmitter and receiver resonator loops is equal to 12 mm, and therefore, the coupling factor between them can be calculated as $k_{23} = 0.0045$, using (3.5) and (3.6). The coupling factor between the source loop and T_X is equal to 0.1. From the two known coupling factors, the relationship between distances d_{12} and d_{23} can be calculated from (3.5), (3.6) and (3.7) as:

$$\frac{k_{12}}{k_{23}} = \frac{\left(\frac{\mu_0 r_1^2 r_2^2 \pi}{2\sqrt{\left(r_2^2+d_{12}\right)^3}}\right)\sqrt{L_2 L_3}}{\left(\frac{\mu_0 r_2^2 r_3^3 \pi}{2\sqrt{\left(r_3^2+d_{23}\right)^3}}\right)\sqrt{L_1 L_2}}. \tag{3.16}$$

After substituting all of the known variables into (3.16), the relationship between the distances d_{12} and d_{23} can be derived as:

$$d_{12} = \frac{0.355689 r_2 d_{23} L_3^{(\frac{1}{6})}}{r_1^{(\frac{1}{3})} r_3^{(\frac{2}{3})} L_1^{(\frac{1}{6})}}. \tag{3.17}$$

The relationship between the distances as described in Eq. 3.17 is simulated in MATLAB, and the obtained results, are presented in Fig. 3.5. It is evident that the relationship between d_{12} and d_{23} can be obtained via the afore-stated mathematical function, the maximum power transmission of the SCMR system can also be achieved at a comparably shorter distance than the system's maximum range. Eminently, the transmission frequency remains unaffected within the whole transmission range, which eliminates the necessity of matching circuits and tuning capacitors [150]. Fig. 3.6 represents the maximum efficiency of the system, if a different load and source resistances are applied. Given the resistance of the source does not have a big impact on the maximum efficiency, the impact of increasing the load resistance is more significant. In order to improve the performance, where the impedance of the source loop does not match the impedance of the load loop, various impedance matching techniques can be used [151, 152]. However, the matching algorithms are not compulsory in this study since this experiment was carried out using a signal generator and a spectrum analyser with 50Ω input source and the load impedance.

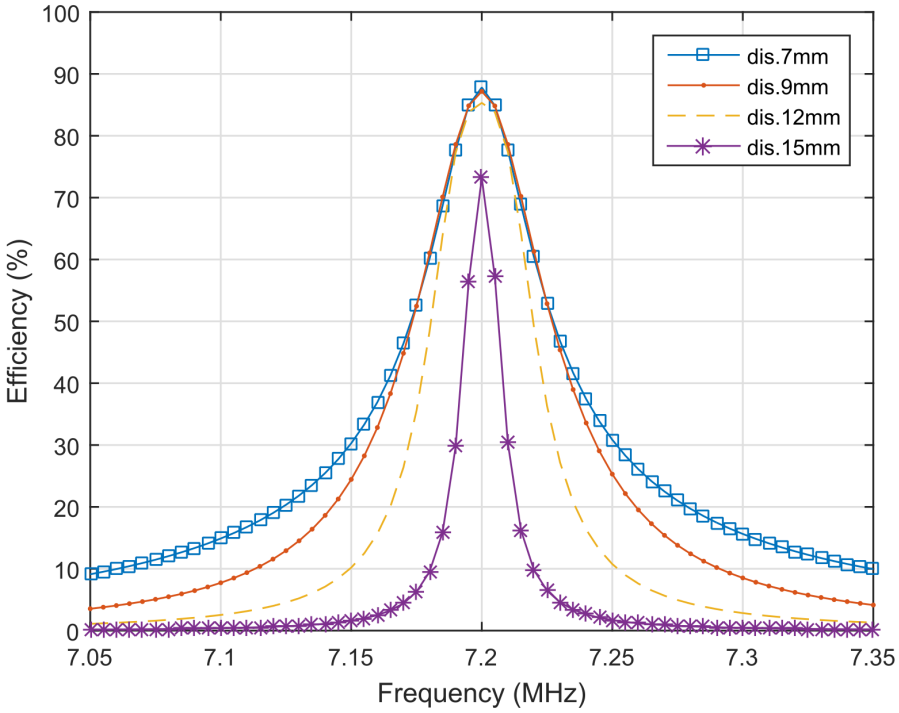

FIGURE 3.5: Simulated efficiency of the hybrid system using (3.17) for the distance (d_{12}).

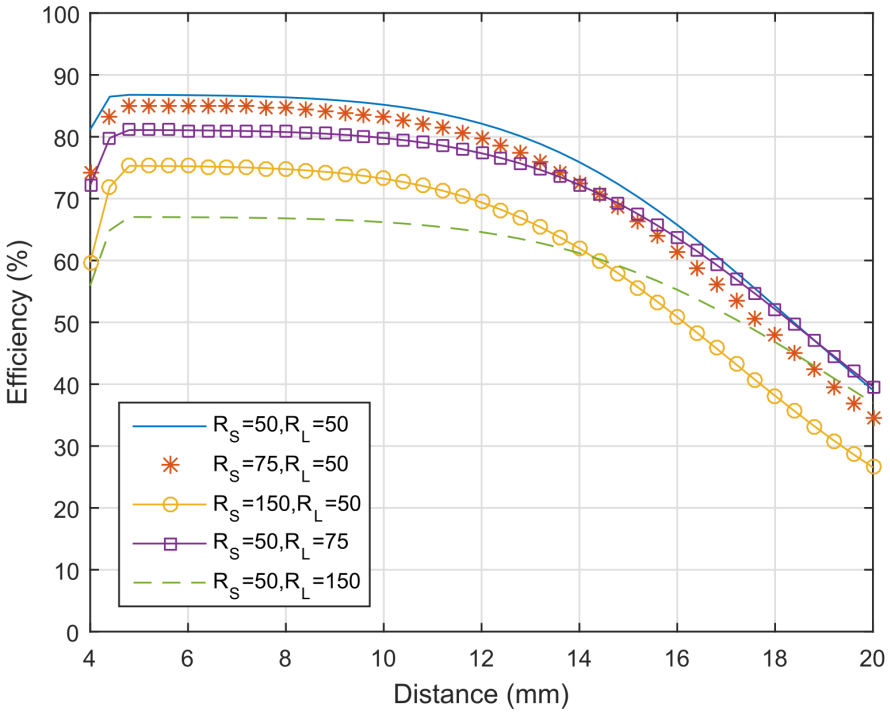

FIGURE 3.6: Maximum efficiency simulated results if the source and load resistance varies at $7.23MHz$.

3.3 Experimental Setup

In this section, an experimental set-up is presented and is then utilized to explore the impact of various system parameters on the performance. In order to verify the calculated results, an appropriate system was built to comply with the calculations' model. The two loops forming the transmitter have the same size forming the SCMR system, and the other two loops are embedded, forming the CSCMR receiver, as shown in Fig. 3.7.

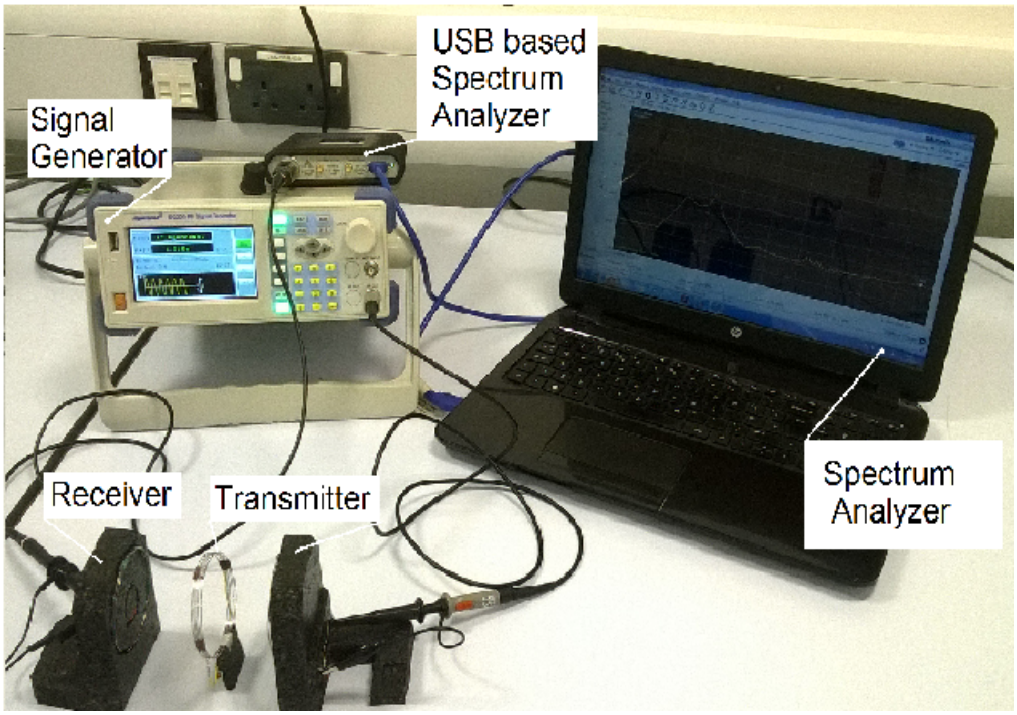

FIGURE 3.7: Practical implementation of the combined CSMR-SCSMR approach.

3.3.1 System Design and Measurement

The transmitter consists of both the source and transmitter resonator loops, and their characteristics can be seen in Table 3.1. The length of inductor wires has been calculated from Eq. 2.12, therefore, the source loop is made of a 2.3 turns of silver-plated insulated copper wire, while the transmitter resonator loop is made of the same wire which contains 5 rotations. The receiver side of the system is made using the same wire where the receiver resonator loop contains 1.6 turns, and the load loop is made of 1.2 turns of the wire. Ceramic capacitors were used to adjust the loops to the same oscillating frequencies.

For measurement purposes, a signal generator was used to send various frequencies to the source loop, while the response was measured using a USB base spectrum analyser. The power generated by a signal generator was 10dBm. The system's efficiency drop was calculated contrasting the system's output power measured with the spectrum analyser and the transmitted power of the signal generator. Finally, the measurement results were displayed using computer-based software communicating with the spectrum analyser.

3.3.2 System Maximum Efficiency

According to the calculation as shown Eq. 3.17, an optimal design of the system presented in Table 3.1, appears when the distance d_{12} is equivalent to $3.4mm$. In this scenario, the maximum efficiency can be achieved when the distance d_{23} is equivalent to $12mm$ as presented in Fig. 3.2. The graphical representation as shown in Fig. 3.8, has been plotted using the measurements where it exhibits the maximum efficiency at a distance equal to $12mm$. The obtained maximum efficiency of the experimental set-up is 79%, which is highly compatible to the 84% calculated efficiency in Section 3.2. The deviation between the results can be attributed to the coil displacements, coil geometry and variation in the electronic components.The lab instruments used during the testing process, can also have an impact on the experiment due to lack of equipment calibration.

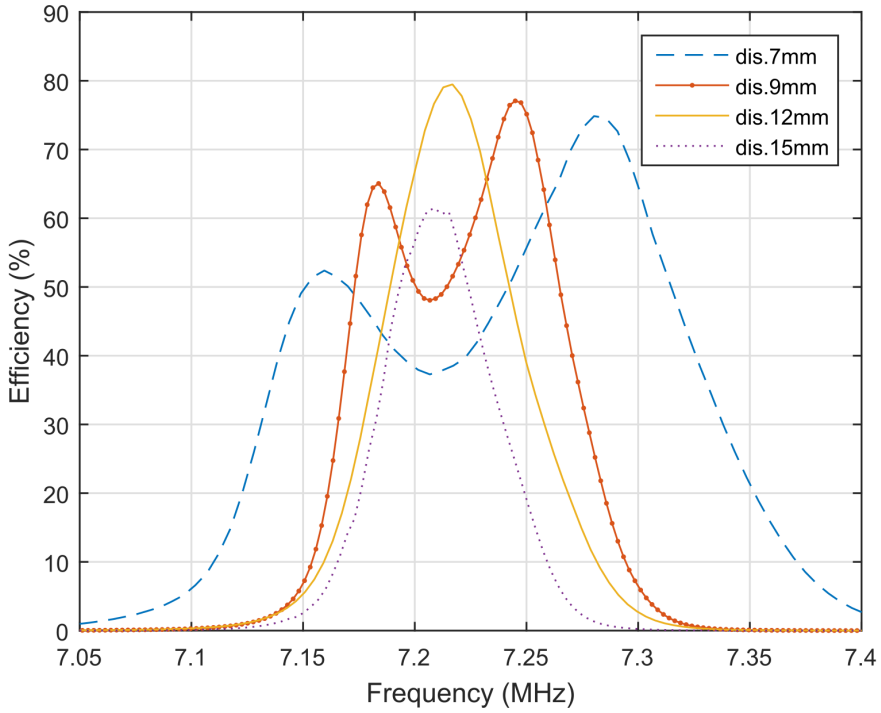

FIGURE 3.8: MATLAB converted results in transmission efficiency (%).

Based on the comparison between the measurements and the calculations, the designed system consists of a resonant frequency 20kHz higher than the calculated one and it also appears to be at 7.22MHz, as shown in Fig. 3.9. The difference in the oscillating frequencies between the calculated and measured systems appears due to the tolerance of the elements that are used in the practical application and mathematical formula approximation. In addition, the inductors that were used to fulfil the experimental purpose may also have tolerance values than the calculated values.

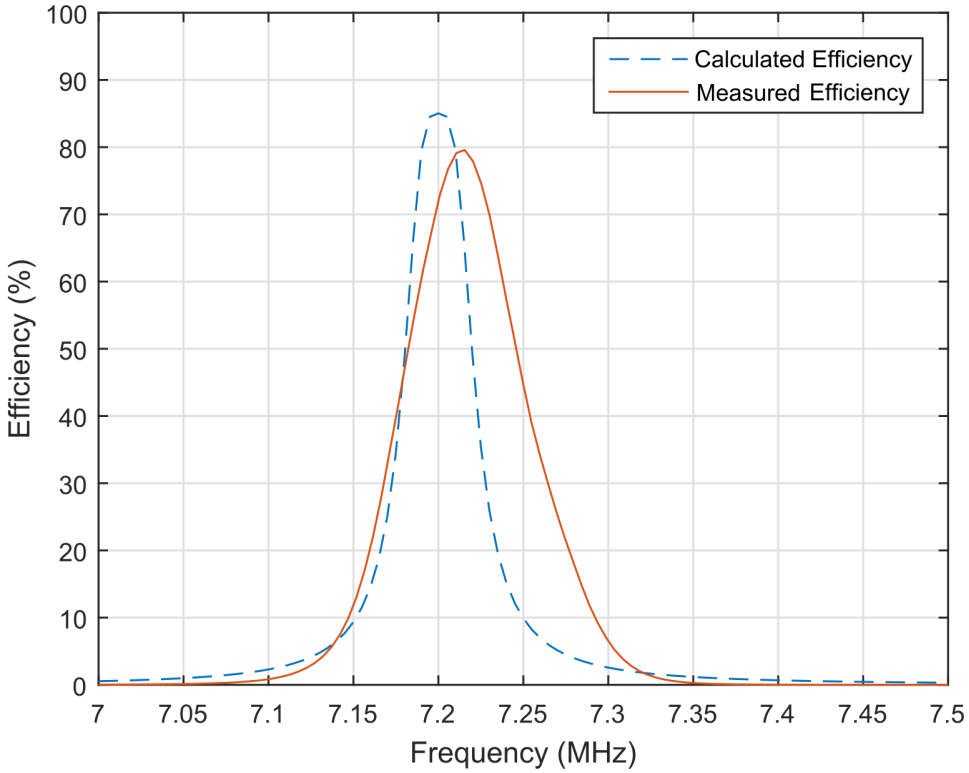

FIGURE 3.9: Frequency misalignment between the mathematical model and the experimental setup at the distance $d_{12} = 3.4mm$ and $d_{23} = 12mm$.

3.3.3 Combined System Efficiency

In order to achieve the maximum efficiency, the distance between the source loop (S) and T_X has to be adjusted according to the distance between the T_X and R_X loops as calculated in (3.17). As presented in Fig. 3.10, the displacement Δd_{23} between the T_X and R_X loops was compensated by adjusting the distance between S and Tx for Δd_{12} in order to achieve the maximum efficiency. The R_X loop in Fig. 3.10 represents the T_X with the embedded load loop, and d_{23max} represents the maximum distance between the transmitting and receiving loops. Fig. 3.11 illustrates a set of measurements commissioned via a combined CSMR-SCSMR system, which exhibits the maximum efficiency over longer distances.

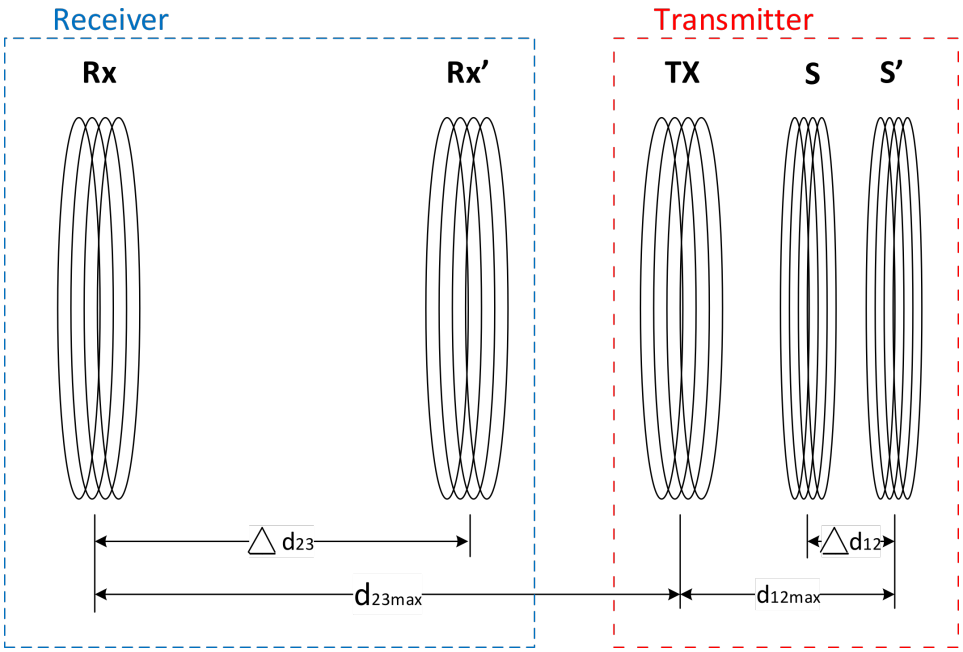

FIGURE 3.10: Maximum efficiency measurements setup.

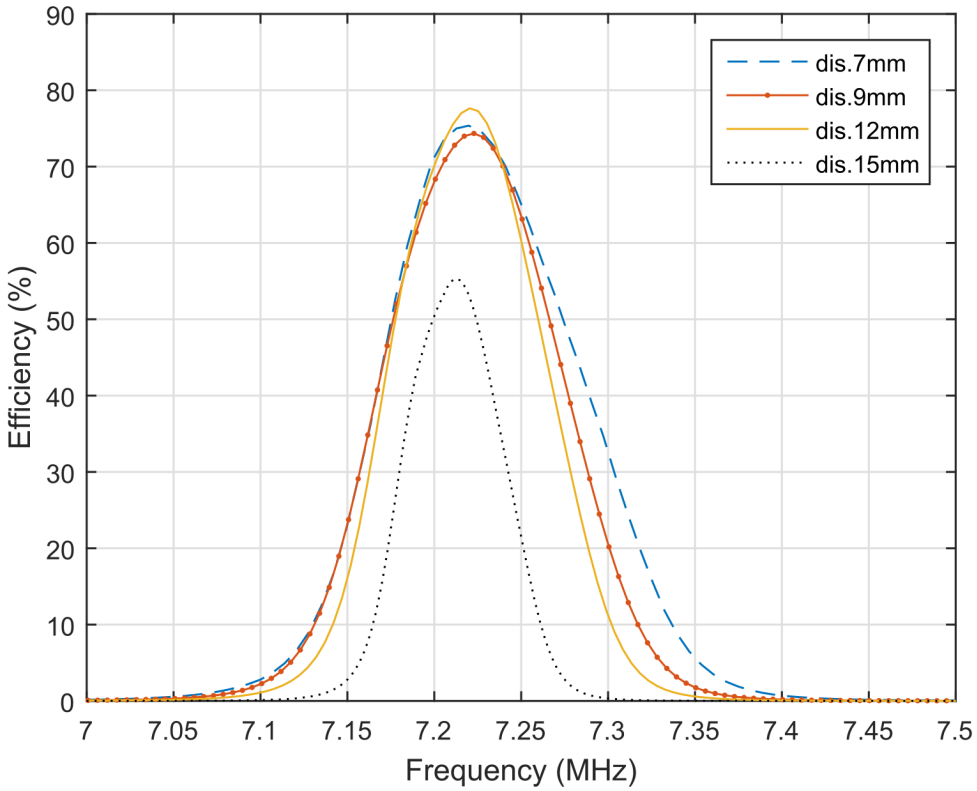

FIGURE 3.11: Measured combined SCMR-CSCMR system the holding maximum efficiency at a frequency of 7.23 *MHz*.

In order to justify the calculated results, the maximum distance d_{12} was

measured at the point where the system demonstrated its maximum efficiency along with the random distance d_{23}. A numerical comparison between the measured and calculated results is presented in Table 3.2.

TABLE 3.2: Comparison between the measured and calculated distances (d_{12}) and variation between the two in %.

d_{23} (mm)	Calculated d_{12} (mm)	Measured d_{12} (mm)	Variation (%)
3	1	1	0
4	1.3	1	23
5	1.6	1.5	6.2
6	1.9	1.8	5.2
7	2.2	2	10
8	2.5	2.3	8
9	2.8	2.6	7.1
10	3.1	2.9	6.4
11	3.4	3.2	5.8
12	3.7	3.6	2.7
13	4	4.1	0.4
14	4.3	4.5	4.6
15	4.6	4.9	6.5
16	4.9	5	2
17	5.2	5.3	1.9
18	5.5	5.6	1.8
19	5.8	5.9	1.7
20	6.1	6.1	0
21	6.4	6.1	4.6

Fig. 3.12 shows a graphical presentation of a comparison between the random distance d_{23} and the measured value of d_{12} against the calculated value, d_{12}.

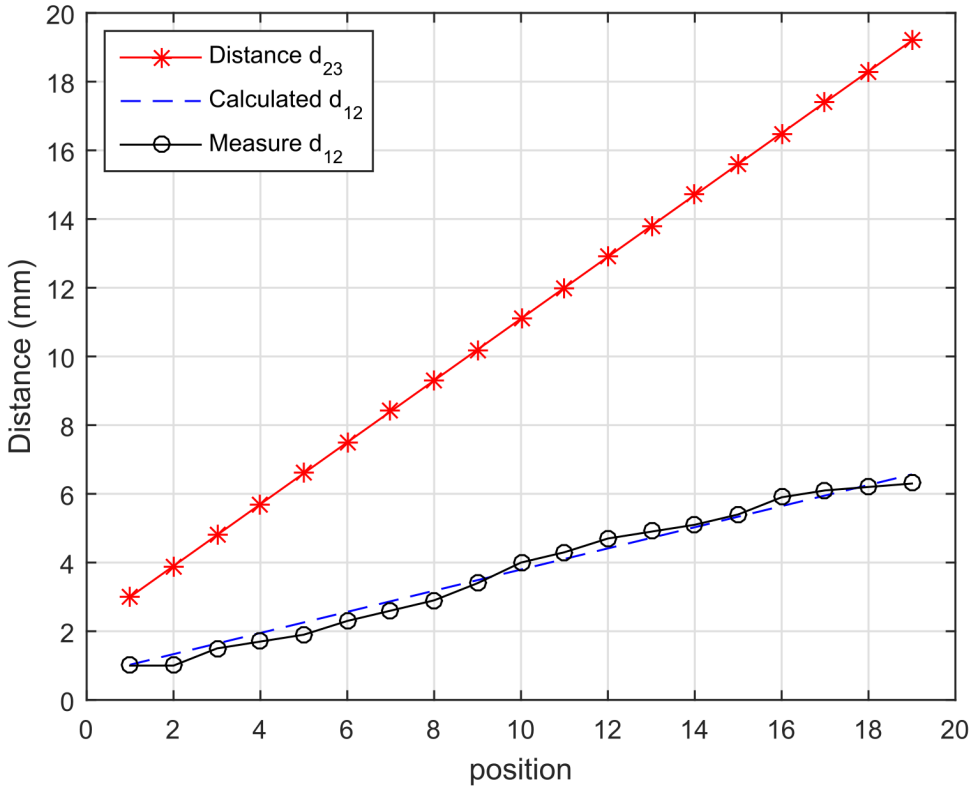

FIGURE 3.12: The relationship between the distances d_{12} and d_{23} and a measured distance d_{12}.

The maximum efficiency of the system was measured by positioning the transmitter at various distances with regards to the receiver, while the distance between the transmitter loop and source loop being adjusted accordingly. In Fig. 3.13, the measured efficiency is compared to the calculated one of the system for multiple random distances, which fits well with the calculated pattern of d_{12} adjustments. It is also evident that the system could demonstrate further higher efficiencies than the obtained maximum efficiency, at shorter distances than the higher distance. The dissimilarities between the measured and mathematically calculated results are also demonstrated in Fig. 3.13. Even though the it was aimed to minimise the parameter variations, clearly the difference was caused due to the variety of the parasitic components which were used for the proposed design. It is also important to note that the inductivity of the air-cored inductor varies upon the spacing variations between the windings. Therefore, the coils' inductivity may slightly change during the measurements. However, the existing small variation in the value of the components may cause efficiency degradations of the system.

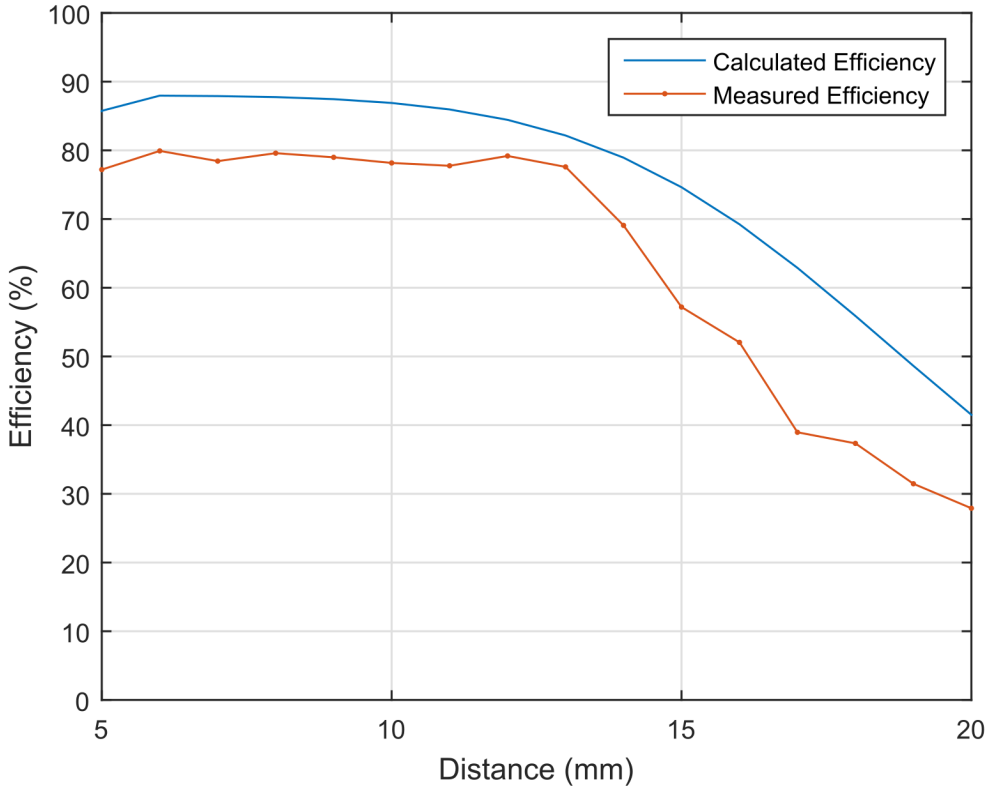

FIGURE 3.13: Comparison between the calculated and measured efficiencies of the system at 7.23MHz.

3.4 Angle and Misalignment

3.4.1 Angle Coverage

The position angle of the transmitter and receiver is also another crucial factor that may impact the system efficiency. In order to measure the efficiency, the angle of the receiver was constantly changed according to the angle of the transmitter, which varied between 0° and 90°, as illustrated in Fig. 3.14. The position of the receiver was also placed at various distances according to the transmitter. For instance, as shown in Fig. 3.10, Δd_{23} indicates the change of the distance between the R'_X to the previous R_X position, which is 1mm. d_{23max} indicates the distance between the final R_X position and the T_X, which is 20mm for our measurements.

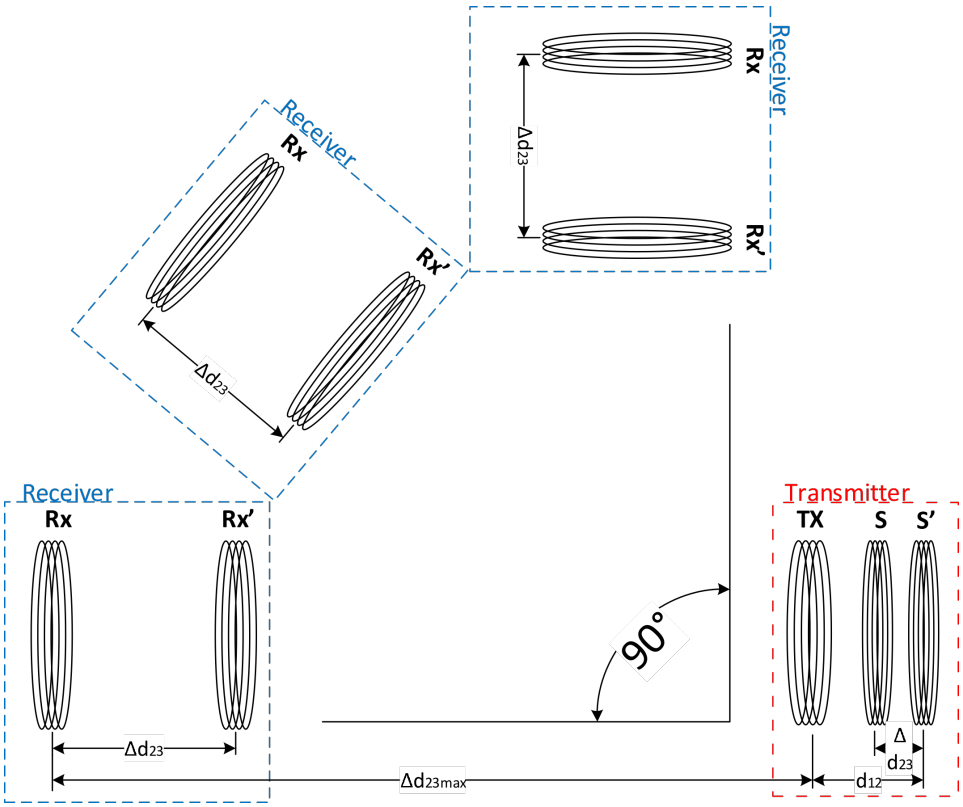

FIGURE 3.14: Positioning of receiver for the measurement of angle efficiency.

Simultaneously, the distance between the T_X and S was adjusted (Δd_{12}) according to the changes made, distance-wise between the T_X and the R_X (Δd_{23}); see Fig. 3.14. This further indicates the changes made to distance d_{12} to achieve the highest efficiency according to the previous measurements. The receiver placement was changed for 30° according to the previous measurements, and the measurement was repeated for new alignment.

As Fig. 3.15 indicates, the maximum efficiency drops in accordance with the angle at which the transmitter is being placed. The greater the angle between transmitter and receiver, the lower the efficiency of the charger, and vice versa. It can also be seen that the angle above 30° highly affects the charging efficiency, as well as the distance at which the charger operates. Furthermore, the angle above 60° reduces the working range of the charger to a few millimetres and drastically decreases the efficiency.

From the measurements, it is evident that for the charger to have high efficiency and the highest possible distance covered, the angle placement must be lower that 30°.

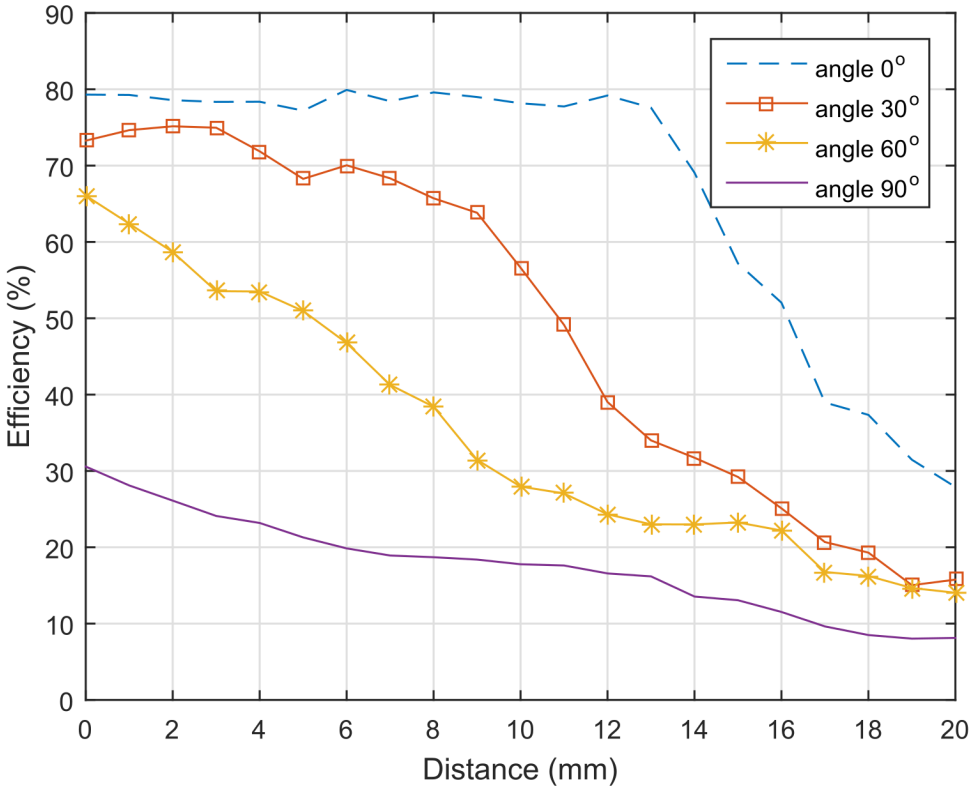

FIGURE 3.15: Measured angle efficiency of the combined system for various angles between transmitter and receiver at $7.23MHz$.

3.4.2 The Impact of the Coils' Misalignment

Misalignment and angle alignment also play a crucial role in the efficiency of WPT systems. For instance the authors in [153, 154] and [155] explored the impact of the misalignment and angle alignment on the two coils which are magnetically coupled in a resonant wireless power system. In addition, this study proposed algorithms capable of adjusting the transmitting frequency to achieve maximum efficiency. Moreover combining the two systems will simultaneously reduce the bulkiness of the receiver coils while enhancing the spatial freedom at the transmitting end.

A misalignment between the transmitter and receiver coils also plays an important role of relevance to the system efficiency. As presented in Fig. 3.16 the measurements were carried out by changing the position of the coverage between the transmitter and receiver loops from 100% coverage down to 10%. The measurements were commissioned at $0°$, $30°$, $60°$ and $90°$ misplacement. The distance between T_X and R_X was also altered by $\Delta d_{23} = 1mm$, up

to d_{23max}, which was equal to $20mm$. The distance between T_X and S was also altered accordingly by Δd_{12}, in order to maximize the system efficiency.

As for the angle covered, the efficiency drops according to the misalignment that occurred. Interestingly, the effect on the efficiency due to the misalignment was indicated as up to 60°, which does not seem to have massively impacted the overall system efficiency. However, over 60° misalignment within the coil structure has degraded the system efficiency drastically while misalignment over 90° has caused severe efficiency drops.

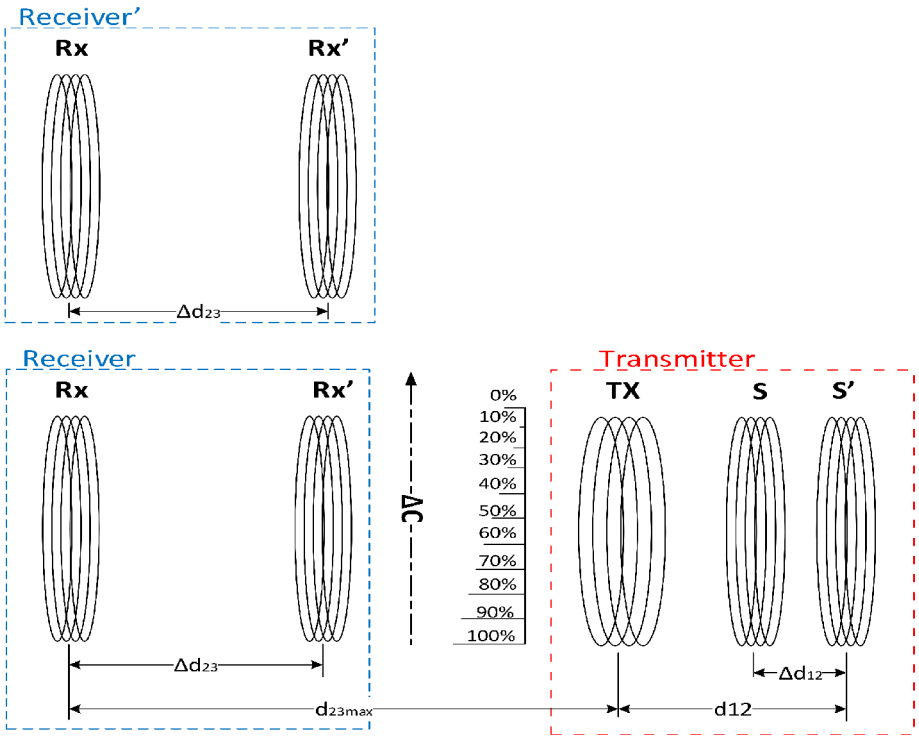

FIGURE 3.16: Positioning of the receiver for the measurement of the misalignment efficiency.

3.5 Charger Efficiency Based on the Measured Results

The proposed wireless power charger design is based on real-time measurements. The charger efficiency is highly sensitive to both coil misalignment and the change of angle between the transmitter and receiver. Moreover, the charger efficiency possesses an inverse relationship with the misalignment and the change of angle. Moreover, the charging efficiency maintains

an inverse relationship with the coil misalignments and the change of angle. Particularly, wireless charger demonstrates its highest efficiency while the maximum distance between the transmitter and receiver is set at $12mm$ with an angular misalignment of 20%. Based on the experimental results in Fig. 3.17, a 50% misalignment may cause approximately 15% of an efficiency drop. From the previous calculation, it can be shown that the starting distance between T_X and R_X will be $5mm$.

The charger transmitter circuit adjusts the distance between the source and transmitter loops to fulfil the changing position requirements of the receiver. However, in order to perform the charging efficiently, the charger must be capable of adjusting the angle to reach the receiver, as shown in Fig. 3.18.

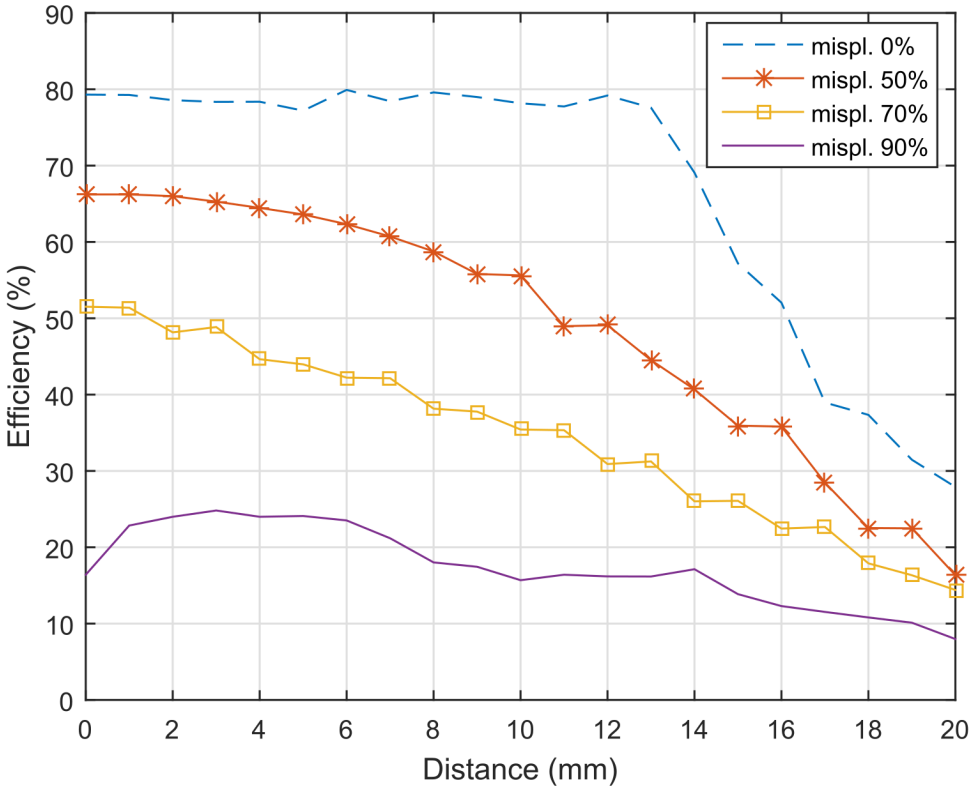

FIGURE 3.17: Measured misalignment efficiency of the combined system for various positions of the receiver at $7.23MHz$.

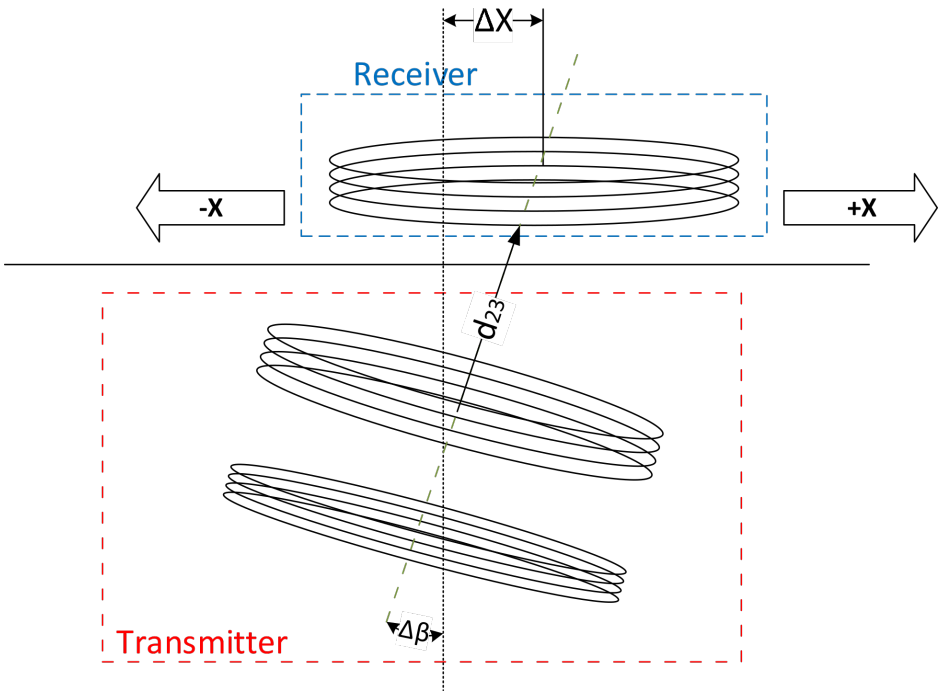

FIGURE 3.18: Diagram of the proposed WPT charger system.

From Fig. 3.19 it is shown that the proposed system exhibits a tolerance of misalignment up to a 50mm radius within the charging pad where the efficiency remains at or above 60%. According to calculations, the efficiency at a 50mm displacement will be 67.6%, while the efficiency at full coverage is just above 79%. Likewise, the overall efficiency loss remains in the range of 10%, providing more flexibility, allowing the device to be charged efficiently within the 50mm radius. The proposed system shows significant improvement in maximum efficiency compared to the maximum efficiency of two loop system [156], where the systems maximum efficiency reaches 72%. Fig. 3.19 illustrates a comparison between the efficiency of the conventional 2-coil system and the proposed system. It is cogently clear that the proposed system consistently exhibits significantly better performance, whereas the efficiency has a lesser negative impact as the distance between elements increases. In contrast to the work proposed in [157], where the efficiency dropped by 20 % when the angle between the transmitter and the receiver reaches 30^{o}, here in proposed method indicates significant improvements with an efficiency drop of 10% under the same circumstances.

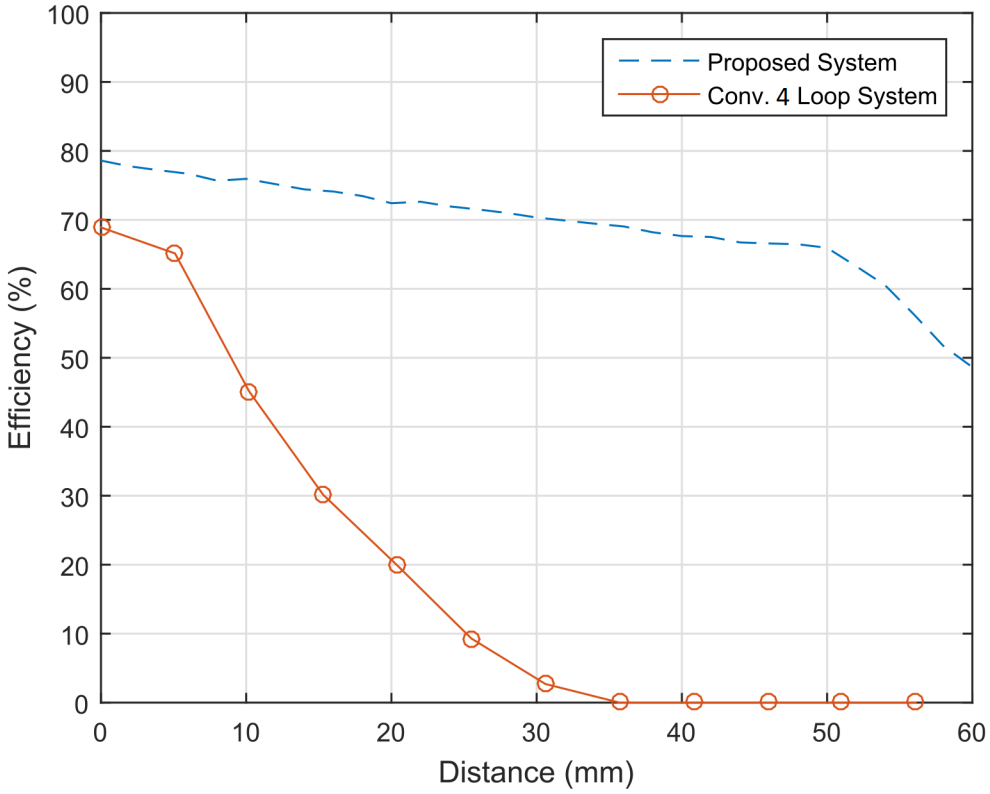

FIGURE 3.19: The proposed charger efficiency after the consideration of misalignment from the centre of the transmitter and angle at 7.23MHz.

At this end, it is worthwhile mentioning that the proposed system may not be always the best option in practical implementations due to its size. However, the improved efficiency and extended operating bandwidth of this system can minimise the size issue. The other attractive advantage of the proposed configuration is its ability to perform well over shorter distances, which is a main drawback of other existing coil resonant systems.

3.6 Chapter Summary

In this chapter a comprehensive analysis of the merged SCMR-CSCMR system supported by the challenges and advantages. Simulated results have been used to support the negative impact on overall system efficiency, due to the varying distance between the transmitter loop and the receiver. With the meticulous distance variations between the source loop and the transmitter resonant loop, system functions at its maximum efficiency. This is achieved at the same frequency as the system's resonant frequency at maximum distance. The key benefit of the system is that the system transmitter performs

sufficiently well enough eliminating a variable frequency power source, simultaneously depreciating the manufacturing costs. The proposed design in this case would attract more applications where the charging systems will be less expensive. Broad range of EV, particularly distinct heights can be charged using the same WPT charging system at its maximum transfer efficiency. The coil alignment of the receiver end complies with the CSCMR hence the proposed design further reduces the size of the receiver. In addition, novel approach also improves the flexibility of the transmitter system, allowing the WPT system to optimise the efficiency with minimum misalignments between the transmitter and receiver. Simulated results have been compared extensively with experimental results which indicate the resemblance between two models. Furthermore, proposed concept offers accelerated degree of freedom for flexible charging. In this case, receiver position can be tweaked to enhance the maximum efficiency without employing multiple coils or adjusting the frequency.

Charging efficiency and the flexibility can be further enhanced by using the system as a part of a multiple coil charger. Results suggest that the proposed system is strongly able to attain higher efficiencies compared to the frequency matching technique, being further close to the maximum efficiency. This further elaborates that the system performance was least affected by either the combined SCMR-CSCMR method or by the distance adjustments between the source loop and transmitter resonator.

Chapter 4

Miniaturization of Two-Loops Strongly Coupled Magnetic Resonance Wireless Power Transfer System

THE way to reduce the size of the WPT system has gained widespread interest among researchers, due to the significantly fast-growing market interest in being included in relatively smaller electronic applications and escalating system limitations in real time conventional applications. There have been numerous research attempts towards the reduction of the coil size while achieving higher efficiency [158, 159]. In [160], embedded loops in an SCMR system have been suggested by the authors. Likewise, Conformal SCMR (CSCMR) system suggests a significant size reduction of the four-loop systems. Authors in [161] have also suggested using metamaterial arrays and a three-coil system to further decrease the size of the receiver. In addition, series-series connected resonant capacitors with a double current rectifier, has been proposed in [162]. Furthermore, the authors showed that this method can be used to simultaneously minimise the current in the secondary coil while the physical parameters of the coil are being reduced. Hence significant reduction of 38% of the total coil weight [163], in case where a selective harmonic approach of the transfer frequency was used.

This chapter presents an investigation of the feasibility of introducing a new set of inductors to the existing transmitter and receiver, to further diminish their size. While the new technique reduces both the size and the overall weight of the coils, with minimum compromise in efficiency. Particularly, this approach further reduces the excessive material which is used for the circuitry, simultaneously minimising both the production costs and weight. With regards to the coil geometry, the resonant WPT system will be

more desirable for both EV and hand-held applications where such a coil can be physically accommodated.

An experimental model was built to validate the analytical results. In order to achieve higher efficiencies at greater range, coils are required to have characteristics such as High Q factor and a stronger k. Q factor can be calculated from Eq. 2.9 where high Q values above the 100 are considered and the values below 100 are considered as low Q factors [164]. High Q is not necessarily an indication of high k, specifically in this case if the T_X and R_X coils are not equally sized. In fact, both the size and coil geometry significantly impact both Q and k separately. The results exhibit that this approach, allows the newly formed WPT circuit to reach its maximum efficiency at similar or lesser coupling factor, as the circuit with the coils are of high Q. Results demonstrate that the proposed system is able to achieve similar efficiencies as a system with larger coils at similar distances, interestingly with further size reduction and weight. This further pinpoints that the high Q of the system can be achieved without higher inductive coils and specifically, lower value capacitors.

The rest of the chapter is organised as follows. Section 4.1 elaborates the proposed WPT model and a thorough mathematical analysis with an insight into the subject has been provided, supported by multiple theoretical equations. System specifications and the calculations are presented in Section 4.2. In Section 4.3, the experimental parameters and the system configuration are described in details. A comparison between the calculations and measured coupling factors, required to reach the maximum efficiency has been discussed in Section 4.4. Finally, the main conclusions of this study are included in Section 4.5.

4.1 Theoretical Analysis of Two-loop Strongly Coupled WPT System

4.1.1 Resonator Tank Design

In highly resonant WPT systems the resonators must have a high resonance factor in order to transfer energy efficiently across the gap between the transmitter and receiver coils. When two resonators are placed close to each other they form an inductive link which allows them to transfer energy via M. Therefore, the tank design is one of the key parameter of the WPT system design. The basic resonant tank designs can be seen in Fig. 4.1, and are based on

the connection between the oscillation components in the circuit. The series-series resonant coupling has capacitor and inductor connected in series in both transmitter and the receiver oscillator, while the series-parallel resonant coupling has only the transmitter oscillator connected in series and the receiver oscillator components are connected in parallel. On the other hand, the parallel-series resonant circuit has the parallel connected inductor and capacitor in the transmitter resonator while the receiver side is connected in series. Lastly, the parallel-parallel connected resonators are shown that both, the transmitter and the receiver resonators inductor and capacitor are connected in parallel.

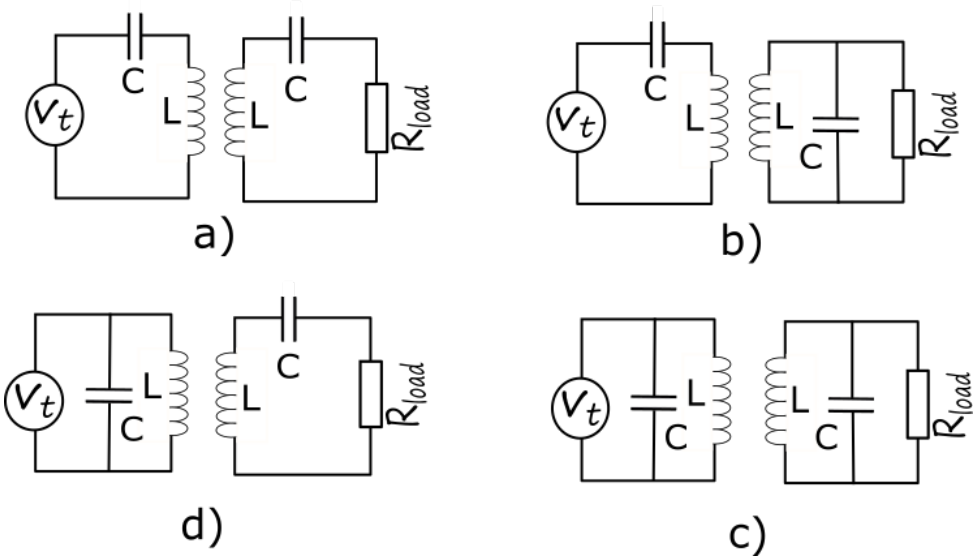

FIGURE 4.1: Basic resonat tank designs; a) series-series, b) series-parallel, c) parallel-series, d) parallel-parallel.

4.1.2 LCL Resonant Circuit

As shown in Fig. 4.2, the proposed system introduces two inductors in parallel with an existing inductor in comparison with the existing structure with a single inductor. The newly added inductors are minimised in size and are positioned in the circuit in a way to have no effect on the mutual inductance link between the transmitter and the receiver coils.

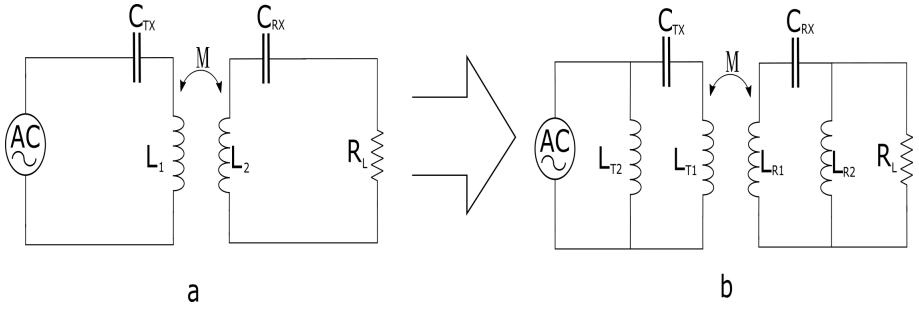

FIGURE 4.2: A comparison between the conventional WPT system with a single set of coils and the proposed technique with an additional coil.

In addition to the existing LC resonant loop, this methodology also introduces two additional inductors, one on each side of the WPT system. At the transmitter end, the new inductor L_{T2} is placed in parallel to the pre-existing LC oscillator and forms a new LCL circuit design. Akin to the transmitter side, the receiver has a new inductor attached in parallel with pre-existing LC circuit and forms a new LCL oscillating circuit on the receiver side. The two newly formed oscillators determine the oscillating frequency of the WPT circuit, at which the transmitted power will be maximised.

Although additional coils were introduced in the existing system architecture, system evidently benefits from the size reduction of the existing resonant coils. The newly added inductors help to fine-tune the coupled circuit into a strongly coupled circuit, without the conventionally expected high Q, which leads to the size reduction of both T_X and R_X resonators.

In addition, to the two inductors L_{T2} and L_{R2}, the circuit contains a frequency generator (AC) which is used as a power source and its input is a sine-wave voltage, while RG represents the internal resistance of the frequency generator. C_{TX} and C_{RX} are the transmitter and receiver capacitors which together with L_{T1}, L_{R1}, L_{T2} and L_{R2} form the LC oscillator. It is important to note that the real inductor already has some self-capacitance reduce value and therefore the loop already has its own oscillating frequency. However, in order to reduce the magnitude of the current and increase the magnitude of the voltage, compensation capacitors must be added [165].

4.1.2.1 Mathematical Analysis of LCL Resonant Circuit

The WPT circuit model of the proposed topology is presented in Fig. 4.3. To analyse the circuit, all branch currents and the voltages should be determined. At the transmitter side, the I_{IN} exhibits the input current and V_A

represents the voltage on the T-node at the transmitter. Henceforth the current I_{IN} is divided into two currents, I_2 and I_3 based on Ampere's law (I_{IN} = I_2 + I_3). At the receiver end, I_4 represents the induced current constructed due to the M between the transmitters coil L_{T1} and receiver coil L_{R1}. Thus, the induced current is further split up into two currents I_5 and I_6 (I_4 = I_5 + I_6) while V_B represents the voltage of the T-node on the receiver side. Load resistance is denoted by R_L, while reactances of the inductors are Z_{T1}, Z_{T2}, Z_{R1} and Z_{R2} and the corresponding internal resistance of the aforementioned inductors are R_{LT1}, R_{LT2}, R_{LR1} and R_{LR2} respectively. The impedance is quantified as Z_X = R_X + $j\omega$ L_X, given that the internal resistance of the inductor and inductance is respectively indicated by the L_X and R_X.

The transferred energy generally oscillates between the coil and the capacitor and the angular frequency at which the energy oscillates, can be mathematically expressed as $\omega_0 = \frac{1}{\sqrt{LC}}$. The proposed design comprises an additional coil, hence the energy which oscillates between the capacitor and the two inductive coils, can be expressed as

$$\omega_0 = \frac{1}{\sqrt{C\left(\frac{1}{L_X} + \frac{1}{L_Y}\right)}} \tag{4.1}$$

The desired oscillating frequency of the system can be further adjusted by the size of inductor and capacitor. To be specific, the distance between the transmitter and receiver coils can be further increased, with a high-quality factor. The quality factor can be derived as

$$Q = \sqrt{\frac{L_X}{C_X}} \frac{1}{R_X}. \tag{4.2}$$

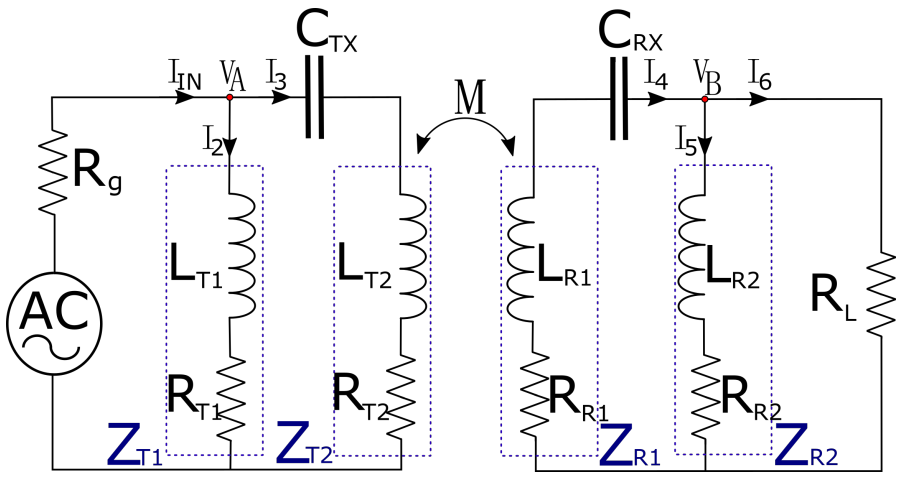

FIGURE 4.3: The circuit diagram of the proposed two-loop resonant WPT system with additional inductor. I_{IN}, I_2, I_3, I_4, I_5 and I_6 represent the currents in each branch, while the Z_{T1}, Z_{T2}, Z_R and Z_{R2} represent reactance of the inductors.

The value of the proposed phenomena can be solely discussed in terms of overall efficiency, which is a comparison between the stored energy, dissipated energy opposing the losses. High-quality factor of the resonator, is a crucial property for a high-resonant WPT system to achieve high efficiency. Given that the resonators are typically manufactured to operate in a relatively narrow frequency band which reduces their probability to interact with surrounding objects. The implication is that, to achieve a high Q, high inductance is required, which eventually increases the physical dimensions of the transmitter and receiver loops. Hence, a new design has been proposed to reduce the size of the transmitter and receiver loops sustaining the state of equilibrium. Particularly, the LCL design herein discussed, in which the inductors are placed in a favourable position, limiting the interaction between the rest of the circuit, but only the T_X and R_X inductors to interact with each other, obtaining the required results. Circuitry of the proposed system in Fig. 4.3, can be analysed via the following set of equations, a derivation of the currents using simple Ohm's law made up of M, resistance (R) and Inductance (L). Currents in the circuit can be simplified as

$$i_2 = \frac{V_A}{(R_{T1} + j\omega L_{T1})} \tag{4.3}$$

$$i_3 = \frac{V_B - (i_4 j\omega M)}{(R_{T2} + j\omega L_{T2} + \frac{1}{j\omega C_{TX}})} \tag{4.4}$$

$$i_4 = \frac{-(V_B + (i_3 j\omega M))}{(R_{R1} + j\omega L_{R1} + \frac{1}{j\omega C_{RX}})} \tag{4.5}$$

$$i_5 = \frac{V_B}{(R_{R2} + j\omega L_{R2})} \tag{4.6}$$

and the voltage V_A can be written as

$$V_A = V_{IN} - ((i_2 + i_3)R_G) \tag{4.7}$$

while the voltage V_B is:

$$V_B = (I_4 - I_5)R_L. \tag{4.8}$$

Calculations can be further simplified, if the capacitive and inductive reactance of the elements are written as

$$\begin{cases} Z_{T1} = R_{LT2} + j\omega L_{LT2} \\ Z_{T2} = R_{LT1} + j\omega L_{LT1} \\ Z_{R1} = R_{LR1} + j\omega L_{LR1} \\ Z_{R2} = R_{LR2} + j\omega L_{LR2} \\ Z_{CTX} = \frac{1}{j\omega C_{TX}} \\ Z_{CRX} = \frac{1}{j\omega C_{RX}} \end{cases} \tag{4.9}$$

Therefore, from these equations the input impedance Z_{IN} can be calculated as

$$Z_{IN} = \frac{(aZ_{T1} + bZ_{T2} + cZ_{R2} + dZ_{T1} + eR_L R_G Z_{R1} + (C_{RX}C_{TX} - M^2)R_L R_G)}{(fZ_{T2} + gZ_{T1} + hR_L Z_{R1} + (C_{RX}C_{TX} - M^2)R_L)} \tag{4.10}$$

where

$$\begin{cases} a = Z_{R2}(Z_{R1} + R_L + C_{RX}) + R_L Z_{R1} + C_{RX} R_L \\ b = (R_G Z_{R1} + (R_L + C_{RX})R_G)Z_{R2} + R_L R_G Z_{R1} + C_{RX} R_L R_G \\ c = ((R_G + C_{TX})Z_{R1} + (R_L + C_{RX})R_G + C_{TX} R_L - M^2 + C_{RX} C_{TX})Z_{R2} \\ d = (R_L R_G + C_{TX} R_L)Z_{R1} + C_{RX} R_L R_G + (C_{RX} C_{TX} - M^2)R_L \\ e = (C_{TX} R_G Z_{R1} + (C_{TX} R_L - M^2 + C_{RX} C_{TX})R_G)Z_{R2} + C_{TX} \\ f = (Z_{R1} + R_L + C_{RX})Z_{R2} + R_L Z_{R1} + C_{RX} R_L \\ g = Z_{T1}(Z_{R1} + R_L) + C_{RX} Z_{R2} + R_L Z_{R1} + C_{RX} R_L \\ h = (C_{TX} Z_{R1} + C_{TX} R_L - M^2 + C_{RX} C_{TX})Z_{R2} + C_{TX}. \end{cases} \tag{4.11}$$

The efficiency of the system η, can be denoted as

$$\eta = \frac{P_{OUT}}{P_{IN}} = \frac{i_{OUT}^2 Z_{IN}}{i_{IN}^2 Z_{EQ}}. \tag{4.12}$$

Therefore, the efficiency of the proposed circuit could be expressed as follows:

$$\eta = \frac{-M R_L Z_{R2} Z_{T1}}{k Z_{T1} + l Z_{T2} + m Z_{R2} + n Z_{T1} + o Z_{R2} + C_{TX} R_L R_G Z_{R1} + p R_L R_G} \tag{4.13}$$

where k, l, m, n, o and p are:

$$\begin{cases} k = (Z_{R1} + R_L + C_{RX})Z_{R2} + R_L Z_{R1} + C_{RX} R_L \\ l = (R_G Z_{R1} + (R_L + C_{RX})R_G)Z_{R2} + R_L R_G Z_{R1} + C_{RX} R_L R_G \\ m = (R_G + C_{TX})Z_{R1} + (R_L + C_{RX})R_G + C_{TX} R_L - M^2 + C_{RX} C_{TX} \\ n = (R_L R_G + C_{TX} R_L)Z_{R1} + C_{RX} R_L R_G + (C_{RX} C_{TX} - M^2)R_L \\ o = C_{TX} R_G Z_{R1} + (C_{TX} R_L - M^2 + C_{RX} C_{TX})R_G \\ p = (C_{RX} C_{TX} - M^2). \end{cases} \tag{4.14}$$

G is gain for the circuit and can be expressed as

$$G = M R_G Z_{T1}(Z_{T2} + C_{TX})((r)Z_{T1} + R_G V_B q Z_{R2} + R_L R_G V_B(q)) \tag{4.15}$$

where q and r can be described as:

$$\begin{cases} q = V_B(Z_{R1} + R_L + C_{RX})Z_{R2} + R_L V_B(Z_{R1} + C_{RX}) \\ r = Z_{T2}(sZ_{T1} + R_G V_B t) + (u + MR_L V_{IN})Z_{R2} + V_B z \end{cases} \tag{4.16}$$

and the s, t, u and z are

$$\begin{cases} s = (Z_{R1} + R_L + C_{RX})Z_{R2} + R_L R_G V_B(Z_{R1} + C_{RX}) \\ t = V_B(R_G(Z_{R1} + R_L + C_{RX}) + C_{TX}(Z_{R1} + C_{RX})) + C_{TX}R_L - M^2 \\ u = R_L(C_{TX}(Z_{R1} + C_{RX}) - M^2) + R_L R_G(Z_{R1} + C_{RX}) \\ z = C_{TX}(Z_{R1} + C_{RX}) + C_{TX}R_L - M^2. \end{cases} \tag{4.17}$$

4.2 Numerical Analysis of Two-loop System

The transmission efficiency and the distance at which the system achieves maximum efficiency, strongly depends on the geometrical design of the loops [166], therefore, M between the two loops is determined as:

$$M_{XY} = M_{YX} = \frac{\Psi_{XY}}{I_X} = \frac{\mu_0 H_Y A_Y}{I_X} = \frac{\mu_0 r_Y^2 r_X^2 \pi}{2\sqrt{(r_X^2 + d^2)^3}}. \tag{4.18}$$

The results obtained from both designs have been contrasted, using the behaviour that all four loops which naturally oscillate at the same frequency, have been designed to have the same inner diameter. The inner diameter of the transmitter and receiver loops were set to be approximately $72mm$ and the frequency at which they oscillate, was set at $9.23MHz$. However, as illustrated in Eq. 4.18, the inner diameter of the loops can be adapted as desired, without influencing the results. It is well understood that the quality factor directly influences the efficiency of the transmission circuit, hence if the inner diameter is reduced, the maximum efficiency of the respective circuit will remain constant, as the coupling factor between the two loops stays same as for the larger system. The remaining loops (L_{T1}, L_{R2}) have a diameter of $2mm$. However, the M between the transmitter L_{T2}, and receiver L_{R1} coils, remains unaffected.

4.2.1 High-Q Coil System Specifications

According to Eq. 4.2, the requirements which determine the Q of the coil are low resistance of the coil and a high ratio between the inductance and the capacitance. The combination of the inductor and the capacitor plays a vital role in defining the oscillating frequency. Therefore, the baseline criteria of the high Q loop properties have been calculated, via Eq. 4.1. Results obtained via the calculations, the elements used in the high Q circuit design are presented in Table 4.1. In addition, the inductance of the T_X (L_1) is set to 186.6μH for the required capacitance of C_1 =1.6pF. For the receiver loop, the inductance L_2 is set at 229.6μH while the capacitance of the receiver is C_2 = 1.3pF. The internal resistance, of the coils is 0.15Ω, given the resistance of the source and load is equal to 50Ω.

TABLE 4.1: Calculated elements of two-loop strongly coupled WPT system with high Q of coils, used to build a practical system.

Capacitance	**Inductance**	**Resistance**	**Resistance**
C_1 = 1.6 pF	L_1 = 186.6 μH	R_{L1} = 0.15 Ω	R_S = 50 Ω
C_2 = 1.3 pF	L_2 = 229.6 μH	R_{L1} = 0.15 Ω	R_L = 50 Ω

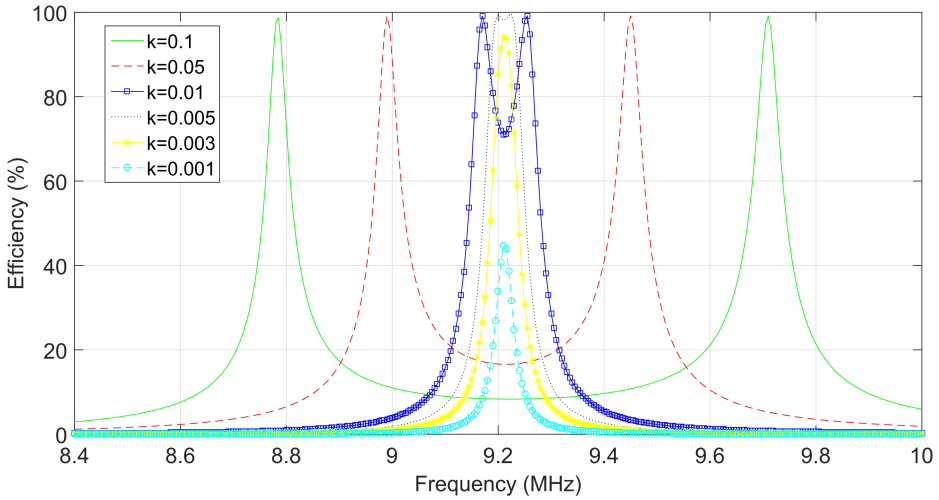

FIGURE 4.4: Calculated efficiency of the system with high-Q of the transmitter and receiver coils, built based on the value of the elements from Table 4.1.

The results obtained from the simulation of the above circuit, are presented in Fig 4.4. It further indicates that, the circuit is over-coupled if the k

between the transmitter and the receiver is 0.1 and the potential maximum efficiency appears in the frequency of $9.27MHz$. Given the coupling factor between the T_X and R_X is 0.005, the system performs at a reasonable efficiency of 97% being suitable for energy transmission. Whilst the k being further decreased, the efficiency also begins to drift accordingly. Particularly, when the coupling factor drifts down to 0.003, system efficiency also decreases to 90% and when the coupling factor is 0.001, system efficiency further decreases the to 43%.

4.2.2 Low-Q Coil System Specifications without Additional Inductor

In contrast to the high Q system, the loops in this system do not require a large capacitance and inductance ratio, as presented in Table 4.2. In order to make the system more cost-effective, standard widely available $15pF$ and $18pF$ capacitors were used in this experiment. The capacitance value for the system with Low Q coil is much higher that that of the capacitors used for high Q design, however the market price per unit is similar. Therefore, to make the loops oscillate at the same frequency as the system with high Q inductors, the T_X must have inductance of 16.37μH and 19.65μH, respectively. The resistance of the inductors is the same as the resistance of the loops with high Q, at 0.15Ω.

TABLE 4.2: Calculated base model of two-loop loosely coupled WPT system. The specification will be later used to build a practical model.

Capacitance	**Inductance**	**Resistance**	**Resistance**
C_1 = 18 pF	L_1 = 16.37 μH	R_{L1} = 0.15 Ω	R_S = 50 Ω
C_2 = 15 pF	L_2 = 19.65 μH	R_{L1} = 0.15 Ω	R_L = 50 Ω

‘

In Fig. 4.5 the calculated performance of the system is presented. As shown in this figure, the system reaches maximum efficiency when the Q between the T_X and R_X is equal to 0.05, which is far higher than the Q required to reach maximum efficiency with high Q of the coil at 0.004. The system with low Q factor reaches efficiency of 15% at the coupling factor of 0.003, which is equivalent to 81% reduction compared to the previous system.

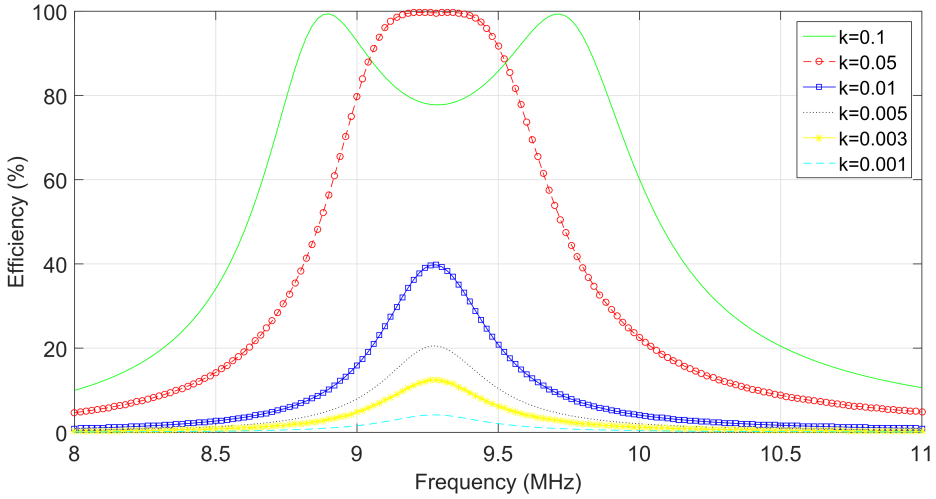

FIGURE 4.5: Efficiency of the system with low-Q factor of the coil without additional inductor, calculated with advanced design system (ADS) software. A coupling factor at which maximum efficiency appears is much higher than that for the system with high Q.

4.2.2.1 Comparisons of a Coupling Factor of Low-Q Coil System and a High-Q Coil System

As mentioned earlier, the quality of the coil affects the coupling factor needed for the system to reach maximum efficiency. In Fig. 4.6 the difference between the two systems is presented. It is evident that the system with low Q value requires higher Q to gain its maximum efficiency. However, the system designed with high Q value has its maximum efficiency at the coupling factor of 0.004 while the system with low Q coils obtains maximum efficiency when the quality factor is 0.05.

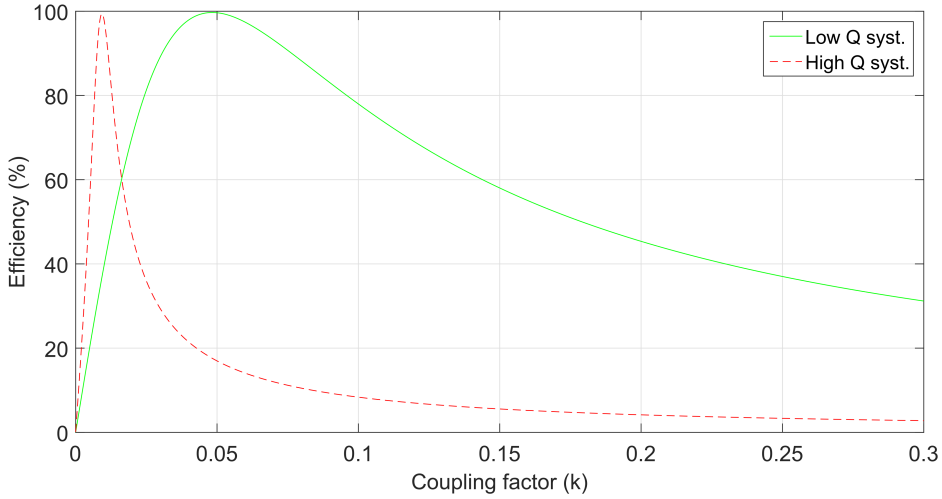

FIGURE 4.6: Comparison between the coupling factor needed for the maximum efficiency to appear for the system with low Q and high Q of the coils.

4.2.3 Low-Q Coil System with Additional Inductor

To enhance the performance of the system with low Q coils, two new inductors are introduced to the existing WPT system. The inductors L_{T1} and L_{R2} are connected in parallel with the transmitter and receiver loops, (L_{T2}, L_{R1}).

4.2.3.1 Determination of the Size of the Additional Inductor

In order to determine the size of the additional coils, the graphical presentation of the effect is presented in Fig. 4.7. It is shown that the increase of the value of the additional inductors connected in parallel to the resonator coil increases the k needed to maximize the efficiency. If $L_{T1} = 2.105\mu H$ and $L_{R2} = 2.359\mu H$, the difference between the coil with additional inductors and low Q coil is minimal. Conversely, if the additional inductors values are too small, as shown in Fig. 4.7, where the $L_{T1} = 0.02105\mu H$ and $L_{R2} = 0.02359\mu H$ are used, the maximum efficiency drops drastically.

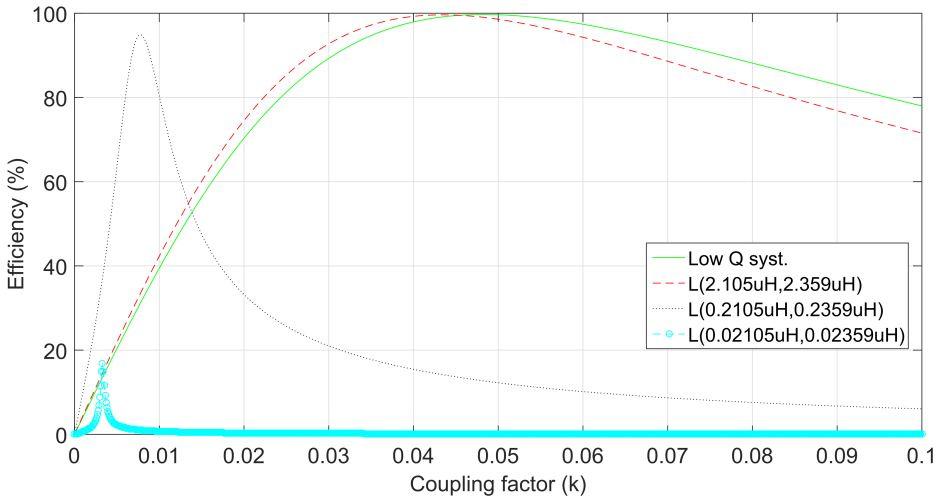

FIGURE 4.7: The effect of the different values of additional inductors on the coupling factor needed to reach maximum efficiency. The coupling factor needed to reach maximum efficiency drops with the decrease of the value of additional inductor.

The size of the additional inductors has to be chosen based on the numerical analysis. In this case, we chose to use $L_{T1} = 0.2105\mu$H and $L_{R2} = 0.2359\mu$H which offer a performance close to that of the system with high Q of the inductor, as shown in Fig. 4.8. To maintain the oscillating frequency of the system at $9.23MHz$ and to use the widely produced capacitors, a trade-off in performance is required. Therefore, the designed system reaches the maximum efficiency at $k = 0.003$, while the system with high Q factor reaches its maximum at $k = 0.004$.

TABLE 4.3: Calculated values of the elements used in the proposed model with two loop loosely coupled WPT system with a low Q of the coils and two additional inductors.

Capacitance	Inductance	Resistance	Resistance
C_{TX} = 18 pF	L_{T2} = 16.37 μH	R_{L2} = 0.15 Ω	R_L = 50 Ω
C_{RX} = 15 pF	L_{T1} = 0.2105 μH	R_{T1} = 0.15 Ω	R_L = 50 Ω
	L_{R1} = 19.65 μH	R_{R1} = 0.15 Ω	
	L_{R2} = 0.2359 μH	R_{R2} = 0.15 Ω	

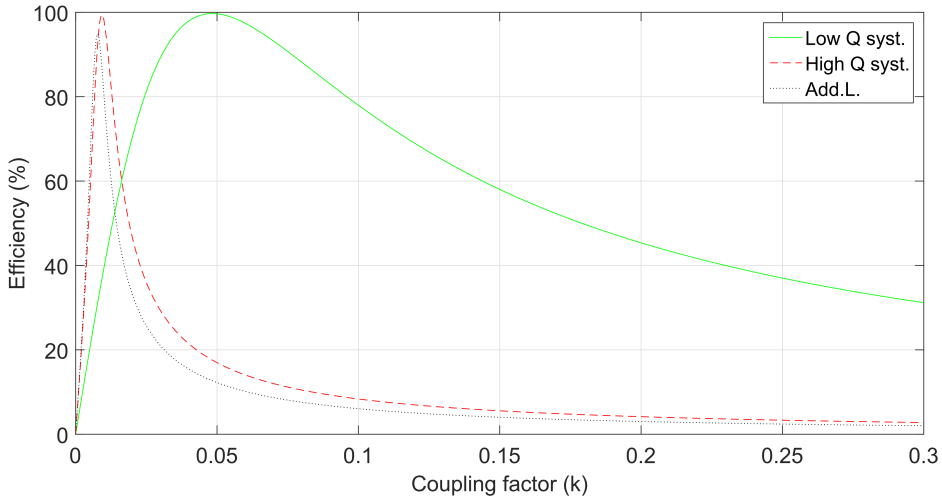

FIGURE 4.8: Comparison of the maximum distance between the T_X and R_X loops of the system with low-Q design, with and without additional inductors and a system with high-Q coil design.

The system specification of the elements is presented in Table 4.3. As it can be seen, the system is a combination of the low Q coils and the additional coils. The calculated performance of the system is presented in Fig. 4.9. As shown in the figure, the system reaches a maximum efficiency of 95% when the coupling factor between the transmitter and receiver is 0.003. This presents high improvement over the system with low Q coils which reaches maximum efficiency at $k = 0.05$. However, an efficiency drop is a major drawback which is a reasonable trade-off in order to reach larger distance without affecting the coils size and weight.

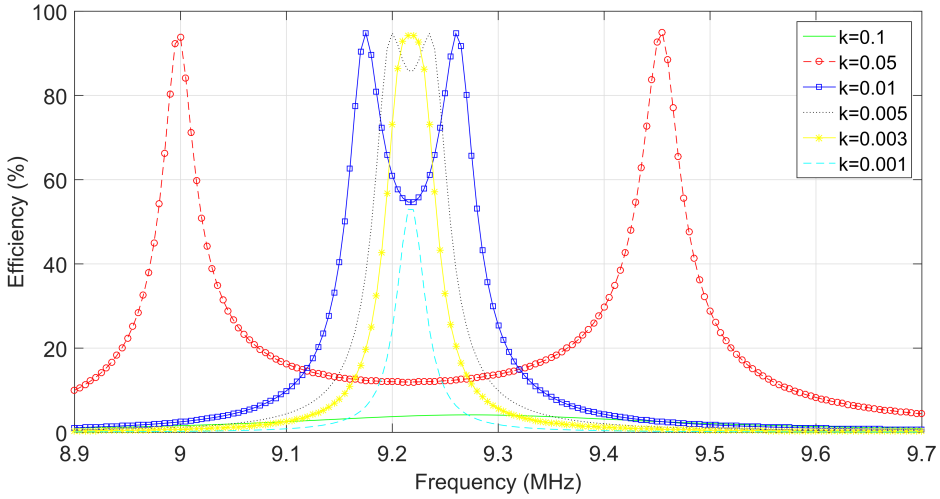

FIGURE 4.9: Calculated efficiency of the proposed system with low Q of the coils with two additional inductors. The coupling factor at which maximum efficiency is much smaller than that for the low Q design without additional coils.

4.2.4 Effect of the Additional Coil Resistance on the System Efficiency

The resistance of the added coils R_{LT2} and R_{LR2} has an important impact on the maximum efficiency thus has been analytically determined via mathematical calculations, which has been the base of the Fig. 4.10. It can be seen that increasing the resistance of the added inductors has a negative effect on the transmission efficiency. When the resistance of the added coils increases from 0.1Ω to 0.5Ω, the system efficiency drops by 10%. A further increase in the coils resistance to 1Ω leads to a drop of efficiency by additional 10% to 70%. From the figure it can be concluded that the increase in resistance leads to a rapid decrease in the system efficiency. However, in the opposite direction, when the resistance decreases, the efficiency improves. As seen from the graph, when the resistance decreases from 0.1Ω to 0.001Ω, the efficiency of WPT system increases by 1%, to 95%. Therefore, in order to reach high efficiency, maintaining a low resistance of added coils R_{LT2} and R_{LR2} is a crucial factor.

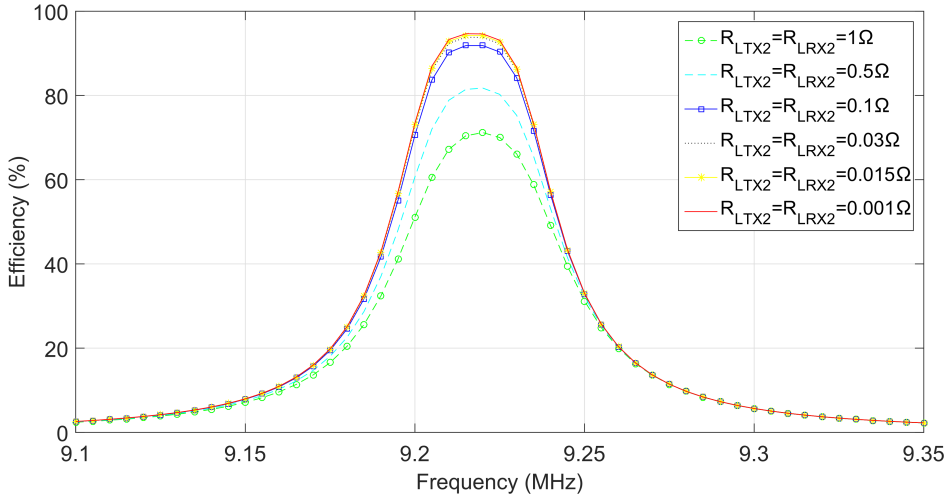

FIGURE 4.10: Effect of different resistance of added coils on the systems efficiency. The smaller the resistance, the higher the efficiency and vice-versa.

4.3 Experimental Setup

An experimental setup is presented in this section. In order to verify the calculated results, an appropriate system was built. A pair of loops were designed for this experiment as shown in Fig. 4.11. The first pair is the conventional T_X and R_X loops shown at the left side of the figure and the second pair is the modified T_X and R_X loops. A practical implementation of the measurement setup can be seen in Fig. 4.12.

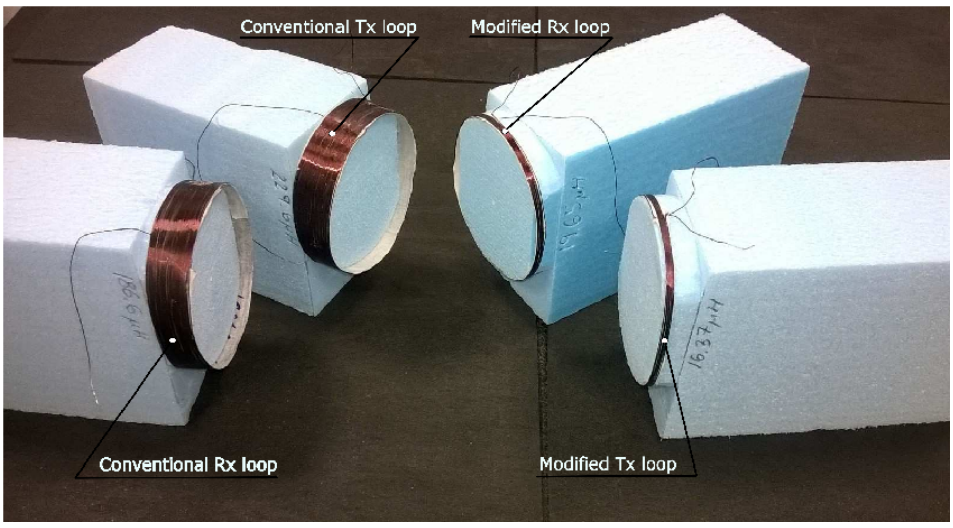

FIGURE 4.11: Comparisons of the coil's sizes.

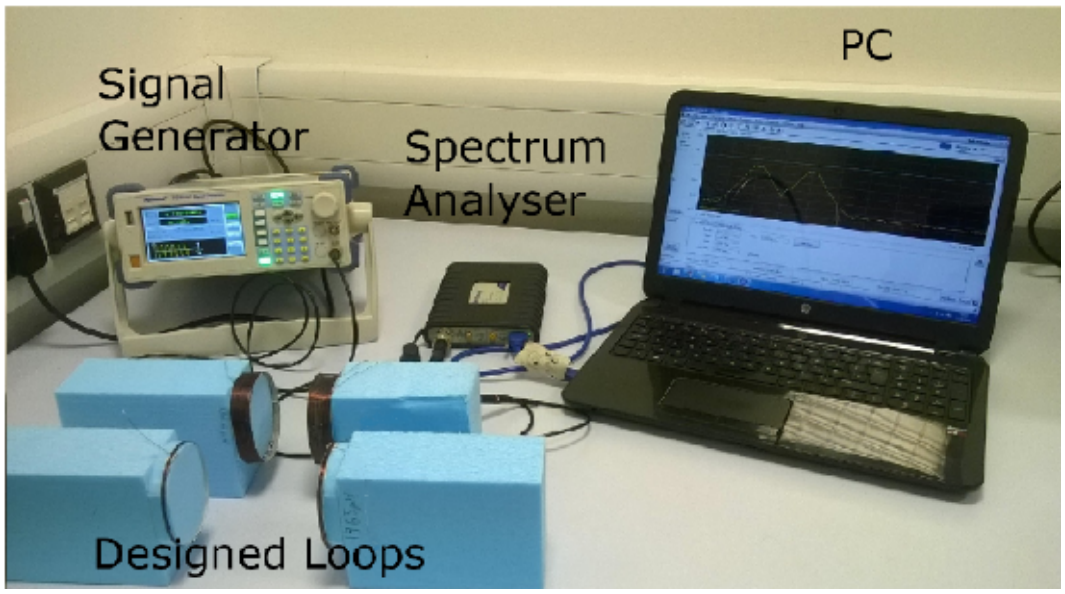

FIGURE 4.12: Measurement set-up of both systems.

4.3.1 System Design and Measurements

Both systems consist of single T_X and R_X loops, made of the same enameled copper wire. The conventional T_X loop with high Q coil, is made of 41 turns while the conventional R_X loop with high Q contains 48 turns as presented in Table 4.1. In contrast, the modified T_X and R_X loops, with additional inductors, are made of only 8 and 9 turns, as presented in Table 4.3. All loops have the same diameter of $72mm$. In addition to the T_X and R_X loops, the proposed system contains two additional inductors made with the same material. The additional inductors L_{T1} and L_{R1} are made of 2 and 3 turns respectively and both have inner diameters of $3mm$. In order to tune the loops to oscillate at the same frequency, ceramic capacitors were used.

A signal generator Digimess SG200 RF was used to provide circuit with various frequency signals, which were applied to the T_X loop. Measuring frequency response of the loops plays important role in order to compare quality of the loops and their oscillating frequency. Its also shows good comparison between the calculated and designed loops performance. The response of the circuit was measured at the R_X loop, and it was carried out by a USB-based spectrum analyser, the Tektronix RSA306. The spectrum analyser was connected to a computer-based software where the results of the measurements were finally displayed.

4.3.2 System Maximum Efficiency

According to the calculation, for the modified system, an optimal efficiency appears when the coupling factor between the T_X and R_X loops is equal to 0.003. As Fig. 4.13 shows a maximum efficiency of the modified system reaches 96% at a frequency of $9.23MHz$. The measurements confirm that the designed system follows the frequency pattern of the calculated system. The maximum efficiency is reached at a frequency of $9.23MHz$, however the maximum efficiency attained is slightly below the calculated value at 89%. The same system at the coupling factor k = 0.01 suffers the effect of frequency splitting and reaches a double peak at frequencies of $9.17MHz$ and $9.26MHz$. The measured results once again confirm the calculated values, a measured double peak maximum efficiency is reached at frequencies of 9.155 and $9.265MHz$. Maximum efficiency is again slightly lower than the calculated values and measured at 85% and 87%, which are 10% and 8% lower than the calculated value.

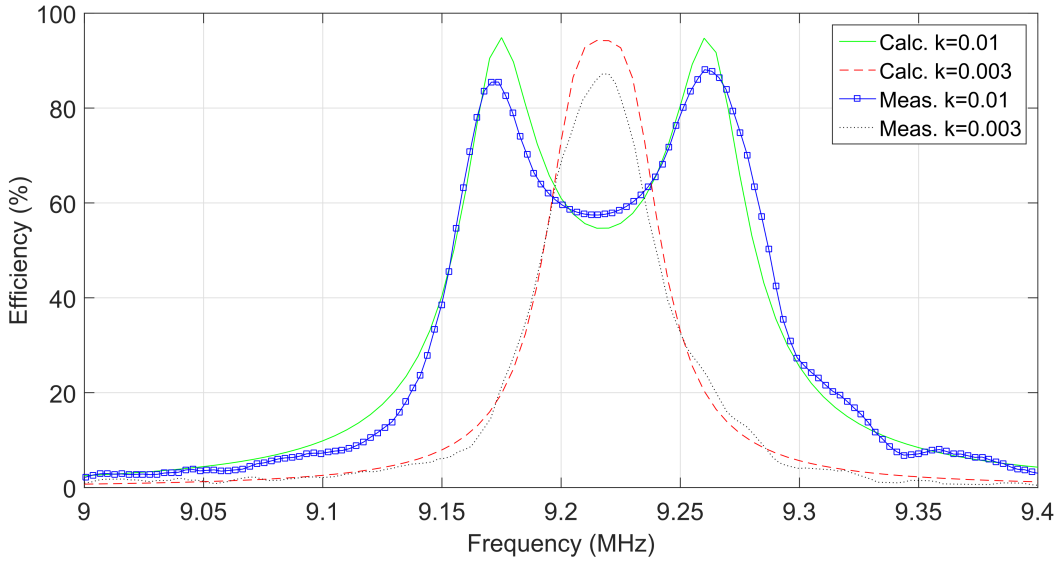

FIGURE 4.13: Comparison between the measured and calculated maximum efficiency and frequency pattern for the modified circuit with additional coils. The results show close similarity of calculated and measured results.

In contrast to the modified loops, the conventional system has slightly wider frequency spectrum. The main reason for this is that in order to use widely produced capacitors for the modified system, the quality factor of the combined coil must be slightly higher than the one from conventional systems in order for both systems to oscillate at the same frequency. That

is also the reason for the efficiency drop at the frequency $9.23MHz$, since the system is already in decline at coupling factor of 0.003, as we can see in Fig. 4.14. Also in Fig. 4.14 it can be seen that the measured efficiency at frequency $9.23MHz$ is 3% below the calculated value, for $k = 0.003$. It is evident that the measured efficiency for both coupling factors, $k = 0.003$ and the $k = 0.01$ resemble the calculated pattern. Double peaks at $9.15MHz$ and $9.28MHz$ as indicated in Fig. 4.14, where $k = 0.01$ indicates a difference of 0.01 and $0.005MHz$ compared to the calculated results.

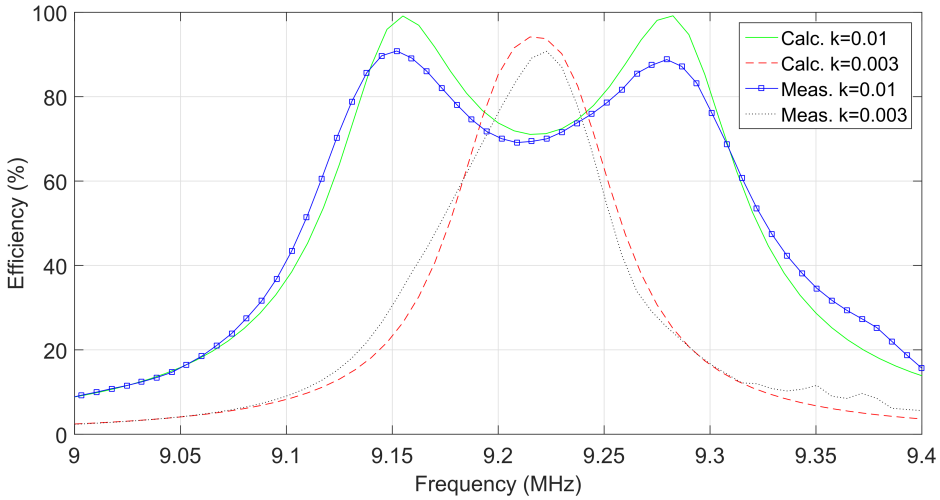

FIGURE 4.14: Comparison between the measured and calculated maximum efficiency and frequency pattern of the conventional system with a high Q of the coil. A designed system shows close similarities with the calculations.

4.4 Comparison of the Size and Efficiency of LCL WPT system

The maximum distance at which the system is able to deliver power with high efficiency is a crucial factor in any WPT system. Up until now a high quality factor of the transmitting and receiving coils was required to efficiently transmit the power on small coupling factor between the two coils. With the proposed method for the maximum distance of the transmission, the quality factor of the transmitting and receiving coils can be made smaller. As shown in Fig. 4.14 the maximum transmission efficiency between the two coils with low quality factor occurs when the coupling factor between them is

equal to 0.05. However, the same two coils can achieve larger maximum distance for the power transfer with the addition of two small inductors L_{T1} and L_{R2} in parallel with the existing inductors. The maximum power transmission between two coils in that case occurs when the coupling factor between the two coils is equal to 0.003, which significantly improves the maximum distance. In both cases, calculated results are compared with the measured as illustrated in Fig. 4.15. It is shown that the maximum efficiency of the two systems appears close to the calculated results.

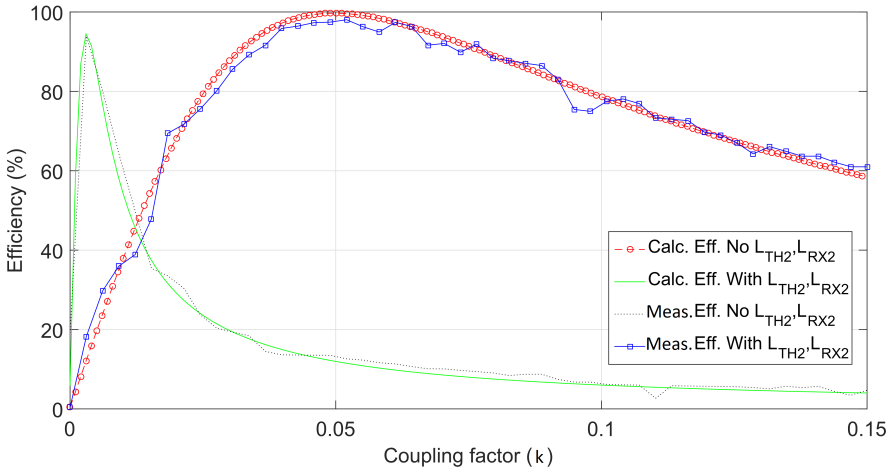

FIGURE 4.15: A comparison between the measured and calculated maximum distances between the low Q design coil with and without added inductor at frequency of 9.23MHz. The system with an additional coils shows an increase in the distance between T_X and R_X at which mximum efficiency occurs.

Similar to the system with low quality of the coils, the new proposed system is compared with the conventional system with a high quality of the transmitter and receiver coils. Fig. 4.16 shows a comparison between the two. As seen from the figure the system with high quality coils reaches its peak when the k between the two coil reaches 0.004 and the maximum efficiency of the proposed design is reached when the coupling factor between the two coils is 0.003. As already mentioned, this occurs due to a desire to use widely available values of the capacitors. From the figure, we can see that the measured results from the prototype system closely follows the calculated results from the model. From the calculations, the maximum efficiency of the proposed system is 7% below that of the conventional model, however the advantages of the proposed design are shown in Table 4.4.

The main advantage of the proposed design is the reduced size of the loops. The length of the transmitter loop in the conventional design is equal

TABLE 4.4: Comparison of the physical parameters of the conventional and modified systems. Proposed system shows a great improvement towards the conventional design.

	Conv. L_{TX}	**Mod. L_{TX}**	**Diff. %**	**Conv. L_{RX}**	**Mod. L_{RX}**	**Diff. %**
Length	15 mm	3 mm	80%	20 mm	4 mm	80%
Weight	7.37 g	1.58 g	78.6%	8.63 g	1.78 g	79.4%
Turns	41	8	80.5%	48	9	81%

to 15mm while that of the proposed design is equal to 3mm. Similar to the transmitter loop, the length of the receiver loop from the proposed design is 4mm, which is a big improvement from the 20mm required for the system from conventional design. Furthermore, the proposed system design has significantly reduced the weight of the WPT transmitter from 7.37g in conventional system to 1.58g while the receiver weight also improved from 8.63g to 1.78g. Both of the above advancements has lead to overall 80% reduction of its size and weight. Therefore, the size reduction offered by the proposed system is achieved at the cost of slight reducing the system efficiency.

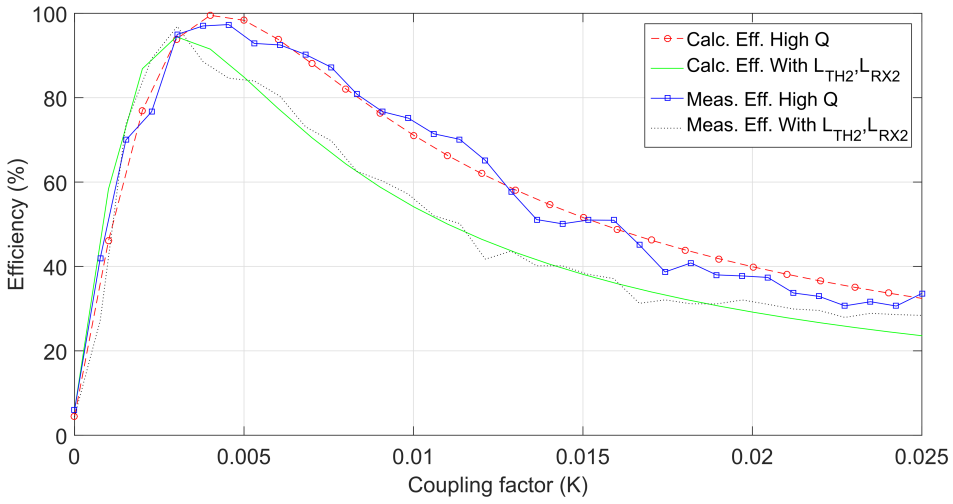

FIGURE 4.16: Comparison between measured and calculated maximum distances between the T_X and R_X coil between the system with high Q coils and the system with added inductor. The results show a similar distance of transmission that can be achieved with both systems.

4.5 Chapter Summary

The proposed methodology reduces the dimensions of the resonators which are comprised in the herein discussed two-loop strongly coupled resonant WPT system. The analytical model of the two-loop, strongly coupled magnetic resonance system with additional inductors, has been developed to further study the relationship between the coil geometry and dimensions with respect to the size of the new inductors and the coupling factor, required to obtain the maximum system transfer efficiency.

The results shed light on the hypothesis of wireless transfer how the coupled mode system efficiency is dependent upon the coupling coefficient. Particularly, how the system obtains its maximum efficiency at a lower coupling coefficient. k is the amount of critical inductive coupling which exists between the coils at a particular distance, which may also vary upon the coil configurations. For instance, if the coils are perfectly coupled then the $k = 1$ and $k = 0.5$ if they are loosely coupled. Similarly, the coupling factor rates the prefect coupling between the independent T_X and R_X, which expresses how much magnetic flux generated in the T_X coil penetrates the R_X coil and determined by the distance between the coils, relative size, shape and lastly the angle [87]. However, here in this chapter the distance between the coils and the size of the inductors, have been taken into account. Additionally, the system transfer efficiency with relevance to the parasitic resistance due to the magnetic field density of the additional inductors has been further examined. The experiment was conducted to validate the analytical results based on the theoretical description.

The novel concept of designing a two-loop resonant WPT circuit which is proposed, replaces the resonant inductors with a high resonant factor, with a set of small inductors which are placed in parallel with an inductor of a low quality factor. The technique allows the newly formed WPT circuit to reach its maximum efficiency at similar or even smaller coupling factor as the circuit designed with the coils of high quality. In contrast, results reflect that the proposed system is significantly able to deliver power at similar efficiencies as the system with larger coils at similar distances. Interestingly, proposed design further reduces the size and weight, being potentially able to manufacture as a hermetically sealed system further optimising the safety feature. Aforementioned multi-coil system optimises the inductive coupling between the elements providing the designer a smaller degree of freedom in size constrained applications.

Furthermore, the analysis indicates that the high quality of the system can be achieved, regardless of the higher inductive coils and specific lower capacitor value. Consequently, smaller inductors are required to specify the oscillating frequency, hence the size of the inductor, is further reduced. A 5% contraction in the WPT transfer efficiency is observed compared to the conventional method. However, the novel architecture trade-off the system efficiency at the cost of the 80% size of the loop is reduced with a 79% weight reduction. The reduced size system is also highly advantageous for strongly coupled systems with a limited thermal budget with less heat generation. It is shown that the simulation results and the measurements during the experiment, exhibit very similar trends, determining that the simulation results also agree well with the theoretical calculations confirming the validity of the theoretical analysis. Despite of the advantages, future research is recommended analysing the complex magnetic quantities and energy exchange characteristics upon the coil geometry.

Chapter 5

Wireless Power Transmission System for Autonomous Charging of EV

ELECTRIC vehicles are regarded as one of the most promising alternatives to fossil fuel vehicles. Statistics indicate that in July 2018, 162,000 plug-in EVs (PEVs) were used on the UK roads. Furthermore, the number of electric car models and brands in the UK market have grown rapidly in the recent years. Today, in the UK, 75 different models of PEVs are available and roughly 20,000 charging points have been installed around the country [167]. It has also been predicted that by 2030, about 60% of all new vehicles sales in the UK will comprise EVs [168]. However, charging cables are still used to connect the cars to the charging stations.

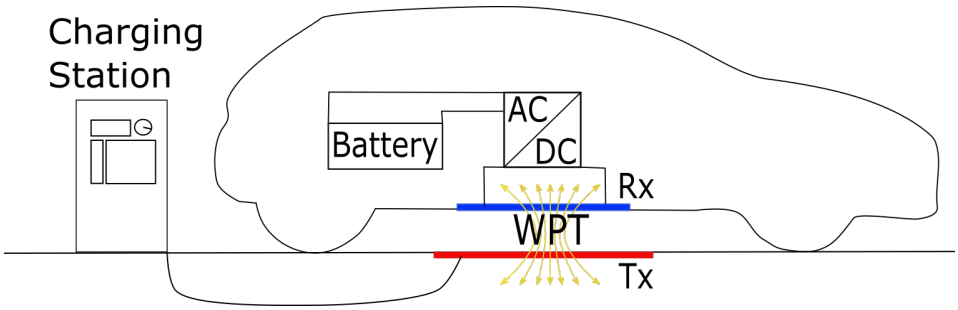

FIGURE 5.1: EV wireless power transmission charging with the charging pad placed under the vehicle.

A conventional EV WPT charger has been illustrated in Fig. 5.1, where the T_X is placed under the EV and the R_X is fitted on its body. The parking spot is designed to offer the driver sufficient parking space and a safe exit. However, spatial freedom in parking spaces is a challenge while designing a WPT transmitter [169]. According to [170], the minimum parking space for a car is $4.8m$ in length and $2.4m$ width. Therefore, the WPT charger should

ideally be able to transfer power with its highest efficiency regardless of the vehicle's position.

Different methods of IWPT have been proposed in recent years. For instance, authors in [171] proposed replacing the circular coil structure of the pad with a quadrature coil combined with DD coil design. The new DD-DDQ coil design can improves the pad's charging zone, thereby reducing the cost of the pad. A tripod was proposed in [172], where the transmitter unit is built with 3 individual charging coils, which are connected to each other in a circular structure. According to the authors, the proposed structure reduces magnetic flux leakage.

Distinct methods to improve spatial freedom of a WPT charger were proposed by [173], where power transmission is combined with a super capacitor (SC) to form an energy buffer. A multi-coil charger was also investigated in [174, 175, 176] to increase the receiver's flexibility based on free positioning of the transmitter. The proposed multi-loop transmitter contains two or more loops that are embedded in the same transmitter. The loop used to transmit power to the receiver is calculated based on the measured results of each individual transmission. The advantage of this method is that power is consistently transmitted with the highest possible efficiency. However, continuous communication between the transmitter and receiver has to be established and numerous measurements have to be made during the charging period and after, to ensure calibration, in case the object repositions.

This chapter presents a novel localisation method for EV charging through WPT. With the proposed technique, the wireless charging system can self-determine the most efficient coil to transmit power to the EV's position, which is detected, based on the sensors activated by its wheels. To ensure optimal charging, our approach involves measuring the transfer efficiency of an individual transmission coil to determine the most efficient one to be used. This not only enhances the charging time but also minimises energy losses by autonomously only activating the coils with the highest transfer efficiencies. The results show that, with the proposed system it is possible to detect the coil with maximum transmitting efficiency without actual power transmission and comparing the measured efficiency. This study also prove that, with the proposed charger set-up, the position of the receiver coil can be detected almost instantly. Therefore, the system saves power and maximises the charging time.

This chapter is structured as follows. Section 5.1 describes the proposed WPT charger model and presents a mathematical analysis. Section 5.2 presents

the system specifications and numerical results. In Section 5.3, the experimental parameters and system configuration are described in detail. The measurement results are discussed in Section 5.4 and the chapter is summarised in Section 5.5.

5.1 Wireless Charging Pads Model

A vital aspect of the car charging pad design is to cover multiple positions of a car in a parking facility. To sense the position of the vehicle, the wheels need to be placed within the pre-marked parking spaces. For experimental purposes, the properties of the three prominent EV models used in the UK have been presented in Table 5.1 [177], and the dimensions of the car have been illustrated in Fig. 5.2. While designing a charging system, the most crucial factors that need to be considered are the distance between the centre of the rear and front wheels (wheelbase), marked as D, as well as the distance between the left and right front wheels (track distance), marked as B.

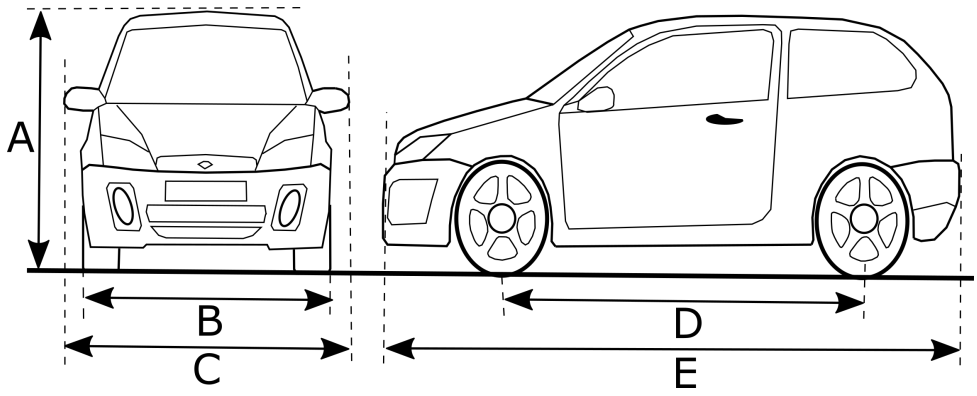

FIGURE 5.2: A car's dimensions; height (A), track distance (B), width (C), wheelbase (D) and length (E).

TABLE 5.1: Dimensions of the three most popular car currently in the UK market.

Model	Height	Width	Wheelbase	Length
Renault Zoe	1562mm	2588mm	2637mm	4084mm
Tesla Model S	1445mm	2960mm	2630mm	4979mm
BMW i3	1598mm	1775mm	2570mm	4006mm

The most common EVs on the UK roads are Renault Zoe, Tesla Model S and BMW i3. With the respect to the dimensions of EVs, shown in Table 5.1, it is evident that despite the similarities between the length of the Renault

Zoe and BMW i3, their widths differ. Tesla Model S is a considerably larger vehicle. Therefore, based on the wheelbase and the track distance, it is possible to determine the model of a vehicle based on the activated sensors. Upon successful determination of the EV's dimension, the system can effectively calculate which T_X is to be used based on the current parking position.

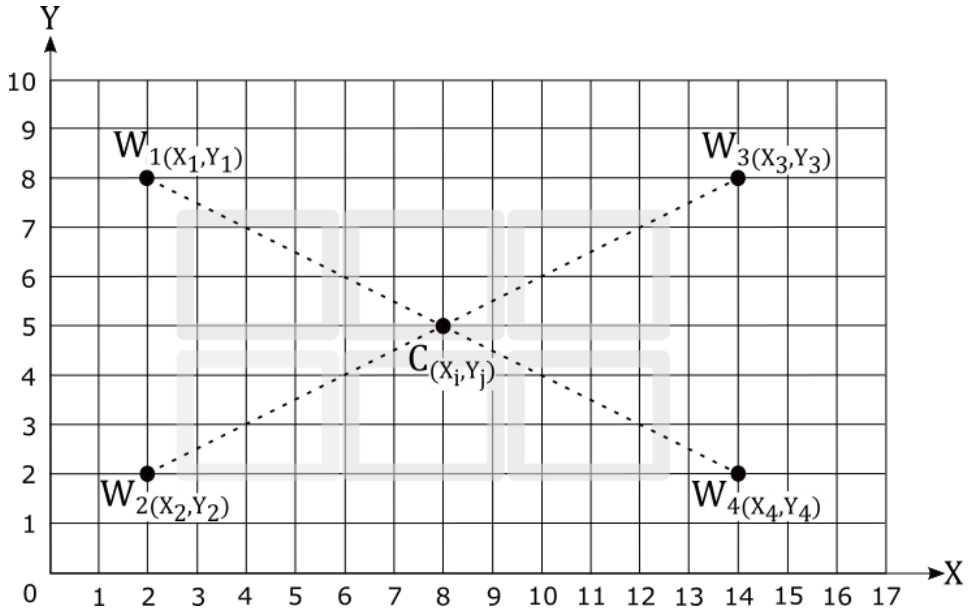

FIGURE 5.3: Two dimensional network of the parking space which is used to calculate the EV's position, size and detect the WPT coil with highest efficiency of charging.

The location of the vehicle in the parking space can be determined by the coordinates within the Cartesian plane, where each of the four vertices of the vehicle has known coordinates as shown in Fig. 5.3. From these coordinates, properties such as the width and length can be determined. The coordinates of each wheel are given by $W_i = W_{(Xi,Yi)}$. To determine the wheelbase and track distance, the distance between the wheels is calculated as follows

$$d_{(Wi,Wj)} = \sqrt{d^2_{(W_{Xi},W_{Xj})} + d^2_{(W_{Yi},W_{Yj})}} \tag{5.1}$$

In the above equation $d_{(Wi,Wj)}$ is the distance between the two measured wheels positions W_i and W_j. The shortest distance is calculated as the distance between the two front wheels, while the longest is the distance of the wheelbase. Based on these results, the car's dimensions can be determined.

To determine which transmitter coil will function at its highest efficiency at the EV's current position, the centre of the car has to be determined. Within

the Cartesian plane, the centre of the EV is determined as the point of intersection of the diagonals. Therefore, the centre of the EV can be calculated as a centre between the two nodes as shown bellow

$$C_{(W_i,W_j)} = \Big(\frac{W_{Xi} + W_{Xj}}{2}\Big), \Big(\frac{W_{Yi} + W_{Yj}}{2}\Big). \tag{5.2}$$

The oscillating frequency of the WPT system is given by $\omega_0 = \frac{1}{\sqrt{LC}}$ where the L and C are the inductance and capacitance of the system respectively. The quality factor of the coil, Q, has a strong impact on the efficiency of the system and it can be expressed as $Q = \sqrt{\frac{L}{C}}\frac{1}{R} = \frac{\omega_0 L}{R}$, where Q decreases as the coil resistance increases. The mutual inductance between the two coils is expressed as $M = k\sqrt{L_T L_R}$, where L_T and L_R are self-inductances of the transmitter and receiver coil and k represents a coupling factor between the two coils. Considering the self-inductances of each coil, the mutual inductance can be calculated as follows

$$M = k\sqrt{\frac{1}{\pi}\mu_0 A}\sqrt{\frac{1}{\pi}\mu_0 B} \tag{5.3}$$

μ_0 represents vacuum permeability and

$$\begin{aligned} A = (-2)\sqrt{(l_1 - r_w)^2 + r_w^2} + \frac{r_w^2}{sinh(l_1 - r_w)} \\ +2\sqrt{(l_1 - r_w)^2 + (w_1 - r_w)^2} + \frac{(r_w - l_1)(l_1 - r_w)}{sinh(l_1 - r_w)} \\ -\frac{(w_1 - r_w)^2}{sinh(r_w)} - 2ln(r_w) - 2(r_w^2 + \sqrt{(w_1 - r_w)^2} \\ +\frac{2r_w^2}{sinh(w_1 - r_w)} + 2\sqrt{2r_w} + \frac{(w_1 - r_w)^2}{sinh(r_w)} + \sqrt{2} \end{aligned} \tag{5.4}$$

$$\begin{aligned} B = (-2)\sqrt{(l_2 - r_w)^2 + r_w^2} + \frac{r_w^2}{sinh(l_2 - r_w)} \\ +2\sqrt{(l_2 - r_w)^2 + (w_2 - r_w)^2} + \frac{(r_w - l_2)(l_2 - r_w)}{sinh(l_2 - r_w)} \\ -\frac{(w_2 - r_w)^2}{sinh(r_w)} - 2ln(r_w) - 2(r_w^2 + \sqrt{(w_2 - r_w)^2} \\ +\frac{2r_w^2}{sinh(w_2 - r_w)} + 2\sqrt{2r_w} + \frac{(w_2 - r_w)^2}{sinh(r_w)} + \sqrt{2}. \end{aligned} \tag{5.5}$$

The length of the loops of the transmitter and receiver coils are represented by l_1 and l_2 respectively, and r_w represents the cross-section radius of the coil. The width of the transmitter loop is denoted by w_1 while the receiver loop width is denoted by w_2. System efficiency is strongly associated with mutual inductance, transmitting frequency and resistance of both coils. It can be calculated as

$$\eta = \frac{k^2\omega^2\sqrt{\frac{\mu_0}{\pi}C^2}\sqrt{\frac{\mu_0}{\pi}D^2}}{R_T R_R(1 + \sqrt{\frac{1}{R_T R_R}k\omega^2\sqrt{\frac{\mu_0}{\pi}C}\sqrt{\frac{\mu_0}{\pi}D}})^2}, \tag{5.6}$$

$$\begin{aligned} C = (-2)ln(r_w) + \frac{(l_1 - r_w)^2}{sinh(r_w)} + \frac{r_w^2}{sinh(l_1 - r_w)} \\ +\frac{2r_w^2}{sinh(-r_w^2 + w_1)} + \frac{(l_1 - r_w)(-l_1 + r_w)}{sinh(-r_w^2 + w_1)} \\ -\frac{(-r_w + w_1)^2}{sinh(l_1 - r_w)} + \sqrt{2} + 2\sqrt{2r_w} - 2\sqrt{(l_1 - r_w)^2 + r_w^2} \\ -2(r_w^2 + \sqrt{(-r_w + w_1)^2}) + 2\sqrt{(l_1 - r_w)^2 + (-r_w + w_1)^2} \end{aligned} \tag{5.7}$$

$$\begin{aligned} D = (-2)ln(r_w) + \frac{(l_2 - r_w)^2}{\sinh(r_w)} + \frac{r_w^2}{\sinh(l_2 - r_w)} \\ +\frac{2r_w^2}{\sinh(-r_w^2 + w_2)} + \frac{(l_2 - r_w)(-l_2 + r_w)}{\sinh(-r_w^2 + w_2)} \\ -\frac{(-r_w + w_2)^2}{\sinh(l_2 - r_w)} + \sqrt{2} + 2\sqrt{2r_w} - 2\sqrt{(l_2 - r_w)^2 + r_w^2} \\ -2(r_w^2 + \sqrt{(-r_w + w_2)^2}) + 2\sqrt{(l_2 - r_w)^2 + (-r_w + w_2)^2}. \end{aligned} \tag{5.8}$$

5.2 Proposed Wireless Charging Pad

The smart WPT proposed in this study is information-centric such that wireless sensor array is integrated with the charging system to a-priori determine the positions of each wheels of the parked vehicle before activating the transmitter coils. Once successfully parked, the weight of the vehicle activates the sensor array underneath the wheels. The control unit senses this outcome as a logic "1" on the input. Based on combination of the sensed logic inputs, the algorithm determines the most suitable coil to transmit power at the given car's position. The control unit activates the corresponding switch on the switching circuit based on the computation. Thereafter, the electrical switch connects the wireless charger in the EV with the transmitter coil, initiating power transmission. The flowchart of the system has been illustrated in Fig. 5.4.

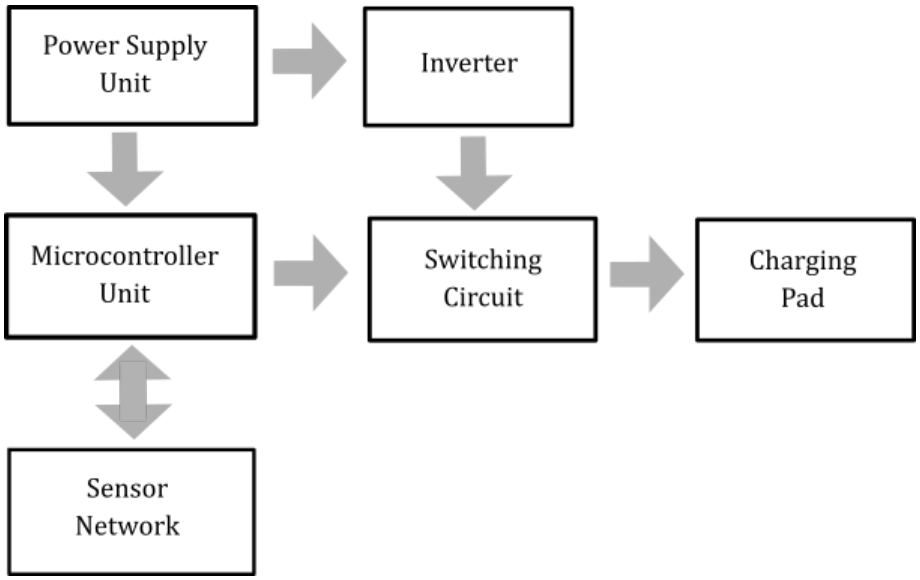

FIGURE 5.4: Block diagram of the proposed charger, with the micro-controller as the main controlling element between the sensors and charging pad.

5.2.1 Wireless Sensor Array Definition

Fig. 5.5 illustrates a parking space model which consists of an inbuilt array of 16 independent sensors. The proposed sensor array can be described as a 4x4 matrix, where each set of four sensors is responsible for determining the position of a wheel. The precision of calculating the car's position can

be optimised by increasing the number of sensors. However, that will simultaneously increase the complexity of the control unit and algorithm. In the end, the cost of implementation will also increase. Alternatively, precision can be enhanced by using existing sensors to measure the position of three or two wheels in diagonal positions. Thus, the algorithms require at least two wheels to be positioned diagonally to determine the charger's position.

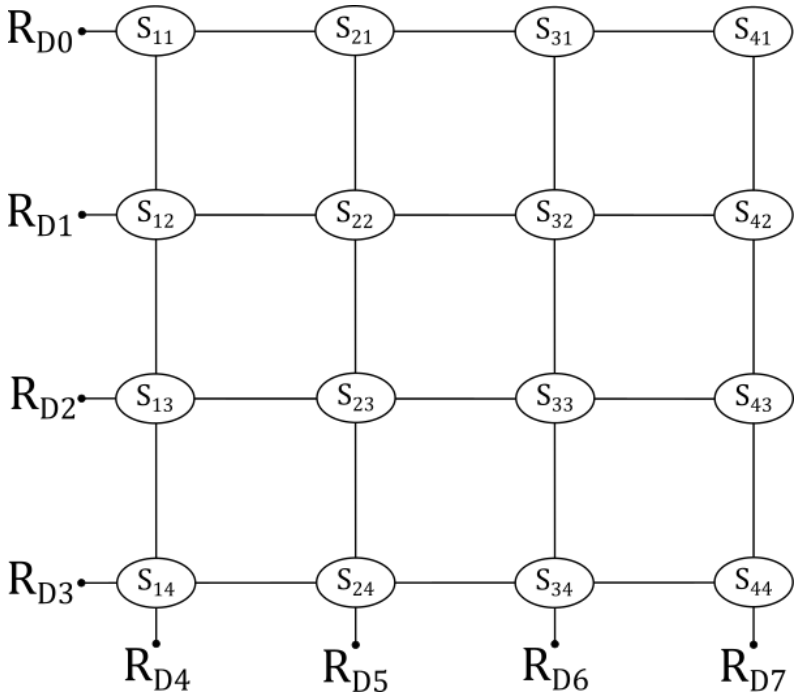

FIGURE 5.5: Charging pad sensor network alignment that senses the car wheels to calculate the position of the car's receiver coil.

As presented in Fig. 5.6, the sensor array underneath each wheel can be considered as an independent system. Each of the four sets of sensors can determine 9 different positions of each wheel, depending on which combination of sensors are activated. For instance, if only sensor $S13$ is activated, the control unit determines that the wheel is positioned on top of the sensor, whereas in the event that sensors S_{13} and S_{14} are activated, the unit will recognise that the wheel is placed in between the two sensors in position 1. If all four sensors are activated, the wheel is considered to be in position 5.

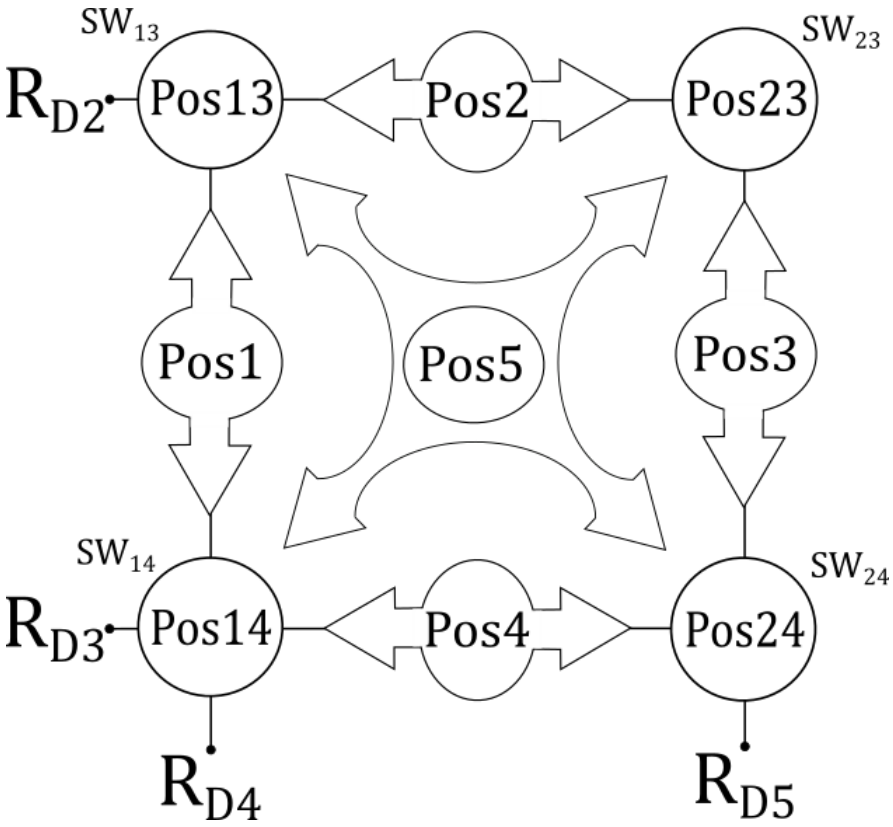

FIGURE 5.6: Sensor network's position under a single wheel, which can determine 9 different placements.

5.2.2 The Control Unit

All feasible combinations of the four sensors under each wheel are presented in Fig. 5.7, which further explains the logic in Fig. 5.6. Furthermore, in the proposed system, logic "1" indicates that the sensor is activated, while "0" indicates otherwise. It is possible to program the system vice versa such that logic "0" indicates that the sensor is active.

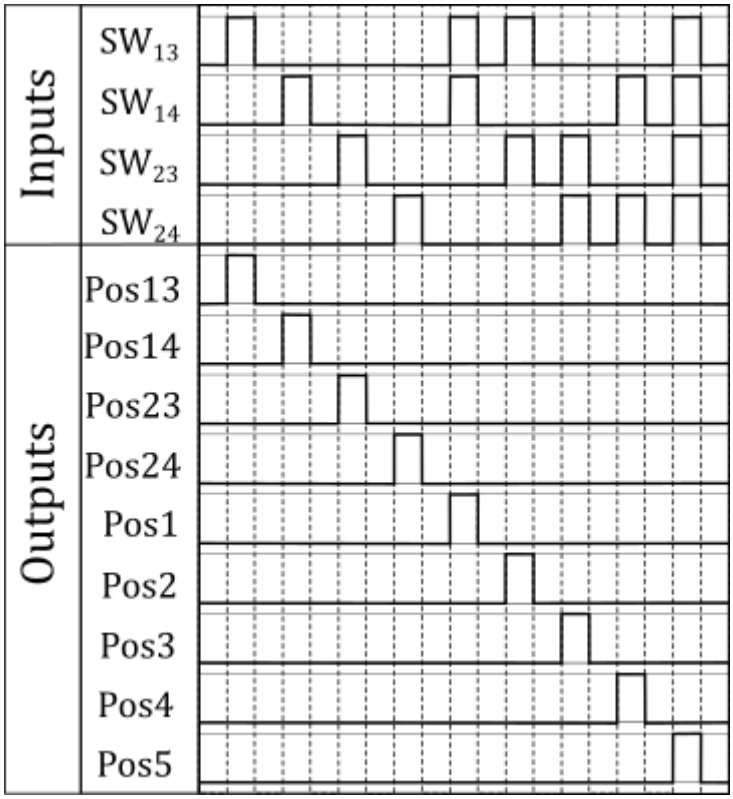

FIGURE 5.7: Outputs of a single wheel position system as seen on micro controller input.

Upon activation of the sensors beneath each wheel, the control unit triggers the corresponding switch to connect the charger to the relevant coil. The proposed coil system consists of six rectangular coils as shown in Fig. 5.8. The open ends of each coil is linked to the connector RB4, which is permanently connected to the inverter. In contrast, the opposite end of the coils are connected to independent switches. Therefore, connection RB0 is linked to switch $SW0$ on the switching board, $RB1$ to $SW1$ and so on. Once the related switch is triggered according to the calculations, the coil with highest efficiency is activated to transmit power to the EV.

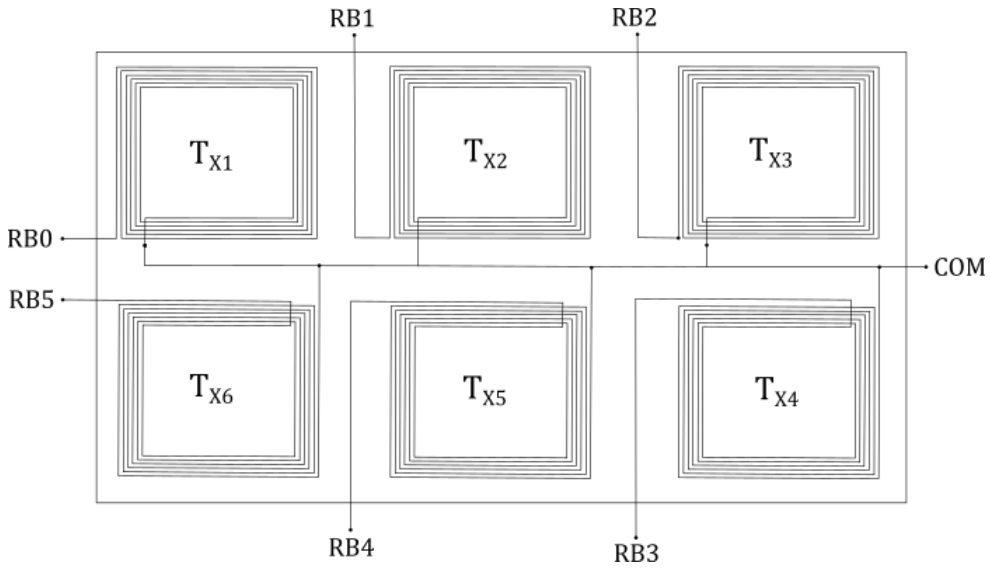

FIGURE 5.8: The connection of the transmitter coils in the charging pad.

5.3 System Design and Practical Implementation

The proposed system is presented in Fig. 5.11. The charging system comprises a power supply unit with an LM7805 voltage regulator that provides stable voltage to both the micro controller and WPT charger. In the control circuit, we used micro controller PIC18F452, as shown in Fig. 5.9, to coordinate the operation of the charging pad. Four of the PICs pins; $RD0$ to $RD3$ are used as outputs. These outputs constantly changes their values from logic "0" to logic "1", of which only one of the outputs can be on logic "1" at any given time. These changes are constantly monitored by the micro-controllers' inputs, $RD4$ to $RD7$ respectively. Furthermore, we developed the algorithm such that the microelectronic converts the input signal by setting one or more outputs on gates $RB0$ to $RB5$ to logic "1" to control the switching board.

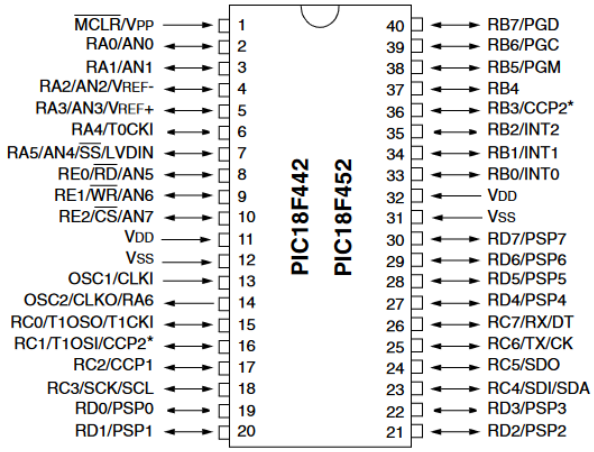

FIGURE 5.9: Pin diagram of PIC18F452 used as a control unit in the experiment.

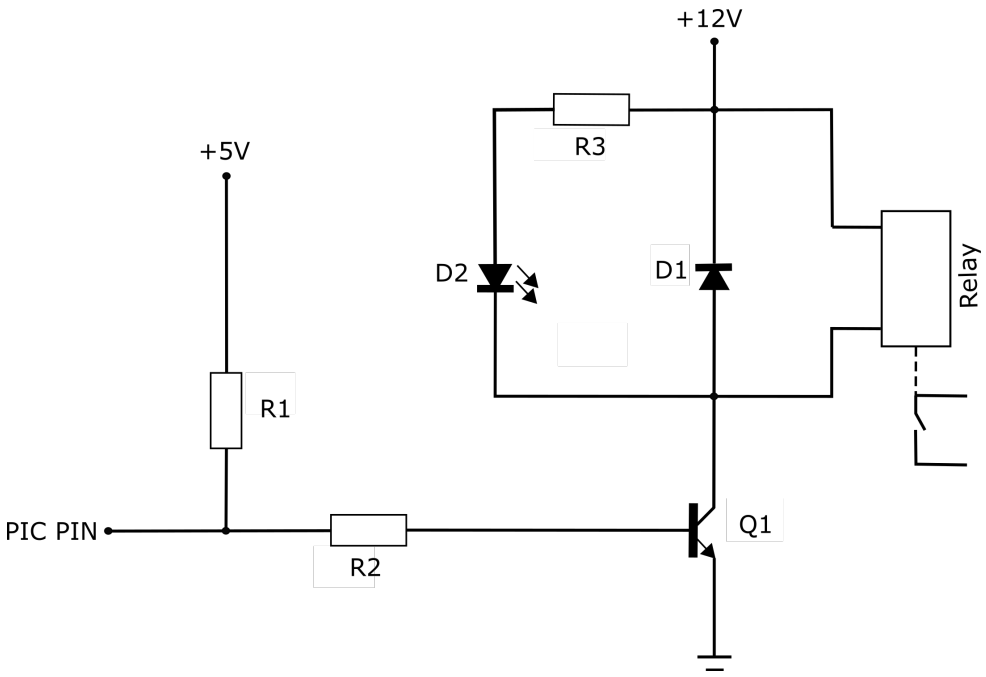

FIGURE 5.10: Connection of a relay via NPN transistor with the output of the micro controller.

As the micro-controller has internal resistance, to pull up logic "1", $+5V$ is not sufficient enough to drive the relay directly from the micro controller. The typical current that is required through the coils to switch the relay is between $25mA$ and $70mA$, therefore an external driving circuit is required. Fig. 5.10, illustrates the relay drive circuit that was used. The NPN transistor $BC547$ was used to control the current through the relay coil. When logic "1" appears on the micro-controller output pin, the transistor opens and closes by logic "0" on the micro controllers output. To drive the transistor

into saturation, the external pull-up resistor $R3$ ($4k7$) is used. This provides the transistor with sufficient current to ensure a gain (h_{fe}) of 100. In addition, the diode $D1$ ($1N2007$) is used as a free wheel diode to protect the transistor against the electromagnetic field that is induced on the coil of the relay when the transistor turns off. The diode ensures that the energy induced on the coil dissipates on the internal resistance of the coil while LED $D2$ is used as an indicator when the relay is switched on.

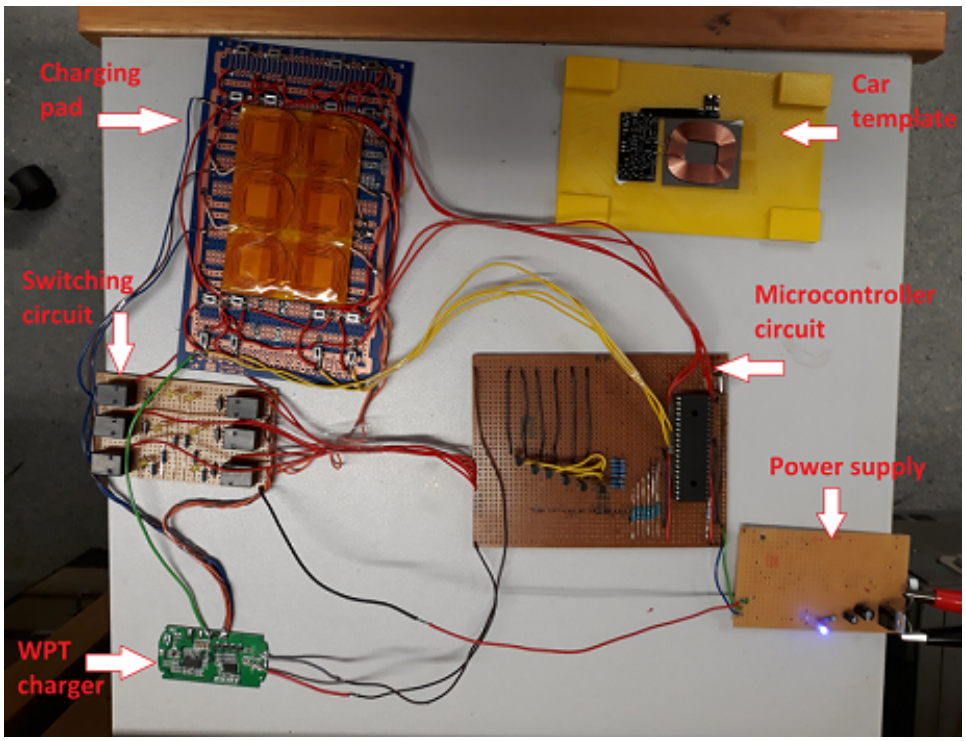

FIGURE 5.11: Practical implementation of the proposed system, with charging pad and a car.

As shown in Fig. 5.11, the designed system consists of a charging pad, which includes a set of six charging coils. Each coil is connected to a separate relay, mounted on the switching board. The relays, controlled by a micro controller, connect the charging coil to the WPT charger. The power provided by the WPT charger is redirected through the relays to a specific coil. A car template is created to simulate the position of the car on the charging pad.

When the car is placed on top of the charging pad, the wheels of the car trigger the sensors in the network. The micro controller determines the car's position and activates the appropriate coil, as shown in Fig. 5.12. Once the coil is activated, the EV charging begins. An LED indicator on the switching circuit indicates which relay is activated. If the car position changes, the change is detected immediately by the sensor network, and the charging coil

changes if necessary.

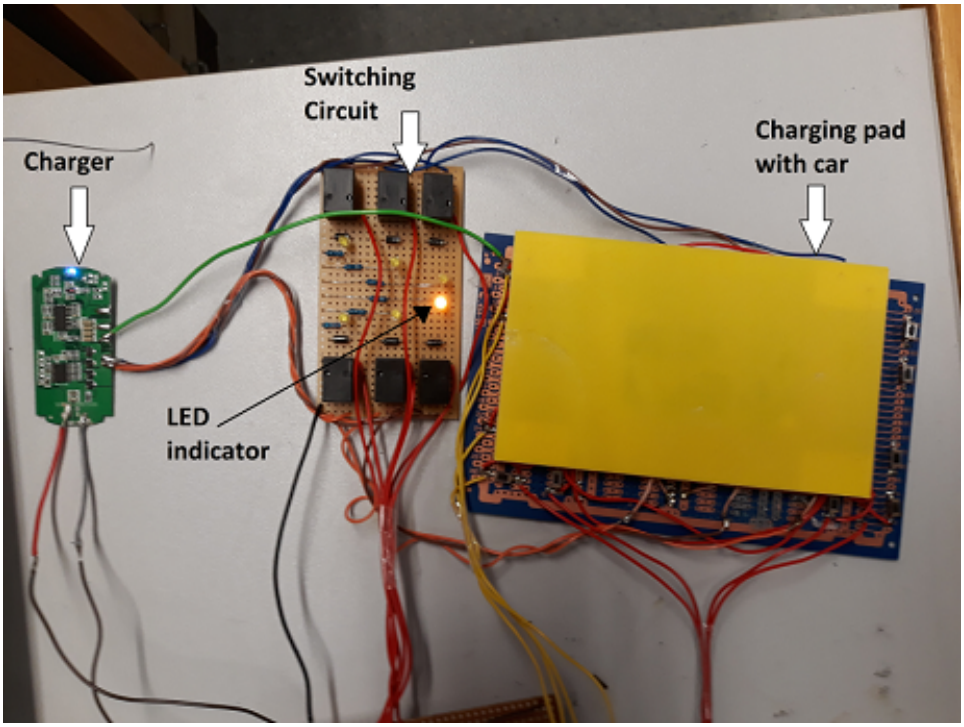

FIGURE 5.12: The charging system with the car parked on the parking space. The LED indicate which coil is active at the certain parking position.

The WPT charger used in this experiment is based on a H-bridge inverter circuit. This ensures that a full square wave voltage is applied to the transmitter coil. The switching frequency of the switches was set on $200kHz$ in order to operate within the QI standards. The circuit diagram of the charger can be seen in Fig. 5.13.

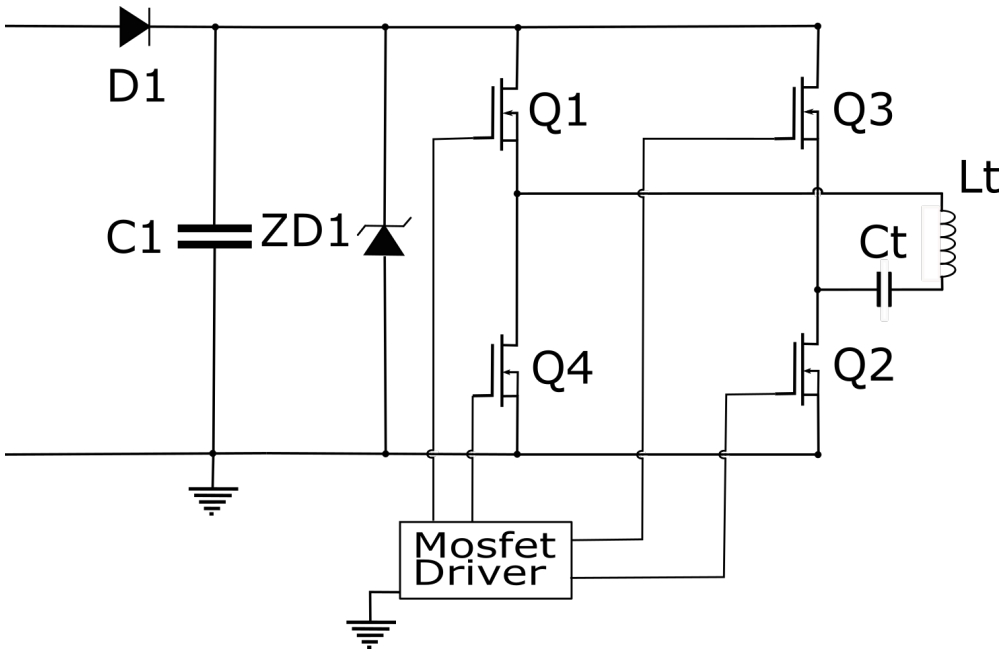

FIGURE 5.13: The circuit diagram of a H-bridge inverter.

5.4 Measured Efficiency and Spatial Freedom of Proposed System

To evaluate the proposed system, the experimental results have been presented in this section. As mentioned, the H-bridge inverts the DC voltage provided by the power supply. The inverted square wave voltage is applied to the transmitter coil. Following this, we measured the output of the inverter and compared that with the received voltage on the receiver coil on a time scale as presented in Fig. 5.14. In the figure, the output voltage of the inverter, presented in blue line is not square shape. This is due to inductance of the transmitter coil. The peak of the output voltage is just below $10V$. This drop from the $12V$ supplied to the inverter represents a significant loss. Nevertheless, the drop in the semiconductor components are expected. The voltage on the receiver side is illustrated as a dotted black line in the same figure. The received voltage is measured when full the transmitter and receiver are fully aligned. At its peak, the received voltage reached $13.5V$.

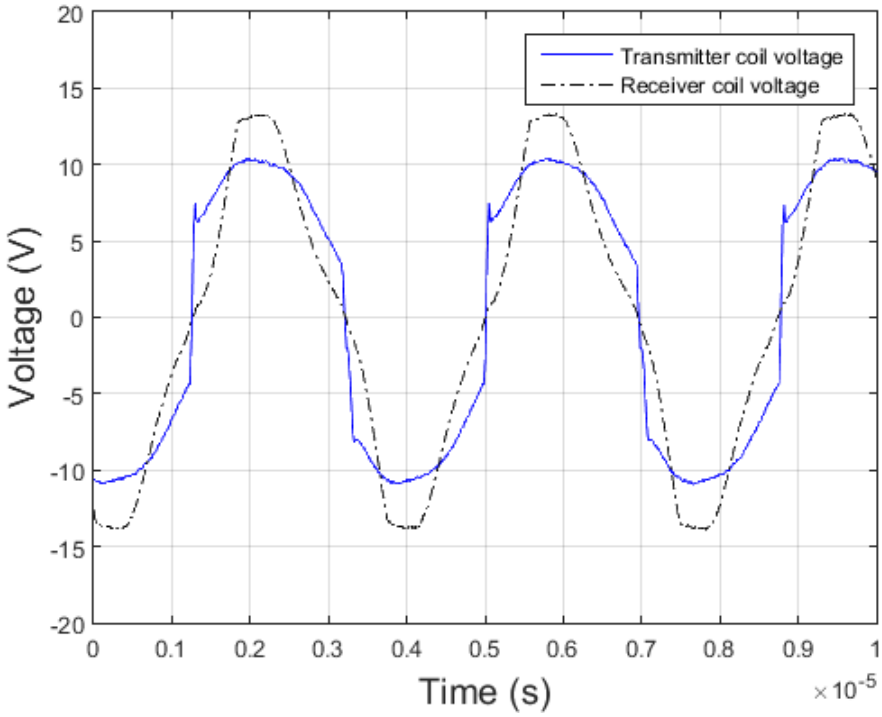

FIGURE 5.14: The comparison between the output voltage on the transmitter side and the received voltage of the receiver.

The transmitter and receiver loops are designed to have a maximum of 50% misalignment between the closest coils. Therefore, the coverage between the transmitter and receiver can be between 100% and 25%. In Fig. 5.15, the measured results of the voltage on the receiver coil for 100, 80, 60 and 30% coverage are presented and compared. The results show that the transmission efficiency drops with increased misalignment between the coils. For instance when the coverage drops to 80%, the voltage measured on the receiver loop drops by $1.5V$. The drop is even more evident when the coverage drops to 30%, where the measured voltage on the receiver reduces to $7.6V$.

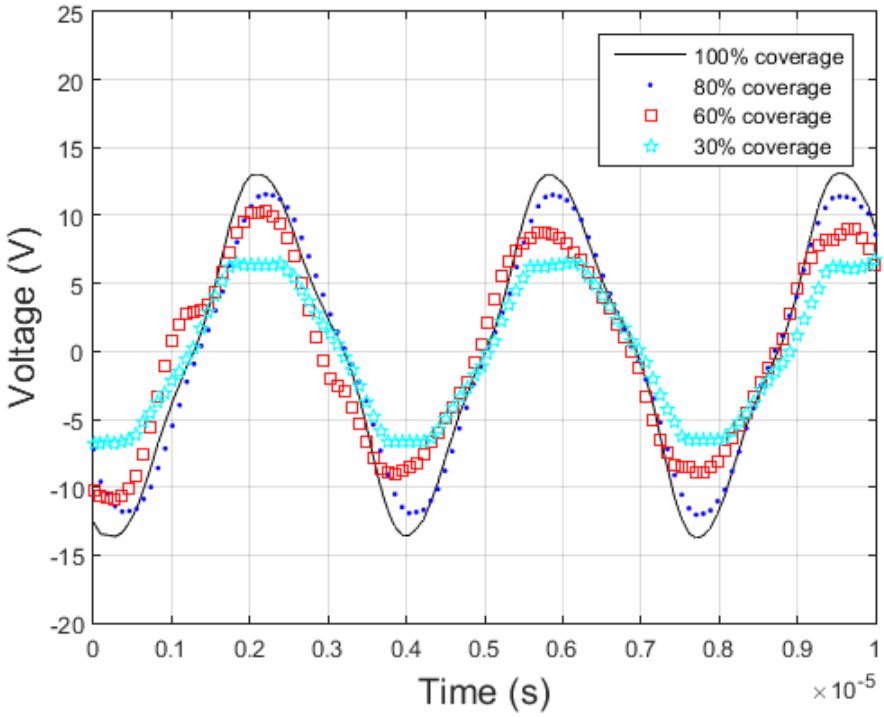

FIGURE 5.15: Voltage measured on the receiver for a changed misalignment between the coils.

According to the results, efficiency of the charging pad depends on the car position. Fig. 5.16 shows the comparisons between the calculated and the measured efficiency drops according to the level of the misplacement. When the coils are perfectly align, the power transfer is maximised. With the increased misplacement between the two coils the efficiency of the transmission also drops. As shown in the figure, the efficiency drops for 10%, if the misalignment between the two coils drops to 52%. The efficiency can be increased by introducing additional coils into the transmitter. This will increase the coverage and prevent the misalignment to drop bellow 25%. At minimum alignment of the coils at 25 %, the efficiency drop in the transmission is 37%, while the calculated results show 30% drop.

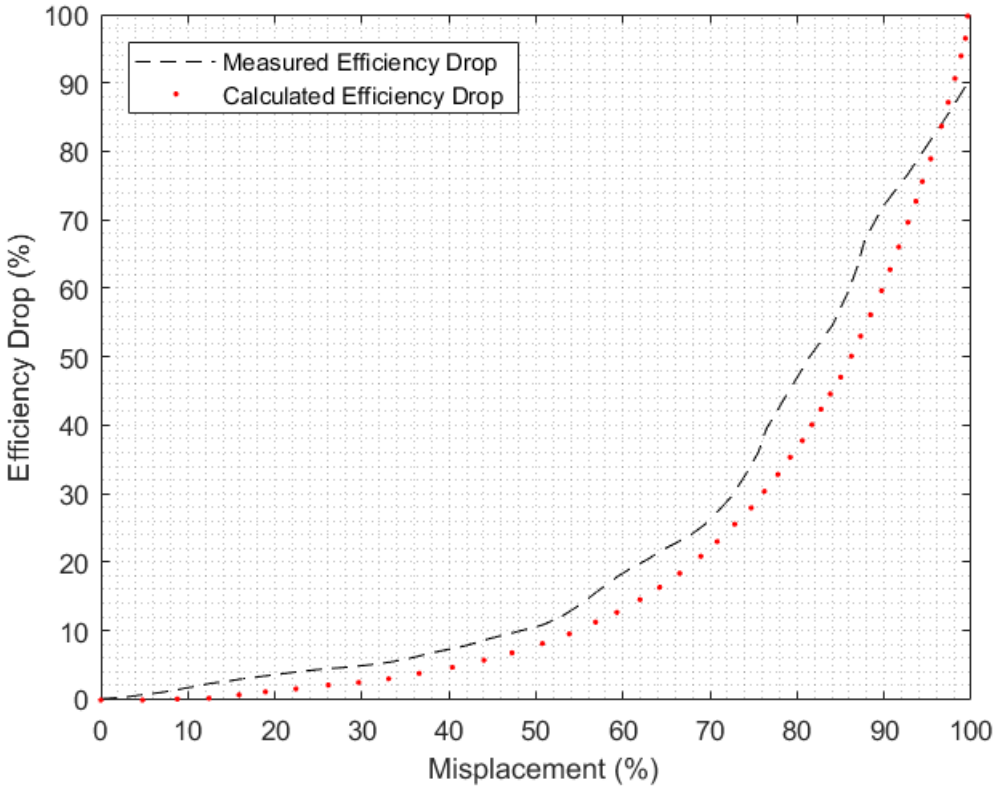

FIGURE 5.16: Efficiency drop caused by the misplacement between the transmitter and receiver coils.

Based on the efficiency drop caused by the misalignment between the transmitter and receiver, the corresponding efficiency of a charging pad is presented in Fig. 5.17. As shown in the figure, the charging pad achieves highest efficiency of 87% when the charging coil is aligned with the receiver coil. On the other hand, the charging efficiency drops when the centre of the receiver coil is in between the four charging coils. In that case, the efficiency of the charging system drops to 52%.

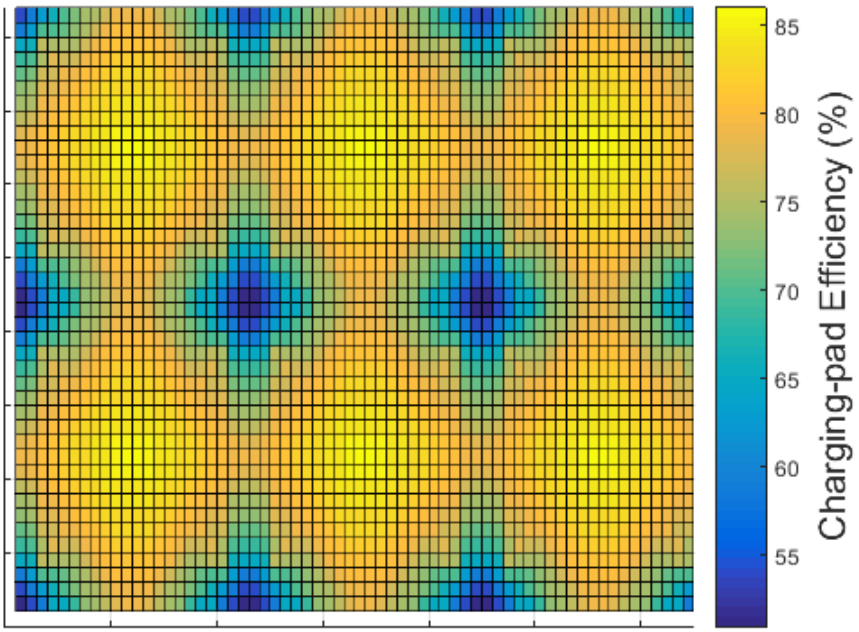

FIGURE 5.17: The efficiency of a charging pad for a whole working surface.

The main advantage of the proposed smart charger is that it offers a reduced response time as presented in Table 5.2. The reaction time needed to respond to the introduction of the receiver coil or a change of the position of the existing receiver coil is compared between the proposed and existing chargers. It has been estimated that the chargers spend $2s$ per coil in its bid to determine the coil with highest transfer efficiency. The time spent for communication was measured for the existing phone charger systems. During that time, the charger sent maximum power to the receiver, measured the efficiency and received a response from the receiver. However, our proposed charging system can determine the EV's position and start the charging of the vehicle within $15ms$, which is the time of a single programme cycle. The comparison of reaction time between the charger and the conventional chargers is presented in Fig. 5.18. It should be noted that power transmitter is decoupled from the sensor network of the charging system, though they are integrated. Therefore, the smart charger can constantly monitor the position of the vehicle without the interrupting the charging.

TABLE 5.2: Response time of a system depends on a number of transmitting coils.

No. of coils	Usual system	Proposed system
1	2s	15ms
2	4s	15ms
3	6s	15ms
4	8s	15ms
5	10s	15ms
6	12s	15ms
7	14s	15ms
8	16s	15ms

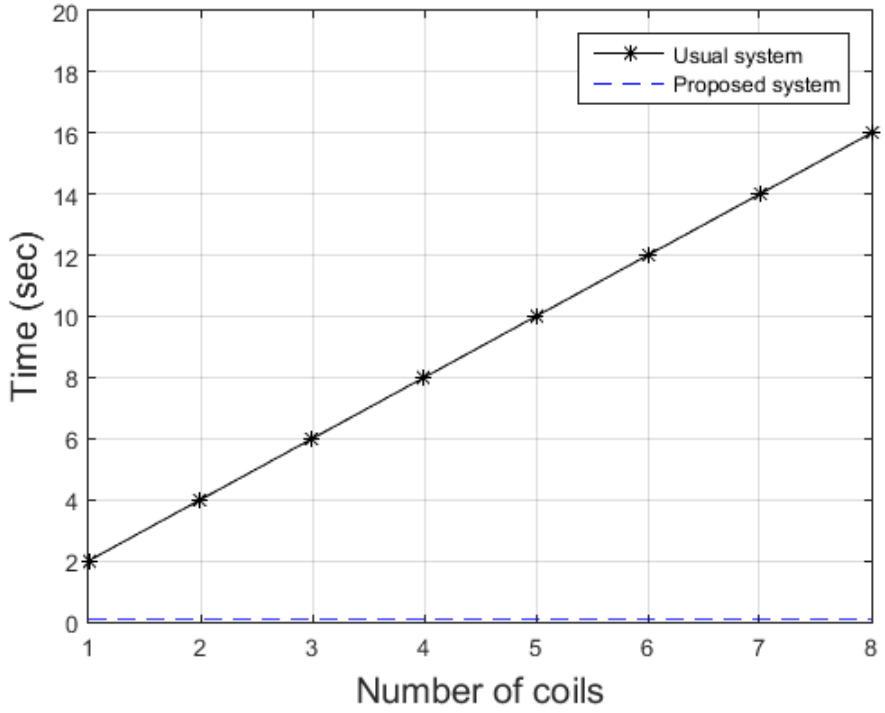

FIGURE 5.18: Comparison of the time needed for the charger to find the coil with maximum efficiency between proposed charger and conventional localization method.

Another important factor to consider in the EV charging is the power during the process of searching and selecting the transmitting coil with maximum efficiency. It has been estimated that the charger loses the same amount of power as the proposed system, which is 2mWh per coil. This estimation is based on the assumption that the full power has to be transmitted from the transmitter to the receiver for at least 1s to measure the efficiency of transmission. Therefore, as shown in Table 5.3, for a system with 6 charging

coils, the lost energy in each position is calculated to be around 12mWh. In contrast, our proposed charging solution does not require any power transmission before selecting the coil with maximum efficiency. In this regard, Fig. 5.19 shows that power consumption of the proposed system is higher for a single coil system however, with higher number of transmitting coils, the power consumption stays the same. In contrast, conventional systems power consumption increases with the number of coils. In contrast, power consumption of a conventional system increases with the number of coils. Considering, that the transmit power of the WPT system for the EV charging may vary from couple of hundreds of watts [110] up to hundreds of kilowatts [109], simultaneously the power losses due to coil search would also significantly increase. With the proposed method, the energy consumption of the charger remains stable at 3mWh regardless of the transmit power variations of the WPT charger.

TABLE 5.3: Power consumption of a system depends on the number of transmitting coils.

No. of coils	Usual system	Proposed system
1	2 mWh	3mWh
2	4mWh	3mWh
3	6mWh	3mWh
4	8mWh	3mWh
5	10mWh	3mWh
6	12mWh	3mWh
7	14mWh	3mWh
8	16mWh	3mWh

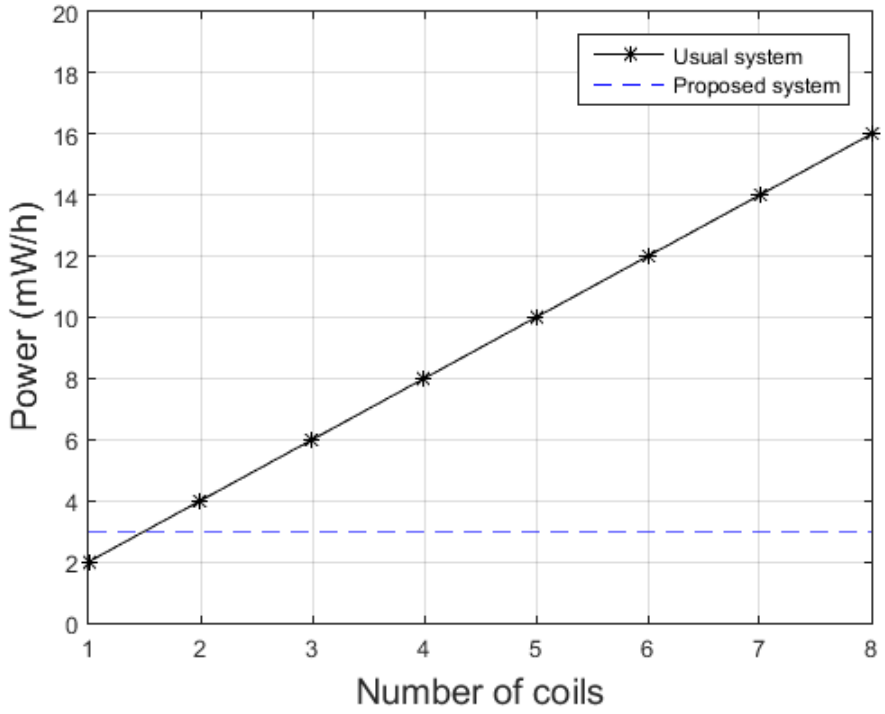

FIGURE 5.19: Comparison between estimated power loss of proposed charger and the charger with measuring method of finding the coil with maximum efficiency.

5.5 Chapter Summary

This chapter investigated a smart charging system for EVs. The system can autonomously determine the position of the receiver coil, which allows the charging pad to utilise only the coil with the highest transfer efficiency to charge the EV. The results show that, with this techniques, the operations of the charging pad can be optimised as the optimal charging coil can be determined almost immediately after the EV is located on the parking spot. Furthermore, the proposed design improves the efficiency of the charging system, as the transmitter is not required to perform measurements on each coil to determine the one with highest efficiency for each location. Thus, our solution eliminates energy losses in the optimal coil selection process, which can be significant in energy intensive systems such as car charging. Finally, the proposed method of charging is more reliable, as the car's position is detected instantly, and recalibration of the charger is not required if the car slips out of position

Chapter 6

Conclusion and Future Work

6.1 Conclusion

In a nutshell, Chapter 6 concludes this thesis, summarising the research findings presented throughout the presents five chapters, the outcomes and the path forward. This work has attempted to provide a new perspective to improve the WP charging capability for EV, addressing the current drawbacks in the market. This thesis explicates WPT technologies, applications and limitations in a systematic framework: inductive coupling WPT, magnetic resonant coupling WPT and electromagnetic radiation. Since the IWPT phenomenon was first introduced, it has come a long way becoming highly desirable, more efficient, smarter and smaller in size.

IWPT falls under the near-field category while electromagnetic radiation is widely being used for far-field WPT. Radiation-based far-field WPT offers high efficiency and longer transmission distances, but it poses a number of challenges for power transfer applications due to radiation and LoS requirements. On the other hand, near-field-based WPT is constrained by transmitter and receiver misalignments, distance and the charging direction of elements. Particularly, magnetic resonant coupling-based WPT addresses the major limitations of inductive coupling, which requires closely coupled elements. It demands precise alignment between the elements. Despite drawbacks such as potential electromagnetic interference due to higher frequency bands and lower efficiencies, resonant-based systems transmit power over long distances through complex circuitry. Hence, each technology can be accommodated based on their merits to ascertain the requirements of consumers. Inductive charging-based applications relatively relies on lower frequencies, functioning at high efficiency with minimum charging period while resonant-based applications may possibly offer a degree of freedom with power transmission between loosely coupled elements, simply trading off efficiency for convenience.

This thesis has also reviewed ongoing and previous research in the field, providing a thorough description, and a perspective on the current problems within EV wireless charging. This work differs from many published approaches as it isolates wireless charging for EV as a whole and addresses how efficiency can be improved in sub-topics, improving one design aspect at a time.

EV technology and ICEVs have been compared from both the customer's point of view and the point of view of environmental impact. Given that EV wireless charging is the focus of this thesis, not only the charging technology but also, a brief yet holistic research on the battery which is to be charged has been presented. Findings based on the literature review on currently used battery technologies have been stated and the potential multidisciplinary drawbacks of each phenomenon that require further research have been identified.

This thesis proposes two design architectures that can be used for EV charging via strongly coupled magnetic resonance using both a two-coil structure and multi-coil structure. The analogy between the geometrical structures has been mathematically detailed and heuristically derived. The relationship between system efficiency, resonant frequency, coupling coefficient and displacement between the elements, of both designs have been further analysed. The efficiency of power transfer depends on frequency. This thesis discusses efficiency in terms of Q and k, which are a function of frequency. In addition, the literature also discusses efficiency as a function of decay constant, but this has not been considered in this thesis, given that all three parameters are directly proportional to the frequency, at a given frequency the k must be higher than Q and decay constant. The theoretical circuit models were established based on the M principle and system efficiency, output power and k were expressed to further simplify the circuit parameter calculations. Suitability of the individual concept has been validated, using both the simulated and calculated system efficiency.

Chapter 3 provides a fundamental yet a cogent description of the limitations of a standalone SCMR system and the means of carefully bringing together both SCMR and CSCMR systems to overcome the system's limitations such as flexibility and manufacturing costs. In a nutshell, with the receiver end with embedded load loop and R_X in plane, the system functions at its maximum efficiency across larger distances. The experimental replication of the SCMR-CSCMR system has been documented, and the experimental

results have compared with the simulation results. The work has also highlighted the influence of vehicle and system positioning. A thorough analysis has been presented upon accommodating the changes to validate the effect on system characteristics, which have been described in great detail. The system successfully attains efficiencies compared to frequency matching techniques, arbitrating the ability to charge EV models with a diverse range of dimensions with an accelerated degree of freedom.

Chapter 4 presents a modified two loop resonant WPT circuit where the inductors with high resonant factor are replaced with a small set of inductors which are placed in parallel with a low–Q inductor. The study indicates that the proposed system design can attain the maximum efficiency at even a smaller k akin to a system with high-Q coils. Interestingly, design concepts presented in this thesis, have further reduced the size and the weight of the system, proving that the higher Q-factor results can be achieved without high-Q inductors and low capacitor value. Therefore, the proposed system indicated 5% contraction of efficiency to achieve the 80% size reduction and 79% weight reduction of the elements, hence can potentially be installed within a compact yet smaller application.

In Chapter 5, SCMR-based smart algorithm has been illustrated, providing a multi-position charging platform that can be installed in a parking space. The system can autonomously identify the location of the receiver and begin the charging process immediately, using only the coil capable of attaining highest efficiency. Even though, the proposed charging pad offers a superior and reliable charging solution, it may have limitations such as assistance of a control algorithm. In future the planning uncertainties need to be met, given the increasing number of vehicles that demand charging. Furthermore, the loading capacity and the impact of extensive charging on the charger need to be measured.

The main objective of this project is to develop an infrastructure to accommodate WPT between different charging platforms and receiver architectures to cater static charging of the batteries comprised in potential applications such as EV, hand-held devices, household equipment etc. Three different WPT architectures have been proposed and have been successfully implemented. An economic evaluation for each architectural structure has not been conducted where assessing the commercial viability does not fall within the project's scope. The cost of the materials, has often been widely debated to justify their manufacturability. As a matter of fact, material costs and

weight mitigate the larger overhead constraints caused due to metal and passive power electronic components. Inductive solution that is smaller, lighter with enhanced efficiency has been discussed while minimising the cost and mass of the system. Hence emerging ultra-capacitors, which instantly deliver and store energy, can be utilised to support design optimisation. The conclusions of this thesis can be summarised as follows.

- Miniaturization of the system can be achieved in a number of ways, by simply combining two or more existing designs or by adding compact system components to the systems.
- The maximum distance between the TX and Rx components, can be enhanced by using additional components, however, this might reduce the transfer efficiency.
- The reduction of weight can be achieved by adding new components to represent the existing system components, which may simultaneously reduce both the size and the weight of the system.
- Strongly coupled inductors are not compulsory to achieve longer distances.
- Early detection of the receiver coil can be achieved with a low power detection circuit, eliminating actual power transmission between the transmitter and receiver.
- Contraction of the distance between the transmitter and the receiver in a four-loop inductive system can be compensated by decreasing the distance between the source and transmitter loop.

6.2 Future Work

The global wireless charging market for EV is growing in leaps and bounds, intending to drive the market share at a significant rate parallel to the surging EV sales. Major industrial players such as Qualcomm, WiTricity and other auto manufacturers, heavily invest in research and development, while the consumer is ready to pay premium prices to own the market trends. The time limitations of the technology such as its shorter range, the lack of charging infrastructure and longer charging durations have been discussed throughout out the study, and a handful of future research possibilities have been emphasised.

This thesis is highly centred on optimising WPT efficiency to accommodate EV charging. Where during the literature review, it is noted that few areas require further research. A vast range of literature or publications addresses physical design and characteristics such as the inductance, coupling and efficiency of WPT. Hence, it can be surmised that the quantum mechanical behaviour of magnetic resonant coupling has been the least addressed areas; however, it has the potential to reveal how reactive forces function in free space to further enhance the efficiency of applications.

6.2.1 Dynamic Charging

IWPT technology has exhibited satisfactory performance in stationary charging, while the vehicle is parked or stopped for a short period of time. Designing a real life-dynamic charging system can be considered as one of the most eminent challenges catering charging facility to a vehicle which is in motion along a dedicated lane, equipped with an IWPT system. Dynamic wireless charging is a promising technology to partially or completely eliminate the stationary charging, through a network of dynamic chargers installed underneath the roads. Dynamic charging would also significantly decrease the demand for higher battery capacity with increased range and the reliability of EVs. However, there are a number of hurdles to skip prior to physically implement such a system. Particularly, losses due to coil misalignments and vehicle tracking would be among the most critical challenges to overcome.

6.2.2 Coil Misalignments

Although this study has proposed coil overlapping in the experimental set up, the design structure may require further research to improve the misalignments with additional circuitry, minimising the material costs. Highest efficiency achieved during the experiment was close to 100% efficiency, which may be achieved by scaling coil characteristics such as its material, diameter and geometry. Given the fact that SCMR-based systems operate in a reactive near-field region, it has a highly limited range. If the systems are built with special meta-materials and tuned to operate at a lower frequency range, the range may be enhanced. There is an open window to further miniaturise the coil architecture using a variety of dielectrics and highly permeable ferromagnetic materials.

6.2.3 Battery Technology

Even though this study has not extensively addressed the limitation of each battery technology to accommodate the aforementioned design architectures, the range could be further improved with enhanced battery solutions or power management solutions; for instance, by employing ultra-capacitors. This study has often assumed that the transmitter pad is located in one place or standing still and the receiver pad is located within the object to be charged, where power transmission occurs in one direction. However, the literature indicates that the notion of bidirectional WPT is emerging as a solution to facilitate charging a neighbouring device which requires charging or returning the extra energy back to the source.

6.2.4 System Architecture

Ensuring widespread adoption of wireless power systems for EV means they are required to move forward and be able to charge EV with electrical propulsion and autonomous cars by 2035. Magnetic resonance based WPT has so far been able to attain high efficiency power transmission at a greater distance, using $6.78MHz$ ISM frequency band. To fulfil the rising demand, magnetic resonant systems require to undergo fundamental changes in both coil technologies, system architecture, and amplifiers. Gallium nitride-based (GaN) class D amplifiers (similar to a conventional DC-AC inverter) and class D zero voltage switching (ZVS) will be highly advantageous to use in wireless power transmission, as they lead to lesser switching losses and have the potential to enhance overall system efficiency. GaN technology itself is a novel addition to the power electronics. However, the introduction of GaN-based amplifiers require an extensive amount of research, covering both its reliability and safety characteristics.

6.2.5 Smart Energy Management

Both the charging platform and vehicle should be developed with smart features to autonomously detect the power demand profile in advance, to trade-off in terms of energy source between the conventional battery and ultra-capacitor system, which will eventually expand the range. Hence the power splitting decision should be made based on a certain policy that determines

the time, the load required and the efficiency boundaries via a form of artificial intelligence (AI). Publications have discussed in-vehicle power management based on a vehicle's forward-propulsion load, but the non-propulsion loads have not been not widely investigated.

Bibliography

[1] N. George and K. Kershaw. "Road Use statistics Great Britain 2017". In: *Road Use statistics Great Britain 2017*. UK Department for Transport. 2017.

[2] T. Parry and Public Enquiries. "Vehicle licensing statistics Annual 2017 Revised". In: *Vehicle licensing statistics: Annual 2017 Government Statistical Release (2018)*. UK Department for Transport. 2018.

[3] A. P. Sample, D. T. Meyer, and J. R. Smith. "Analysis, experimental results, and range adaptation of magnetically coupled resonators for wireless power transfer". In: *IEEE Tran. on Ind. Electronics* 58.2 (2011), pp. 544–554.

[4] A. Sultanbek, A. Khassenov, Y. Kanapyanov, M. Kenzhegaliyeva, and M. Bagheri. "Intelligent wireless charging station for electric vehicles". In: *Internat. Siberian Conf. on Control and Communications (SIBCON) 2017*. IEEE. 2017, pp. 1–6.

[5] C. A. Tucker. "Transmission of wireless power by magnetic resonance". PhD thesis. University of Reading, 2013.

[6] A. Kurs, A. Karalis, R. Moffatt, J. D. Joannopoulos, P. Fisher, and M. Soljačić. "Wireless power transfer via strongly coupled magnetic resonances". In: *science* 317.5834 (2007), pp. 83–86.

[7] J. Zhou, B. Luo, X. Zhang, and Y. Hu. "Extendible load-isolation wireless charging platform for multi-receiver applications". In: *IET Power Electronics* 10.1 (2017), pp. 134–142.

[8] J. V. de Almeida and R. S. Feitoza. "Metamaterial-Enhanced Magnetic Coupling: An Inductive Wireless Power Transmission System Assisted by Metamaterial-Based u-Negative Lenses". In: *IEEE Microwave Magazine* 19.4 (2018), pp. 95–100.

[9] Z. Li, C. Zhu, J. Jiang, K. Song, and G. Wei. "A 3-kW wireless power transfer system for sightseeing car supercapacitor charge". In: *IEEE Transactions on Power Electronics* 32.5 (2017), pp. 3301–3316.

[10] A. A. S. Mohamed, C. R. Lashway, and O. Mohammed. "Modeling and feasibility analysis of quasi-dynamic WPT system for EV applications". In: *IEEE tran. on transportation electrification* 3.2 (2017), pp. 343–353.

[11] D. Patil, M. K. McDonough, J. M. Miller, B. Fahimi, and P. T. Balsara. "Wireless Power Transfer for Vehicular Applications an Overview and Challenges". In: *IEEE Tran. on Transportation Electrification* 4.1 (2018), pp. 3–37.

[12] B. Regensburger, S. Sinha, A. Kumar, J. Vance, Z. Popovic, and K. K. Afridi. "Kilowatt-scale large air-gap multi-modular capacitive wireless power transfer system for electric vehicle charging". In: *Applied Power Electronics Conf. and Exposition (APEC), 2018 IEEE*. IEEE. 2018, pp. 666–671.

[13] A. Barakat, K. Yoshitomi, and R. K. Pokharel. "Design Approach for Efficient Wireless Power Transfer Systems During Lateral Misalignment". In: *IEEE Transactions on Microwave Theory and Techniques* 66.9 (2018), pp. 4170–4177.

[14] WiTricity. *DRIVE: Electric Vehicles*. Ed. by WiTricity Corporation. June 2018. URL: http://witricity.com/products/automotive/.

[15] M. Bhagat and S. Nalbalwar. "Wireless Transfer of Solar Power for Charging Mobile Devices in a Vehicle". In: (2017).

[16] J. C. Maxwell. *A treatise on electricity and magnetism*. A Treatise on Electricity and Magnetism v. 1-2. Dover Publications, 1954. URL: https://books.google.co.uk/books?id=HbUPAQAAMAAJ.

[17] F. Marra, L. Zhang, and J. G. Lyng. "Radio frequency treatment of foods: review of recent advances". In: *Journal of food engineering* 91.4 (2009), pp. 497–508.

[18] A. S. Marincic. "Nikola Tesla and the Wireless Transmission of Energy". In: *IEEE Power Engineering Review* PER-2.10 (1982), pp. 58–59. ISSN: 0272-1724. DOI: 10.1109/MPER.1982.5519923.

[19] C. K. Lee, W. X. Zhong, and S. Y. R. Hui. "Recent progress in mid-range wireless power transfer". In: *2012 IEEE Energy Conversion Congress and Exposition (ECCE)*. 2012, pp. 3819–3824.

[20] S. C. Nambiar and M. Manteghi. "A simple wireless power transfer scheme for implanted devices". In: *2014 United States Nat. Committee of URSI Nat. Radio Science Meeting (USNC-URSI NRSM)*. 2014, pp. 1–1. DOI: 10.1109/USNC-URSI-NRSM.2014.6928003.

[21] E. C. Okress, W. C. Brown, T. Moreno, G. Goubau, N. I. Heenan, and R. H. George. "Microwave power engineering". In: *IEEE Spectrum* 1.10 (1964), pp. 76–76. ISSN: 0018-9235. DOI: 10.1109/MSPEC.1964.6501190.

[22] J. J. Schlesak, A. Alden, and T. Ohno. "A microwave powered high altitude platform". In: *1988., IEEE MTT-S Internat. Microwave Symp. Digest*. 1988, 283–286 vol.1. DOI: 10.1109/MWSYM.1988.22031.

[23] B. Strassner and K. Chang. "Microwave Power Transmission: Historical Milestones and System Components". In: *Proceedings of the IEEE* 101.6 (2013), pp. 1379–1396. ISSN: 0018-9219. DOI: 10.1109/JPROC.2013.2246132.

[24] J. O. McSpadden and J. C. Mankins. "Space solar power programs and microwave wireless power transmission technology". In: *IEEE Microwave Magazine* 3.4 (2002), pp. 46–57. ISSN: 1527-3342. DOI: 10.1109/MMW.2002.1145675.

[25] A. K. RamRakhyani, S. Mirabbasi, and M. Chiao. "Design and optimization of resonance-based efficient wireless power delivery systems for biomedical implants". In: *IEEE Tran. on Biomedical Circuits and Systems* 5.1 (2011), pp. 48–63.

[26] X. Lu, P. Wang, D. Niyato, D. I. Kim, and Z. Han. "Wireless Charging Technologies: Fundamentals, Standards, and Network Applications". In: *IEEE Commun. Surveys Tutorials* 18.2 (2016), pp. 1413–1452. ISSN: 1553-877X. DOI: 10.1109/COMST.2015.2499783.

[27] G. Kiruthiga, M. Y. Jayant, and A. Sharmila. "Wireless charging for low power applications using Qi standard". In: *2016 Internat. Conf. on Commun. and Signal Processing (ICCSP)*. 2016, pp. 1180–1184. DOI: 10.1109/ICCSP.2016.7754338.

[28] Y. J. Park, B. Jang, S. M. Park, H. C. Ryu, S. J. Oh, S. Y. Kim, Y. Pu, S. S. Yoo, K. C. Hwang, Y. Yang, M. Lee, and K. Y. Lee. "A Triple-Mode Wireless Power-Receiving Unit With 85.5Efficiency for A4WP, WPC, and PMA Applications". In: *IEEE Tran. on Power Electronics* 33.4 (2018), pp. 3141–3156. ISSN: 0885-8993. DOI: 10.1109/TPEL.2017.2703153.

[29] X. Wei, Z. Wang, and H. Dai. "A Critical Review of Wireless Power Transfer via Strongly Coupled Magnetic Resonances". In: *Energies* 7.7 (2014), pp. 4316–4341. ISSN: 1996-1073. URL: http://www.mdpi.com/1996-1073/7/7/4316.

[30] C. S. Wang, G. A. Covic, and O. H. Stielau. "Power transfer capability and bifurcation phenomena of loosely coupled inductive power transfer systems". In: *IEEE Tran. on Ind. Electronics* 51.1 (2004), pp. 148–157. ISSN: 0278-0046. DOI: 10.1109/TIE.2003.822038.

[31] Z. Pantic and S. M. Lukic. "Framework and Topology for Active Tuning of Parallel Compensated Receivers in Power Transfer Systems". In: *IEEE Tran. on Power Electronics* 27.11 (2012), pp. 4503–4513. ISSN: 0885-8993. DOI: 10.1109/TPEL.2012.2196055.

[32] N. Shinohara. "Power without wires". In: *IEEE Microwave Magazine* 12.7 (2011), S64–S73.

[33] M. Kesler. "Highly resonant wireless power transfer: safe, efficient, and over distance". In: *Witricity corporation* (2013), pp. 1–32.

[34] T. Hiramatsu, X. Huang, M. Kato, T. Imura, and Y. Hori. "Wireless charging power control for HESS through receiver side voltage control". In: *Applied Power Electronics Conference and Exposition (APEC), 2015 IEEE*. IEEE. 2015, pp. 1614–1619.

[35] F. Musavi, M. Edington, and W. Eberle. "Wireless power transfer: A survey of EV battery charging technologies". In: *Energy Conversion Congress and Exposition (ECCE), 2012 IEEE*. IEEE. 2012, pp. 1804–1810.

[36] M. H. Kline. *Capacitive power transfer*. Tech. rep. California Univ. Berkeley Dept. of Electrical Eng. and Computer Sci., 2010.

[37] Jiejian J. Dai, Daniel C D. C. Ludois, et al. "A survey of wireless power transfer and a critical comparison of inductive and capacitive coupling for small gap applications". In: *IEEE Trans. Power Electron* 30.11 (2015), pp. 6017–6029.

[38] F. Lu, H. Zhang, H. Hofmann, and C. C. Mi. "A double sided LCLC compensated capacitive power transfer system for electric vehicle charging". In: *IEEE Tran. on Power Electronics* 30.11 (2015), pp. 6011–6014.

[39] F. Lu, H. Zhang, H. Hofmann, and C. C. Mi. "An Inductive and Capacitive Combined Wireless Power Transfer System With LC Compensated Topology". In: *IEEE Tran. on Power Electronics* 31.12 (2016), pp. 8471–8482.

[40] A. Costanzo, M. Dionigi, F. Mastri, M. Mongiardo, G. Monti, J. A. Russer, P. Russer, and L. Tarricone. "Conditions for a load independent operating regime in resonant inductive WPT". In: vol. 65. 4. IEEE, 2017, pp. 1066–1076.

[41] M. Rozman, M. Fernando, B. Adebisi, K. M. Rabie, R. Kharel, A. Ikpehai, and H. Gacanin. "Combined conformal strongly-coupled magnetic resonance for efficient wireless power transfer". In: *Energies* 10.4 (2017), p. 498.

[42] K. Hassan, S. Pan, and P. Jain. "Multiple receiver wireless power charger for mobile electronic devices in near field". In: *Industrial Electronics for Sustainable Energy Systems (IESES), 2018 IEEE International Conference on*. IEEE. 2018, pp. 426–433.

[43] S. Kim, I. K. Cho, J. I. Moon, S. I. Jeon, and J. I. Choi. "5W wireless power transmission system with coupled magnetic resonance". In: *2013 5th IEEE Internat. Symp. on Microwave, Antenna, Propag. and EMC Tech. for Wireless Commun.* 2013, pp. 255–258. DOI: 10.1109/MAPE.2013.6689880.

[44] M. Rozman, K. M. Rabie, and B. Adebisi. "Wireless Power and Communication Transmission for Industrial Robots". In: *2018 11th International Symp. on Commun. Systems, Networks Digital Signal Proc. (CSNDSP)*. 2018, pp. 1–5. DOI: 10.1109/CSNDSP.2018.8471796.

[45] S. Prengel, M. Helwig, and N. Modler. "Lightweight coil for efficient wireless power transfer: Optimization of weight and efficiency for WPT coils". In: *2014 IEEE Wireless Power Transfer Conference*. 2014, pp. 96–99. DOI: 10.1109/WPT.2014.6839603.

[46] B. Li, Y. Geng, F. Lin, Z. Yang, and S. Igarashi. "Design of Constant Voltage Compensation Topology Applied to WPT System for Electrical Vehicles". In: *2016 IEEE Vehicle Power and Propulsion Conference (VPPC)*. 2016, pp. 1–6.

[47] R. Zhang and C. K. Ho. "MIMO Broadcasting for Simultaneous Wireless Information and Power Transfer". In: *IEEE Tran. on Wireless Commun.s* 12.5 (2013), pp. 1989–2001. ISSN: 1536-1276. DOI: 10.1109/TWC.2013.031813.120224.

[48] G. Yilmaz and C. Dehollain. *Wireless power transfer and data communication for neural implants: case study: epilepsy monitoring*. Springer, 2017.

[49] B. Lu. *Solid state microwave generator*. US Patent App. 15/237,081. 2017.

[50] Z. Harouni, L. Cirio, L. Osman, A. Gharsallah, and O. Picon. "A Dual Circularly Polarized 2.45-GHz Rectenna for Wireless Power Transmission". In: *IEEE Antennas and Wireless Propag.n Letters* 10 (2011), pp. 306–309. ISSN: 1536-1225. DOI: 10.1109/LAWP.2011.2141973.

[51] E. Henderson and M. Holderman. "Technology applications that support space exploration". In: *47th AIAA/ASME/SAE/ASEE Joint Propulsion Conference & Exhibit*. 2011, p. 5570.

[52] X. Yang, W. Geyi, and H. Sun. "Optimum design of wireless power transmission system using microstrip patch antenna arrays". In: *IEEE Antennas and Wireless Propag. Letters* 16 (2017), pp. 1824–1827.

[53] A. Ahmad, M. S. Alam, and R. Chabaan. "A comprehensive review of wireless charging technologies for electric vehicles". In: *IEEE Tran. on Transportation Electrification* 4.1 (2018), pp. 38–63.

[54] L. Summerer and O. Purcell. "Concepts for wireless energy transmission via laser". In: *Europeans Space Agency (ESA)-Advanced Concepts Team* (2009).

[55] F. Steinsiek. "Wireless power transmission experiment as an early contribution to planetary exploration missions". In: *54th International Astronautical Congress of the International Astronautical Federation, the International Academy of Astronautics, and the International Institute of Space Law*. 2003, R–3.

[56] M. Mori, H. Kagawa, and Y. Saito. "Summary of studies on space solar power systems of Japan Aerospace Exploration Agency (JAXA)". In: *Acta Astronautica* 59.1-5 (2006), pp. 132–138.

[57] Q. Zhang, W. Fang, Q. Liu, J. Wu, P. Xia, and L. Yang. "Distributed laser charging: A wireless power transfer approach". In: *IEEE Internet of Things Journal* (2018).

[58] M. Sugino and T. Masamura. "The wireless power transfer systems using the Class E push pull inverter for industrial robots". In: *Wireless Power Transfer Conference (WPTC), 2017 IEEE*. IEEE. 2017, pp. 1–3.

[59] I. Mayordomo, T. Dräger, J. A. Alayón, and J. Bernhard. "Wireless power transfer for sensors and systems embedded in fiber composites". In: *2013 IEEE Wireless Power Transfer (WPT)*. 2013, pp. 107–110. DOI: 10.1109/WPT.2013.6556894.

[60] J. Shin, S. Shin, Y. Kim, S. Ahn, S. Lee, G. Jung, S. Jeon, and D. Cho. "Design and Implementation of Shaped Magnetic Resonance Based Wireless Power Transfer System for Roadway Powered Moving Electric Vehicles". In: *IEEE Tran. on Ind. Electronics* 61.3 (2014), pp. 1179–1192. ISSN: 0278-0046. DOI: 10.1109/TIE.2013.2258294.

[61] H. Widmer, N. P. Cook, and L. Sieber. *Wireless power transmission in electric vehicles*. US Patent 9,561,730. 2017.

[62] K. Tachikawa, M. Kesler, and O. Atasoy. "Feasibility Study of Bi directional Wireless Charging for Vehicle to Grid". In: *SAE Technical Paper* (2018), pp. 01–0669.

[63] N. Shinohara. "Wireless power transmission progress for electric vehicle in Japan". In: *Radio and Wireless Symposium (RWS), 2013 IEEE*. IEEE. 2013, pp. 109–111.

[64] H. Matsumoto. "Research on solar power satellites and microwave power transmission in Japan". In: *IEEE microwave magazine* 3.4 (2002), pp. 36–45.

[65] Y. Shi, L. Xie, Y. T. Hou, and H. D. Sherali. "On renewable sensor networks with wireless energy transfer". In: *2011 Proceedings IEEE INFOCOM*. 2011, pp. 1350–1358. DOI: 10.1109/INFCOM.2011.5934919.

[66] W. Wang, V. Srinivasan, and K. C. Chua. "Using mobile relays to prolong the lifetime of wireless sensor networks". In: *Proceedings of the 11th annual international conference on Mobile computing and networking*. ACM. 2005, pp. 270–283.

[67] K. N. Mude, M. T. Outeiro, and A. Carvalho. "In-motion wireless power transfer: Technology, infrastructure, challenges and market scenario". In: *2017 IEEE Internat. Conf. on Industrial Technology (ICIT)*. IEEE. 2017, pp. 1550–1554.

[68] A. O. Leung, W. J. Luksemburg, A. S. Wong, and M. H. Wong. "Spatial distribution of polybrominated diphenyl ethers and polychlorinated dibenzopdioxins and dibenzofurans in soil and combusted residue at Guiyu, an electronic waste recycling site in southeast China". In: *Environmental science & technology* 41.8 (2007), pp. 2730–2737.

[69] C. Liu, A. P. Hu, and X. Dai. "A contactless power transfer system with capacitively coupled matrix pad". In: *Energy Conversion Congress and Exposition (ECCE), 2011 IEEE*. IEEE. 2011, pp. 3488–3494.

[70] M. Kline, I. Izyumin, B. Boser, and S. Sanders. "Capacitive power transfer for contactless charging". In: *Applied Power Electronics Conf. and Exposition (APEC), 2011 Twenty-Sixth Annual IEEE*. IEEE. 2011, pp. 1398–1404.

[71] R. G. Dickie. *Toothbrush oscillating head*. US Patent 6,536,066. 2003.

[72] J. Choi, Y. H. Ryu, D. Kim, N. Y. Kim, C. Yoon, Y. K. Park, S. Kwon, and Y. Yang. "Design of high efficiency wireless charging pad based on magnetic resonance coupling". In: *Radar Conference (EuRAD), 2012 9th European*. IEEE. 2012, pp. 590–593.

[73] H. Ju and R. Zhang. "Throughput maximization in wireless powered communication networks". In: *IEEE Trans. on Wireless Commun.* 13.1 (2014), pp. 418–428.

[74] R. Fiorello, A. J. Campanella, K. L. Hall, M. P. Kesler, K. Kulikowski, and E. R. Giler. *Wireless powered television*. US Patent 9.160.203. 2015.

[75] M. P. Kesler, A. J. Campanella, K. L. Hall, A. Karalis, A. B. Kurs, and Q. Li. *Wireless powered projector*. US Patent App. 13/267.757. 2012.

[76] S. W. Ham, J. X. Kuang, and D. J. Vanoni. *Wireless power for heating or cooling*. US Patent App. 12/849,710. 2011.

[77] J. Chiao. "Batteryless wireless gastric implants". In: *WAMICON 2014*. 2014, pp. 1–4. DOI: 10.1109/WAMICON.2014.6857808.

[78] P. Hou, Y. Cheng, M. Jia, L. Feng, and Q. Ding. "Site to site wireless power transmission for medical endoscopes". In: *2010 3rd Internat. Conf. on Biomedical Engineering and Informatics*. Vol. 5. 2010, pp. 2101–2103. DOI: 10.1109/BMEI.2010.5639991.

[79] J. Zhiwei and Z. Bingquan. "A new type receiving set of wireless power transmission systems for gastrointestinal robot". In: *2015 IEEE PELS Workshop on Emerging Technologies: Wireless Power (2015 WoW)*. 2015, pp. 1–4. DOI: 10.1109/WoW.2015.7132850.

[80] K. A. Townsend, J. W. Haslett, T. K. K. Tsang, M. N. El-Gamal, and K. Iniewski. "Recent advances and future trends in low power wireless systems for medical applications". In: *Fifth Internat. Workshop on System on Chip for Real Time Applications (IWSOC'05)*. 2005, pp. 476–481. DOI: 10.1109/IWSOC.2005.96.

[81] A. Lymberis. "Smart wearable systems for personalised health management: current RD and future challenges". In: *Engineering in Medicine and Biology Society, 2003. Proceedings of the 25th Annual International Conference of the IEEE*. Vol. 4. IEEE. 2003, pp. 3716–3719.

[82] D. P. Williams. "On optimal AUV track-spacing for underwater mine detection". In: *2010 IEEE Internat. Conf. on Robotics and Automation (ICRA)*. IEEE. 2010, pp. 4755–4762.

[83] K. Lam, R. S. Bradbeer, P. K. S. Shin, Kenneth K. Ku, and P. Hodgson. "Application of a real time underwater surveillance camera in monitoring of fish assemblages on a shallow coral communities in a marine park". In: *OCEANS 2007*. IEEE. 2007, pp. 1–7.

[84] A. Askari, R. Stark, J. Curran, D. Rule, and K. Lin. "Underwater wireless power transfer". In: *2015 IEEE Wireless Power Transfer Conference (WPTC)*. 2015, pp. 1–4. DOI: 10.1109/WPT.2015.7139141.

[85] T. Assaf, C. Stefanini, and P. Dario. "Autonomous underwater biorobots: A wireless system for power transfer". In: *IEEE Robotics & Automation Magazine* 20.3 (2013), pp. 26–32.

[86] J. Manikandan, S. Akash, A. Vishwanath, R. Nandakumar, V. K. Agrawal, and M. Korulla. "Design and development of contactless battery charger for underwater vehicles". In: (2015).

[87] D. Van Wageningen and T. Staring. "The Qi wireless power standard". In: *Power Electronics and Motion Control Conference (EPE/PEMC), 2010 14th International*. IEEE. 2010, S15–25.

[88] X. Lu, P. Wang, D. Niyato, D. I. Kim, and Z. Han. "Wireless charging technologies: Fundamentals, standards, and network applications". In: *IEEE Commun. Surveys AND Tutorials* 18.2 (2016), pp. 1413–1452.

[89] IEEE. "IEEE Standard for Safety Levels with Respect to Human Exposure to Radio Frequency Electromagnetic Fields, 3 kHz to 300 GHz". In: *IEEE Std C95.1-2005 (Revision of IEEE Std C95.1-1991)* (2006), pp. 1–238. DOI: 10.1109/IEEESTD.2006.99501.

[90] S. J. Orfanidis. "Electromagnetic waves and antennas". In: (2002).

[91] H. Vazquez-Lealr, A. Gallardo del Angel, CR. astaneda Sheissa, and F. J. Gonzalez-Martinezr. "The phenomenon of wireless energy transfer: experiments and philosophy". In: *Wireless Power Transfer Principles and Engineering Explorations*. InTech, 2012.

[92] C. Liao, J. Li, and S. Li. "Design of LCC impedance matching circuit for wireless power transfer system under rectifier load". In: *CPSS Tran. on Power Electronics and Applications* 2.3 (2017), pp. 237–245. ISSN: 2475-742X. DOI: 10.24295/CPSSTPEA.2017.00022.

[93] Q. Wang, W. Che, G. Monti, M. Mongiardo, M. Dionigi, and F. Mastri. "Conjugate image impedance matching for maximizing the gains of a WPT link". In: *2018 IEEE MTT-S Internat. Wireless Symp. (IWS)*. 2018, pp. 1–3. DOI: 10.1109/IEEE-IWS.2018.8400873.

[94] S. Lee and R. D. Lorenz. "Development and Validation of Model for 95Wireless Power Transfer Over a 30-cm Air Gap". In: *IEEE Tran. on Ind. Applications* 47.6 (2011), pp. 2495–2504. ISSN: 0093-9994. DOI: 10.1109/TIA.2011.2168555.

[95] T. C. Beh, T. Imura, M. Kato, and Y. Hori. "Basic study of improving efficiency of wireless power transfer via magnetic resonance coupling based on impedance matching". In: *2010 IEEE Internat. Symp. on Ind. Electronics* (2010), pp. 2011–2016. ISSN: 2163-5137.

[96] H. Hao, G. A. Covic, and J. T. Boys. "An Approximate Dynamic Model of LCL-T Based Inductive Power Transfer Power Supplies". In: *IEEE Tran. on Power Electronics* 29.10 (2014), pp. 5554–5567. ISSN: 0885-8993. DOI: 10.1109/TPEL.2013.2293138.

[97] M. M. Al-Asadi, A. P. Duffy, A. J. Willis, K. Hodge, and T. M. Benson. "A simple formula for calculating the frequency-dependent resistance of a round wire". In: *Microwave and Optical Technology Letters* 19.2 (1998), pp. 84–87.

[98] N. Xi and C. R. Sullivan. "An improved calculation of proximity-effect loss in high-frequency windings of round conductors". In: *IEEE 34th Annual Conf. on Power Electronics Specialist (PESC)*. Vol. 2. 2003, 853–860 vol.2. DOI: 10.1109/PESC.2003.1218168.

[99] O. D. Momoh and M. O. Omoigui. "An overview of hybrid electric vehicle technology". In: *Vehicle Power and Propulsion Conference, (VPPC'09)*. IEEE. 2009, pp. 1286–1292.

[100] T. Ishizaki, G. Kitano, and K. Mikami. "Mobile wireless power transfer system for electric vehicles". In: *2014 IEEE Wireless Power Transfer Conf.* 2014, pp. 142–145. DOI: 10.1109/WPT.2014.6839575.

[101] M. Ayman, S. Gurhari, S. Hagspiel, M. Fellah, and A. Rousseau. "Impact of real world drive cycles on PHEV fuel efficiency and cost for different powertrain and battery characteristics". In: *World Electric Vehicle Journal* 3.1 (2009), pp. 186–195.

[102] L. O. Valøen and M. I. Shoesmith. "The effect of PHEV and HEV duty cycles on battery and battery pack performance". In: *PHEV 2007 Conference*. 2007, pp. 4–5.

[103] P. Bauer, Y. Zhou, J. Doppler, and N. Stembridge. "Charging of electric vehicles and impact on the grid". In: *13th Mechatronika 2010*. 2010, pp. 121–127.

[104] C. Duan, C. Jiang, A. Taylor, and K. Bai. "Design of a zero-voltage-switching large-air-gap wireless charger with low electrical stress for Plugin Hybrid Electric Vehicles". In: *2013 IEEE Transportation Electrification Conference and Expo (ITEC)*. 2013, pp. 1–5. DOI: 10.1109/ITEC.2013.6574507.

[105] S. Hu, J. Deng, C. Mi, and M. Zhang. "Optimal design of line level control resonant converters in plug-in hybrid electric vehicle battery chargers". In: *IET Electrical Systems in Transportation* 4.1 (2014), pp. 21–28. ISSN: 2042-9738. DOI: 10.1049/iet-est.2013.0016.

[106] Kevin Morrow, Donald Karner, and James Francfort. "Plug-in hybrid electric vehicle charging infrastructure review". In: *US Department of Energy-Vehicle Technologies Program* 34 (2008).

[107] M. Yilmaz and P. T. Krein. "Review of Battery Charger Topologies, Charging Power Levels, and Infrastructure for Plug-In Electric and Hybrid Vehicles". In: *IEEE Transactions on Power Electronics* 28.5 (2013), pp. 2151–2169. ISSN: 0885-8993. DOI: 10.1109/TPEL.2012.2212917.

[108] Anamika Dubey and Surya Santoso. "Electric vehicle charging on residential distribution systems: Impacts and mitigations". In: *IEEE Access* 3 (2015), pp. 1871–1893.

[109] Aviva Brecher, David Arthur, et al. *Review and evaluation of wireless power transfer (WPT) for electric transit applications*. Tech. rep. John A. Volpe National Transportation Systems Center (US), 2014.

[110] G. Buja, M. Bertoluzzo, and K. N. Mude. "Design and Experimentation of WPT Charger for Electric City Car". In: *IEEE Transactions on Industrial Electronics* 62.12 (2015), pp. 7436–7447. ISSN: 0278-0046. DOI: 10.1109/TIE.2015.2455524.

[111] S. Lukic and Z. Pantic. "Cutting the Cord: Static and Dynamic Inductive Wireless Charging of Electric Vehicles". In: *IEEE Electrification Magazine* 1.1 (2013), pp. 57–64. ISSN: 2325-5897.

[112] Young Jang, Seungmin Jeong, and Min Lee. "Initial energy logistics cost analysis for stationary, quasi-dynamic, and dynamic wireless charging public transportation systems". In: *Energies* 9.7 (2016), p. 483.

[113] B. G. Pollet, I. Staffell, and J. I. Shang. "Current status of hybrid, battery and fuel cell electric vehicles: From electrochemistry to market prospects". In: *Electrochimica Acta* 84 (2012), pp. 235–249.

[114] T. R. Hawkins, B. Singh, G. Majeau-Bettez, and A. H. Strømman. "Comparative environmental life cycle assessment of conventional and electric vehicles". In: *Journal of Industrial Ecology* 17.1 (2013), pp. 53–64.

[115] J. W. Brennan and T. E. Barder. "Battery Electric Vehicles vs. Internal Combustion Engine Vehicles". In: *A United States-Based Comprehensive Assessment* (2016).

[116] J. Loughran. *Japan's first electric car battery recycling plant to sell old batteries at half price*. 2018. URL: `https : eandt . theiet . org` (visited on 10/15/2018).

[117] S. T. Myung, F. Maglia, K. J. Park, C. S. Yoon, P. Lamp, S. J. Kim, and Y. K. Sun. "Nickel-rich layered cathode materials for automotive lithium-ion batteries: achievements and perspectives". In: *ACS Energy Letters* 2.1 (2016), pp. 196–223.

[118] L. Wang, X. Liu, H. Li, W. Im, and J. Kim. "Power electronics enabled energy management for energy storage with extended cycle life and improved fuel economy in a PHEV". In: *2010 IEEE Energy Conversion Congress and Exposition*. 2010, pp. 3917–3922. DOI: `10.1109/ECCE.2010.5617792`.

[119] G. Buja, M. Bertoluzzo, and K. N. Mude. "Design and experimentation of WPT charger for electric city car". In: *IEEE Tran. on Ind. Electronics* 62.12 (2015), pp. 7436–7447.

[120] B. Hauke. "Basic calculation of a boost converter's power stage". In: *Texas Instruments, Application Report November* (2009), pp. 1–9.

[121] E. Noh and K. Kangwook. "Design of a transmitter coil for use in two wireless power transmission standards". In: *2015 IEEE Wireless Power Transfer Conference (WPTC)*. 2015, pp. 1–3.

[122] M. X. Chen and K. W. E. Cheng. "Design of flat magnetic core for inductively coupled coils in high efficiency wireless power transfer application". In: *2017 7th Internat. Conf. on Power Electronics Systems and Applications Smart Mobility, Power Transfer Security (PESA)*. 2017, pp. 1–7.

[123] J. P. K. Sampath, A. Alphones, and H. Shimasaki. "Coil design guidelines for high efficiency of wireless power transfer (WPT)". In: *2016 IEEE Region 10 Conference (TENCON)*. 2016, pp. 726–729. DOI: 10.1109/TENCON.2016.7848098.

[124] C. Bibirica, S. Cristian, L. Ene, and M. Iordache. "Improving the performance of PCB inductors for WPT systems using magnetic shields". In: *2017 5th Internat. Symp. on Electrical and Electronics Engineering (ISEEE)*. 2017, pp. 1–5. DOI: 10.1109/ISEEE.2017.8170637.

[125] T. Kim, S. Yoon, J. Yook, G. Yun, and W. Y. Lee. "Evaluation of power transfer efficiency with ferrite sheets in WPT system". In: *2017 IEEE Wireless Power Transfer Conf. (WPTC)*. 2017, pp. 1–4. DOI: 10.1109/WPT.2017.7953894.

[126] H. Choi, S. Lee, and C. Cha. "Optimization of geometric parameters for circular loop antenna in magnetic coupled wireless power transfer". In: *2014 IEEE Wireless Power Transfer Conf.* 2014, pp. 280–283. DOI: 10.1109/WPT.2014.6839563.

[127] J. Cho, J. Sun, H. Kim, J. Fan, Y. Lu, and S. Pan. "Coil design for 100 KHz and 6.78 MHz WPT system: Litz and solid wires and winding methods". In: *2017 IEEE Internat. Symp. on Electromag. Compatibility Signal Power Integrity (EMCSI)*. 2017, pp. 803–806. DOI: 10.1109/ISEMC.2017.8077977.

[128] H. Rossmanith, M. Doebroenti, M. Albach, and D. Exner. "Measurement and Characterization of High Frequency Losses in Nonideal Litz Wires". In: *IEEE Tran. on Power Electronics* 26.11 (2011), pp. 3386–3394. ISSN: 0885-8993. DOI: 10.1109/TPEL.2011.2143729.

[129] S. L. Ho, J. Wang, W. N. Fu, and M. Sun. "A comparative study between novel witricity and traditional inductive magnetic coupling in wireless charging". In: *IEEE Tran. on Mag.* 47.5 (2011), pp. 1522–1525.

[130] D. W. Lee, K. P. Hwang, and S. X. Wang. "Fabrication and analysis of high-performance integrated solenoid inductor with magnetic core". In: *IEEE Tran. on Magnetics* 44.11 (2008), pp. 4089–4095.

[131] A. Sultanbek, A. Khassenov, Y. Kanapyanov, M. Kenzhegaliyeva, and M. Bagheri. "Intelligent wireless charging station for electric vehicles". In: *2017 Internat. Siberian Conf. on Control and Commun. (SIBCON)*. 2017, pp. 1–6. DOI: 10.1109/SIBCON.2017.7998497.

[132] J. P. K. Sampath, D. M. Vilathgamuwa, and A. Alphones. "Efficiency Enhancement for Dynamic Wireless Power Transfer System With Segmented Transmitter Array". In: *IEEE Tran. on Transportation Electrification* 2.1 (2016), pp. 76–85. ISSN: 2332-7782. DOI: 10.1109/TTE.2015.2508721.

[133] H. Hu. "Optimal and Miniaturized Strongly Coupled Magnetic Resonant Systems". In: (2016).

[134] T. C. Beh, T. Imura, M. Kato, and Y. Hori. "Basic study of improving efficiency of wireless power transfer via magnetic resonance coupling based on impedance matching". In: *IEEE Internat. Symp. on Ind. Electronics (ISIE) 2010*. IEEE. 2010, pp. 2011–2016.

[135] P. Hu, J. Ren, and W. Li. "Frequency-splitting-free synchronous tuning of close-coupling self-oscillating wireless power transfer". In: *Energies* 9.7 (2016), p. 491.

[136] J. Park, Y. Tak, Y. Kim, Y. Kim, and S. Nam. "Investigation of adaptive matching methods for near-field wireless power transfer". In: *IEEE Tran. on Antennas and Propag.* 59.5 (2011), pp. 1769–1773.

[137] N. Oodachi, K. Ogawa, H. Kudo, H. Shoki, S. Obayashi, and T. Morooka. "Efficiency improvement of wireless power transfer via magnetic resonance using transmission coil array". In: *Proc. IEEE Antennas and Propagat. Int. Symp.(APSURSI)*. 2011, pp. 1707–1710.

[138] D. Liu, H. Hu, and S. V. Georgakopoulos. "Novel topologies of misalignment insensitive SCMR wireless power transfer systems". In: *Antennas and Prop. Society Internat. Symp. (APSURSI), 2014 IEEE*. IEEE. 2014, pp. 1341–1342.

[139] F. Jolani, Y. Yu, and Z. Chen. "Enhanced planar wireless power transfer using strongly coupled magnetic resonance". In: *Electronics Letters* 51.2 (2015), pp. 173–175.

[140] O. Jonah, S. V. Geogakopoulos, and M. M. Tentzeris. "Strongly Coupled Wireless Power Transfer with Conformal Structures". In: *Proc. IEEE Antennas Propagat. Soc. Int. Symp. Lake Buena Vista FL*. 2013.

[141] K. Bao, H. Hu, and S. V. Georgakopoulos. "Design considerations of conformal SCMR system". In: *Proc. IEEE Wireless Power Transransfer Conf. (WPTC)*. 2015, pp. 1–3.

[142] H. Hu, K. Bao, J. Gibson, and S. V. Georgakopoulos. "Printable and conformal strongly coupled magnetic resonant systems for wireless powering". In: *IEEE 15th Annual Wireless and Microwave Technology Conf. (WAMICON)*. IEEE. 2014, pp. 1–4.

[143] J. Gibson, K. Bao, H. Hu, and S. V. Georgakopoulos. "Wireless charging for Li-Ion battery using a printable Conformal SCMR". In: *Proc. IEEE Antennas and Propagat. Soc. Int. Symp. (APSURSI), 2014*. 2014, pp. 1349–1350.

[144] H. Hoang and F. Bien. "Maximizing Efficiency of Electromagnetic Resonance Wireless Power Transmission Systems with Adaptive Circuits". In: *Wireless Power Transfer - Principles and Engineering Explorations*. InTech, 2012, pp. 272–. ISBN: 978-953-307-874-8. DOI: 10.5772/25829. URL: http://www.intechopen.com.

[145] O. Jonah and S. V. Georgakopoulos. "Wireless power transfer in concrete via strongly coupled magnetic resonance". In: *IEEE Tran. on Antennas and Propag.* 61.3 (2013), pp. 1378–1384.

[146] P. T. Theilmann and P. M. Asbeck. "An Analytical Model for Inductively Coupled Implantable Biomedical Devices With Ferrite Rods". In: *IEEE Trans. Biomedical Circuits and Syst.* 3.1 (2009), pp. 43–52. ISSN: 1932-4545. DOI: 10.1109/TBCAS.2008.2004776.

[147] A. Karalis, J. D. Joannopoulos, and M. Soljacic. "Efficient wireless non-radiative mid-range energy transfer". In: *Annals of physics* 323.1 (2008), pp. 34–48.

[148] G. Bouattour, B. Kallel, K. Sasmal, O. Kanoun, and N. Derbel. "Comparative study of resonant circuit for power transmission via inductive link". In: *12th Internat. Multi Conf. on Syst. Signals and Devices (SSD) 2015*. IEEE. 2015, pp. 1–6.

[149] H. Hu and S. V. Georgakopoulos. "Design of optimal and broadband conformal SCMR systems". In: *IEEE Antennas and Propag. Soc. Internat. Symp. (APSURSI)*. 2014, pp. 1345–1346.

[150] X. Li, X. Dai, Y. Li, Y. Sun, Z. Ye, and Z. Wang. "Coupling coefficient identification for maximum power transfer in WPT system via impedance matching". In: *IEEE PELS Workshop on Emerging Technologies: Wireless Power Transfer (WoW) 2016*. IEEE. 2016, pp. 27–30.

[151] R. Vijaykumar, A. S. Edison, and W. W. Brey. "Inductively-coupled frequency tuning and impedance matching in HTS-based NMR probes". In: *IEEE Tran. on Applied Superconductivity* 27.4 (2017), pp. 1–5.

[152] Y. Huang, N. Shinohara, and T. Mitani. "Impedance matching in wireless power transfer". In: *IEEE Tran. on Microwave Theory and Techniques* 65.2 (2017), pp. 582–590.

[153] F. Liu, Y. Yang, D. Jiang, X. Ruan, and X. Chen. "Modeling and Optimization of Magnetically Coupled Resonant Wireless Power Transfer System with Varying Spatial Scales". In: *IEEE Trans. Power Electron.* PP.99 (2016), pp. 1–1. ISSN: 0885-8993. DOI: 10.1109/TPEL.2016.2581840.

[154] X. Mou, O. Groling, and H. Sun. "Energy-efficient and adaptive design for wireless power transfer in electric vehicles". In: *IEEE Tran. on Ind. Electronics* 64.9 (2017), pp. 7250–7260.

[155] X. Xie, R. W. G. Bucknall, and K. Yearwood. "Simulation study of a magnetic coupled resonant wireless energy transfer and storage system for electric vehicles under dynamic condition". In: *Australasian Universities Power Engineering Conf. (AUPEC) 2015*. IEEE. 2015, pp. 1–6.

[156] D. Liu, H. Hu, and S. V. Georgakopoulos. "Misalignment sensitivity of strongly coupled wireless power transfer systems". In: *IEEE Trans. Power Electron* 32.7 (2017), pp. 5509–5519.

[157] D. Daerhan, O. Jonah, H. Hu, S. V. Georgakopoulos, and M. M. Tentzeris. "Novel highly-efficient and misalignment insensitive wireless power transfer systems utilizing Strongly Coupled Magnetic Resonance principles". In: *2014 IEEE 64th Electronic Components and Technology Conference (ECTC)*. 2014, pp. 759–762. DOI: 10.1109/ECTC.2014.6897370.

[158] H. Lee, S. Kang, Y. Kim, and C. Jung. "Small-sized metallic and transparent film resonators for MR-WPT system". In: *Electronics Letters* 52.8 (2016), pp. 650–652.

[159] H. Hu, D. Liu, and S. V. Georgakopoulos. "Miniaturized strongly coupled magnetic resonant systems for wireless power transfer". In: *IEEE Internat. Symp. on Antennas and Prop. (APSURSI), 2016*. IEEE. 2016, pp. 155–156.

[160] M. Kiani, U. I. Jow, and M. Ghovanloo. "Design and optimization of a 3-coil inductive link for efficient wireless power transmission". In: 5.6 (2011), pp. 579–591.

[161] S. H. Kang, C. W. Jung, et al. "Wireless power transfer for mobile devices with consideration of ground effect". In: *Wireless Power Transfer Conference (WPTC), 2015 IEEE*. IEEE. 2015, pp. 1–4.

[162] T. Fujita, T. Yasuda, and H. Akagi. "A wireless power transfer system with a double-current rectifier for EVs". In: *Energy Conversion Congress and Exposition (ECCE), 2016 IEEE*. IEEE. 2016, pp. 1–7.

[163] M. Mahdavifard, A. Poorfakhraei, and F. Tahami. "A novel method for reduction of coil weight and size in wireless power transfer". In: *Power Electronics, Drive Systems & Technologies Conference (PEDSTC), 2017 8th*. IEEE. 2017, pp. 395–400.

[164] T. Kim, B. Kim, J. Yook, G. Yun, and W. Y. Lee. "High Q-factor compact coils having non-uniform wire width for wireless power transfer system". In: *2016 URSI Asia-Pacific Radio Science Conference (URSI AP-RASC)*. 2016, pp. 854–857. DOI: 10.1109/URSIAP-RASC.2016.7601279.

[165] Y. Geng, B. Li, Z. Yang, F. Lin, and H. Sun. "A high efficiency charging strategy for a supercapacitor using a wireless power transfer system based on LCC compensation topology". In: *Energies* 10.1 (2017), p. 135.

[166] H. Hu and S. V. Georgakopoulos. "Analysis and design of conformal SCMR WPT systems with multiple resonators". In: *Antennas and Propagation Society International Symposium (APSURSI), 2014 IEEE*. IEEE. 2014, pp. 1347–1348.

[167] M. Contestabile, M. Alajaji, and B. Almubarak. "Will current electric vehicle policy lead to cost-effective electrification of passenger car transport?" In: *Energy Policy* 110 (2017), pp. 20–30.

[168] Y. A. Sha'aban, A. Ikpehai, B. Adebisi, and K. M. Rabie. "Bi-directional coordination of plug-in electric vehicles with economic model predictive control". In: *Energies* 10.10 (2017), p. 1507.

[169] W. Zhang, T. Zhang, Q. Guo, L. Shao, N. Zhang, X. Jin, and J. Yang. "High-efficiency wireless power transfer system for 3D, unstationary free-positioning and multi-object charging". In: *IET Electric Power Applications* 12.5 (2018), pp. 658–665.

[170] Planning Policy Team and Southampton City Council. "Parking Standards Supplementary Planning Document (SPD)". In: *city* 23.8083 (2011), p. 4912.

[171] M. Budhia, J. T. Boys, G. A. Covic, and C. Y. Huang. "Development of a single-sided flux magnetic coupler for electric vehicle IPT charging systems". In: *IEEE Tran. on Ind. Electronics* 60.1 (2013), pp. 318–328.

[172] S. Kim, G. A. Covic, and J. T. Boys. "Tripolar pad for inductive power transfer systems for EV charging". In: *IEEE Tran. on Power Electronics* 32.7 (2017), pp. 5045–5057.

[173] S. Ruddell, U. K. Madawala, D. J. Thrimawithana, and M. Neuburger. "A novel wireless converter topology for dynamic EV charging". In: *Transportation Electrification Conference and Expo (ITEC), 2016 IEEE*. IEEE. 2016, pp. 1–5.

[174] C. Xu, Y. Zhuang, H. Han, C. Song, Y. Huang, and J. Zhou. "Multi-coil high efficiency wireless power transfer system against misalignment". In: *2018 IEEE MTT-S Internat. Wireless Symp. (IWS)*. IEEE. 2018, pp. 1–3.

[175] P. Liang, Q. Wu, H. D. Brüns, and C. Schuster. "Efficient modeling of multi-coil wireless power transfer systems using combination of full-wave simulation and equivalent circuit modeling". In: *2018 IEEE Internat. Symp. on Electromag. Compat. and 2018 IEEE Asia-Pacific Symp. on Electromagnetic Compatibility (EMC/APEMC)*. IEEE. 2018, pp. 466–471.

[176] L. Ye P. Tan C. Liu and T. Peng. "Modeling and experimentation of multi-coil switching coupler for wireless power transfer systems". In: *Energy Conversion Congress and Exposition (ECCE), 2017 IEEE*. IEEE. 2017, pp. 2579–2583.

[177] C. Lilly. *Electric car market statistics*. Ed. by nextgreencar. June 2018. URL: `www.nextgreencar.com/electric-cars/statistics/`.